# FUNCTIONAL ELECTRICAL STIMULATION INDUCED CYCLING USING REPETITIVE LEARNING AND PASSIVITY-BASED CONTROL

By

VICTOR HAZAEL DUENAS FONTES

A DISSERTATION PRESENTED TO THE GRADUATE SCHOOL
OF THE UNIVERSITY OF FLORIDA IN PARTIAL FULFILLMENT
OF THE REQUIREMENTS FOR THE DEGREE OF
DOCTOR OF PHILOSOPHY

UNIVERSITY OF FLORIDA

2018

To God, for being the source of life and inspiration, to my mother Lourdes, my father Victor, and my brother Samuel, for their invaluable support

ACKNOWLEDGMENTS

I am very grateful to my advisor and mentor Dr. Warren E. Dixon for his continuous guidance, support, and patience throughout this academic journey. He has provided invaluable advice to focus on meaningful high-quality problems and strive for excellence in research. As a mentor, his ongoing motivation and immense experience have positively shaped my vision to pursue an academic career. The collaboration-based culture developed in the NCR lab has facilitated my learning across different topics and impacted the way I interact with my colleagues. I am fortunate to have received this unique technical and professional training as I prepare for my academic career. I would like to express my gratitude to my family and friends who have constantly supported and encouraged me emotionally and spiritually during my doctorate program. I would also like to extend my gratitude towards my committee members Dr. Carl Crane, Dr. Scott Banks, and Dr. Karim Oweiss for their time and the valuable recommendations they have provided to improve this dissertation. I would also like to thank past and present members of the NCR lab for the countless discussions that have helped shape the ideas in this dissertation. I am thankful for the financial support provided by the Mechanical and Aerospace department at the University of Florida.

TABLE OF CONTENTS

LIST OF TABLES

LIST OF FIGURES

Abstract of Dissertation Presented to the Graduate School
of the University of Florida in Partial Fulfillment of the
Requirements for the Degree of Doctor of Philosophy

FUNCTIONAL ELECTRICAL STIMULATION INDUCED CYCLING USING REPETITIVE LEARNING AND PASSIVITY-BASED CONTROL

By

Victor Hazael Duenas Fontes

May 2018

Chair: Warren E. Dixon
Major: Mechanical Engineering

Neurological conditions (NCs) that result in movement disorders greatly affect a person's independence and mobility. Rehabilitative procedures and activity-based therapy have shown a potential to facilitate neurological reorganization and recovery based on the concept of motor learning by active, intense, and repetitive task completion. Assistive devices and technologies such as powered exoskeletons and brain computer interfaces have been recently coupled with functional electrical stimulation (FES) to provide training in the upper and lower body for people with NCs. FES is a common technology used to elicit muscle contractions to achieve a motor task. Stationary FES-cycling has been recommended to activate multiple lower-limb muscles and facilitate long duration exercises to yield physiological and functional benefits. The use of motorized assistance in FES-cycling is intended to facilitate consistent, continuous exercise especially at early stages of rehabilitation where spasticity and stimulation hypersensitivity are limiting factors in patient populations. Switching control is inherent in FES-cycling since multiple lower limb muscles are needed to produce a coordinated movement. Moreover, switching between multiple muscle groups and an electric motor makes the overall closed-loop system a switched system. A particular characteristic of cycling is its inherent periodic nature. Hence, iterative and repetitive learning controllers are suitable for motorized FES-cycling. Therefore motivation exists to develop learning

control algorithms that can take advantage of the periodicity of the desired tracking trajectories in FES-cycling while guaranteeing stability of the human-machine closed-loop system.

In Chapter 1, motivation for motorized FES-cycling as a rehabilitation treatment is developed along with a survey of closed-loop learning control methods relevant for the tracking objectives presented in the subsequent chapters of the dissertation. In Chapter 2, a nonlinear stationary cycle and rider dynamic model with autonomous state-dependent switching is introduced. The stimulation pattern switches across multiple lower-limb muscle groups based on the effectiveness of producing functional torque during the crank cycle, and the electric motor provides assistance when the muscle groups yield low torque production. The controllers developed in subsequent chapters are designed for this uncertain and nonlinear rider-cycle model with switched control inputs.

In Chapter 3, a switched learning controller is developed by exploiting the continuous operation of the cycle and the periodic nature of cadence tracking in cycling. No previous study has developed a repetitive learning controller (RLC) for cadence tracking while considering the switching effects between lower-limb muscles and an electric motor. A Lyapunov-based stability analysis that invokes a LaSalle-Yoshizawa corollary for nonsmooth systems is used to guarantee asymptotic tracking. The developed controller was tested during FES-cycling experiments in five able-bodied individuals and three participants with NCs. The added value of the RLC in cadence tracking is illustrated by comparing the results of two trials with and without the learning feedforward term. The results indicate that the RLC yields a lower mean root-mean- squared (RMS) cadence tracking error.

In Chapter 4, the design of a distributed RLC that commands an independent learning feedforward term to each of the six stimulated lower-limb muscle groups and an electric motor during the tracking of a periodic cadence trajectory is examined. The

controller exploits the periodicity of the desired cadence trajectory to learn from previous control inputs for each muscle group and electric motor. The motivation of this chapter is to leverage the idea of distributed learning control that has recently developed in the fields of multi-agent systems, network control, and large-scale systems to investigate FES-cycling since the multiple activation of lower-limb muscles is needed to perform cooperative tracking. The switched controller with distributed RLC was evaluated in experiments with seven able-bodied individuals and five participants with NCs.

In Chapter 5, the activation of the lower-limb muscles is performed via a novel spatial repetitive learning control to achieve torque tracking. Cadence regulation is achieved by the electric motor using a robust sliding-mode controller. The idea of spatial learning control is used to investigate the objective of torque tracking defined by a spatially periodic function of the crank position. A desired torque trajectory is constructed based on the crank position and determined by the kinematic efficiency of the rider to elicit active torque. The learning controller takes advantage of the periodicity of the desired torque trajectory to provide a feedforward input to the stimulated muscles. A passivity-based analysis is developed to ensure stability of the torque and cadence closed-loop error systems. The muscle torque and electric motor controllers were implemented in experiments with five able-bodied individuals and three participants with movement disorders.

Chapter 6 highlights the contributions of the developed techniques and provides future research extensions.

# CHAPTER 1
# INTRODUCTION

## 1.1 Background

Functional Electrical Stimulation (FES) technologies seek to enhance the quality of life of people with movement disorders. Neurological conditions (NCs) that result in movement disorders greatly affect a person's independence and mobility. The use of robotic devices and the artificial activation of muscles via FES aim to restore mobility and actuation function in paralyzed limbs and promote active movements for people with constrained neurological motor control. Functional electrical stimulation (FES) is a common technology used to elicit muscle contractions to achieve a motor task [1]. The use of closed-loop FES control has been successfully implemented in contracting isolated ex vivo muscles [2], upper-limb tasks [3–5], locomotion (including stepping, standing, and walking) with neuroprostheses [6–10], and lower-limb cycling with and without motorized assistance [11–14]. FES applied to lower-limb muscles has allowed individuals with spinal cord injury (SCI) to stand and step for short distances, which has improved their sitting balance and posture [15]. Active lower-limb cycling with FES significantly improved the walking ability of stroke participants versus cycling without FES [16]. Additionally, improvements in joint movement coordination in the upper limbs with FES [5] and postural control and muscle strength after lower-limb FES-cycling have been reported for stroke participants [16]. Also, FES-cycling was found to be effective in promoting muscle strength and motor recovery in individuals post-acute stroke in [17]. In [18], a long-term FES-cycling study with twenty-five participants with SCI found important gains in neurological, motor, and sensory function and increased muscle volume and strength. Hence, FES-cycling has been suggested as a rehabilitation strategy for people with NCs to improve motor skills due to its simplicity, availability, and low risk (e.g., compared to fall risks in locomotion). Motorized FES-cycling is recommended as an effective exercise to activate lower-limb muscles, thus exploiting

the physiological benefits of the stimulation [19, 20], and extend the exercise duration due to the assistance provided by the electric motor.

Robotic devices have been used to assist neurologically impaired individuals in completing repetitive movements, and to quantify kinematic variables to assess the level of motor recovery during clinical studies [21, 22]. Repetition of a movement pattern through robotic control contributes to motor learning and rehabilitation [21]. Thus the facilitation of adaptive neurological reorganization and recovery of the human motor systems after a neurological lesion has been based on the concept of motor learning by intense, repetitive task completion [23–25]. Further results have shown that motor learning is promoted primarily during motor tasks where robotic assistance is provided only as needed to promote active engagement, if possible, of the user [22, 26]. Hence, the development of a cycling protocol that delivers high intensity repetitive active exercise is desired. Additionally, motorized assistance can aid in obtaining repeatable exercise by only assisting the electrically stimulated lower-limb muscles as needed.

Closed-loop controllers have been developed to provide robustness to the nonlinear dynamics of the cycle-rider system, including the uncertain nonlinear muscle activation dynamics [11–14, 27–29]. FES controllers developed in [12–14, 30, 31] use high-gain feedback to ensure robustness to the system's uncertainty. However, such high frequency control methods often lead to accelerated fatigue [32, 33]. High gain feedback can yield uncomfortable stimulation intensity and amplify high frequency aspects of the feedback signal contributing to muscle fatigue. Motivate d by the desire to reduce high-gain/high-frequency feedback, an important goal is to develop adaptive and/or learning controllers for FES-cycling.

Switching control is inherent in FES-cycling since multiple lower limb muscles are needed to produce a coordinated movement. Switching between multiple muscle groups is desired to achieve metabolic efficiency. In results such as [11, 34, 35] an electric motor is included to provide assistance during regions of the crank cycle where

muscle stimulation is less effective in producing torque. The goal in such results is to maximize the muscle contribution during regions of the crank cycle where efficient torque production occurs and to extend the overall exercise duration by activating the electric motor during low muscle torque output regions. Switching between multiple muscle groups and the electric motor makes the overall system a switched system. Since stability of individual subsystems doesn't guarantee stability of the overall system [36], additional analysis is required. For example, results such as [12] ensure stability of the overall switched system by developing reverse dwell time conditions based on known exponential convergence rates, where a sliding mode control design provides the negative definite bound on the Lyapunov function derivative. However, a technical challenge to design adaptive and/or learning controllers with a switching control input is that a negative-definite bound on the time derivative of the Lyapunov function candidate is unlikely without persistence of excitation.

Learning control methods, such as iterative learning control (ILC) and repetitive learning control (RLC)[1] , improve tracking performance of repetitive or periodic (state or time) processes by utilizing control inputs from previous cycles, iterations, or periods [37–40]. The main difference between RLC and ILC is that RLC is intended for continuous operation with no resetting of the initial conditions, whereas ILC addresses repetitive tracking tasks to be performed over a finite interval, where historically, the initial conditions are set to the same value (resetting condition) on each trial [38, 41]. In different practical applications, ILC and RLC have been realized to handle state, trajectory and time periodicities for continuous and discrete cases [40, 42]. The use of learning control does not require an explicit mathematical model of the uncertainties

[1] The acronym RLC is used interchangeably throughout this dissertation to refer to a particular repetitive learning controller or to repetitive learning control (control methodology).

present in the system, rather, the control strategy exploits the repeated or periodic motion to learn the uncertainties. Rehabilitation tasks such as cycling are repetitive/periodic naturally, and hence, ILC/RLC is an attractive method to adaptively adjust to the person's unique attributes. Compared to adaptive control, ILC/RLC methods don't require the uncertainty in the system to be linearly parameterizable (LP). This relaxation of the structure of uncertainty is beneficial given the lack of an exact model in applications that involve human-machine interaction, especially for participants with NCs. ILC and RLC have been extensively applied for tracking of nonlinear systems to ensure asymptotic convergence and boundedness of the learning inputs [43–46]. Lyapunov- and passivity-based tools have been utilized to synthesize ILC and RLC controllers for finite interval tasks with states resetting after each trial [38, 41] and for continuous operation in the time horizon without resetting [44, 46], respectively.

ILC and RLC methods have been implemented in in FES studies. In results such as [41], [47], and [48] the use of ILC with FES has been investigated during planar and unconstrained upper arm tasks for clinical rehabilitation in stroke and multiple sclerosis (MS) populations. However, most of the developed ILC controllers required preliminary model identification procedures, the dynamics were linearized, and limited information was given regarding the switching muscle dynamics. In [49], ILC was implemented for foot trajectory tracking during swing phase in gait using a drop foot neuroprosthesis. A brain-computer interface with FES was developed for upper limbs motor rehabilitation using ILC in [50]. In [51], a FES repetitive controller was implemented for tremor suppression at the wrist. A single study applied ILC for FES-cycling in computer simulation [52]. However there is no previous work using learning control techniques in FES-cycling while developing a Lyapunov-based stability analysis that takes into consideration the switching effects between multiple muscle groups and an electric motor. In Chapter 3, the development of RLC in the context of switched control is introduced for cadence tracking in FES-cycling.

Recent literature in learning control has studied the development of a distributed or decentralized learning approach has been developed in the fields of multi-agent systems, network control, and large-scale systems. In [53], a distributed ILC approach was realized for trajectory tracking of a group of quadrotors, where each vehicle learns from its own and its neighbor's previous inputs during past repetitions. Consensus-based learning control was designed to learn periodic uncertainties where an auxiliary control is designed for each follower agent to track the leader in [54]. A distributed adaptive iterative learning technique was implemented for consensus tracking for a class of nonlinear multi-agent systems in [55]. In [56], a multi-agent formation problem is studied with switching topologies utilizing a distributed algorithm where agents learn to execute a cooperative task via repetition. A distributed optimization-based ILC algorithm was developed in [57] to address a large-scale building temperature control problem where the centralized system is separated into several subsystems that share communication. In Chapter 4, a distributed repetitive learning is investigated for FES-cycling since multiple lower-limb muscles require activation to achieve a cadence tracking objective.

Several objectives have been identified for the design of assistive devices, such as strength training (control of resistive torque to enhance power output) and cardiovascular improvements (focused on lower resistive torque, but longer exercise duration) [22, 58, 59]. In cycling, closed-loop switching control has been used to activate lower-limb muscles and engage an electric motor to cooperatively track cadence [11, 60]. However, motivation also exists to maximize the torque output produced by the activation of lower-limb muscles for strength training and building muscle mass [35]. The dual objective of torque and cadence tracking, i.e., power tracking, has been studied in several FES-cycling protocols. In [34], a procedure for system identification and the use of linear feedback control was developed for power tracking. In [29], a higher-order sliding mode control was designed to track a power trajectory between 5 and 10 Watts

(W). A Lyapunov method using a switched dwell-time analysis was designed for power control in [61]. In [62], a discrete-time analysis was developed for torque tracking, where the controller was updated once at the beginning of each crank cycle. However, none of the previous results exploit the repetitive/periodic nature of cycling during power tracking. Hence, the development of learning control algorithms that can take advantage of the periodicity of FES-cycling while guaranteeing stability of the human-machine closed-loop system is desired.

The selection of tracking trajectories for human-robot applications is an important design consideration in rehabilitative procedures. Torque trajectories for human-assisted locomotion have been based on time, joint angles, mechanical phase-variables, and electromyographic signals [63–66]. The relationship between lower-limb joint angles and joint torques has been utilized to regulate net joint power, especially in lower limb exoskeletons [9, 63]. For cycling, a mechanical power analysis was developed in [67] using a two-legged pedaling model to determine the energy generation by knee extensor and flexor joint torques through the upstroke and downstroke regions of the crank cycle. In [68] a transfemoral amputee pedaled a bicycle with assistance from a powered prosthetic device, where the joint torque references were generated using the knee joint power distribution (as a function of crank angle) presented in [67]. Therefore motivation exists in cycling to select crank position-dependent desired torque trajectories, where the kinematic efficiency of the rider is exploited to evoke muscle torque in favorable regions of the crank cycle.

Since people undergoing movement therapy often have diminished torque producing capacity, an electric motor is typically used to assist FES-cycling; however, the use of an electric motor raises an additional concern for safe interaction between the rider and the motor. Safety is a fundamental factor, especially for applications involving people with NCs that result in paralysis, spasticity, and tremor, etc. Motivated to ensure safe human-robot interaction, passivity theory has been used to design controllers in

numerous applications including exercise machines and exoskeletons [58, 59]. Closed-loop controllers that ensure passivity in the human-robot system are desirable due to their compliant behavior, which also results in safe performance [58]. Several adaptive controllers have been developed that ensure passivity for trajectory tracking of fully actuated robot manipulators [69, 70]. Moreover in recent years, passivity is often used to examine the feedback interconnections of complex systems, such as hybrid and switched systems [71, 72]. Hence, passivity is a powerful tool to be exploited for the design of adaptive and learning controllers in the context of switched systems such as FES-cycling.

More recently, spatial iterative learning methods have been developed to address the fact that many tracking tasks are not periodic in the time domain, but rather periodic in the spatial domain (state-based periodicity) [73–77]. In [73], a spatial-based ILC was developed based on path errors updates and progress along the path. In [74], an adaptive compensator was developed to reject a state-based periodic disturbance. In [75], the spatial periodicity of rotary machine systems was exploited to develop an adaptive controller to update the parametric estimates and the input signal. A spatial projection was developed in [76] to develop a framework to leverage the spatial repeatability typically found in human motor learning experiments. In [77], a space-based barrier function was developed to show convergence and boundedness of the state tracking of a system modeled with spatial periodicities. In Chapter 5, the idea of spatial learning control to investigate the objective of torque tracking defined by a spatially periodic function of the crank position.

## 1.2 Outline of the Dissertation

Chapter 2 describes the switched dynamic model of the cycle-rider nonlinear system. The nonlinear model of the motorized cycle-rider system presented in Chapter 2 is used for the design of learning switching controllers in subsequent chapters. A stimulation activation pattern switches across the quadriceps femoris, hamstrings, and

gluteal muscle groups, which exploits the kinematic effectiveness of the rider, and an electric motor is coupled to the drive chain. The properties and assumptions used in the subsequent chapters are also listed in Chapter 2.

In Chapter 3, a RLC is designed based on a saturated feedforward learning input to track a desired periodic cadence with known period on a stationary recumbent FES-cycle. The RLC is developed to deal with the periodic tracking control problem without the need to enforce a resetting condition by exploiting the continuous operation of the cycle. The electric motor provides assistance as needed during the regions of the cycle crank where the muscle groups are not activated due to torque transfer inefficiencies. Experimental validation on five healthy individuals and three participants with neurological conditions NCs are presented and discussed. Comparative results of two trials with and without the learning feedforward term are presented to establish the benefits of the RLC. The results indicate that the inclusion of the RLC term in the switching controller yields a lower average root-mean-squared (RMS) cadence tracking error compared to the trial where the learning term was turned off. A common Lyapunov-like function is constructed by adding a Lyapunov-Krasovskii like term to account for the periodicity of the system's desired states. Although a negative semi-definite bound is obtained on the Lyapunov derivative, as opposed to the negative definite bound typically required for switched systems, asymptotic tracking over the time horizon of the overall switched system is ensured through the use of a corollary to the LaSalle-Yoshizawa theorem for nonsmooth systems [78, Corollary 2].

In Chapter 4, a distributed RLC approach (i.e., an independent learning feedforward input is designed for each actuator) is implemented for cooperative cadence tracking between the lower-limb muscles and the electric motor. The distributed feedforward learning terms compensate for the periodic dynamics based on the desired cadence tracking trajectory. The switched learning controller is implemented without the requirement of any identification procedure despite the parametric uncertainty in the system.

Due to the construction of a filtered tracking error, the distributed RLC affects both cadence and position tracking. A Lyapunov-based stability analysis guarantees asymptotic tracking via the invariance-like corollary exploited in Chapter 3. Experimental results are reported for seven able-bodied individuals and five participants with different NCs.

In Chapter 5, the design of torque and cadence controllers is examined for power tracking in FES-cycling. The idea of spatial learning control is used to investigate the objective of torque tracking defined by a spatially periodic function of the crank position. Specifically, a switched FES controller with spatial learning control is designed to track a desired state-periodic torque trajectory by stimulating lower-limb muscles. The periodic desired torque trajectory is designed based on the knee kinematic effectiveness of the rider, which varies as a function of the crank angle. In parallel, a robust sliding-mode controller is designed for the electric motor to achieve cadence tracking. Because every crank cycle (i.e., a full revolution) is completed within different time periods, the spatial periodicity of the torque trajectory is leveraged to update the learning controller based on the crank position. A passivity-based analysis is developed to ensure stability of the torque (muscle control) and cadence (motor control) subsystems. Experimental results on five able-bodied individuals and three participants with NCs demonstrate the feasibility of the torque and cadence controllers.

Chapter 6 concludes the dissertation. A summary of the dissertation is provided along with a discussion on potential extensions and future research directions based on the results developed in previous chapters.

The experimental results presented in this dissertation quantify the cycling performance using position, cadence, and torque from the sensors fitted in the cycle. A key contribution of this dissertation is the proof of feasibility and stability of the aforementioned learning controllers validated in experiments with people with NCs such as stroke, spinal cord injury, spina bifida, and multiple sclerosis. Future work outside of the scope of this dissertation may focus on analyzing standard clinical outcome measures resulting

from the implementation of closed-loop learning controllers for FES-cycling and the challenges related to clinical adoption.

# CHAPTER 2
# FES-CYCLING DYNAMIC MODEL

## 2.1 Dynamic Model

In this chapter, a nonlinear model of a stationary FES-cycling system is presented that includes uncertainty and norm bounded disturbances [11, 12].

### 2.1.1 Stationary Cycle and Rider Dynamic Model

A motorized recumbent stationary cycle and a two-legged rider can be modeled as a single degree-of-freedom system with the following dynamics [12]

$$M(q)\ddot{q} + V(q,\dot{q})\dot{q} + G(q) + P(q,\dot{q}) + c_d\dot{q} + d(t) = \tau_a(q,\dot{q},t) + \tau_e(t), \tag{2-1}$$

where $q : \mathbb{R}_{\geq t_0} \to \mathcal{Q}$ denotes the positive clockwise measurable crank angle, and $\mathcal{Q} \subseteq \mathbb{R}$ denotes the set of crank angles contained between [0,2$\pi$), and $t_0 \in \mathbb{R}$ is the initial time; $M : \mathcal{Q} \to \mathbb{R}_{>0}$, denotes the inertial effects of the rider and cycle; $V : \mathcal{Q} \times \mathbb{R} \to \mathbb{R}$ and $G : \mathcal{Q} \to \mathbb{R}$ denote the centripetal-Coriolis, and gravitational effects, respectively; $P : \mathcal{Q} \times \mathbb{R} \to \mathbb{R}$ denotes the effects of passive viscoelastic tissue forces in the rider's joints; $c_d \in \mathbb{R}_{>0}$ denotes the viscous damping parameter in the cycle; and $d : \mathbb{R}_{\geq t_0} \to \mathbb{R}$ denotes the disturbances applied by the rider and unmodeled effects in the system; $\tau_a : \mathcal{Q} \times \mathbb{R} \times \mathbb{R}_{\geq t_0} \to \mathbb{R}$ denotes the net active torque produced by the lower limb muscle contractions; and $\tau_e : \mathbb{R}_{\geq t_0} \to \mathbb{R}$ denotes the torque applied about the cycle crank axis by the electric motor. The full system is represented by a closed kinematic chain, thus when the orientation of a segment (i.e., the crank angle) is specified for a 4-bar linkage system, the orientation of the remaining segments (i.e., knee- or hip-joint angles) are defined. Figure 2-1 depicts the single DOF dynamic system and the switching regions for the muscle groups and electric motor determined by the crank angle.

The model in (2-1) can be generalized as

$$\tau_c(\dot{q},\ddot{q}) + \tau_r(q,\dot{q},\ddot{q},t) = \tau_e(t), \tag{2-2}$$

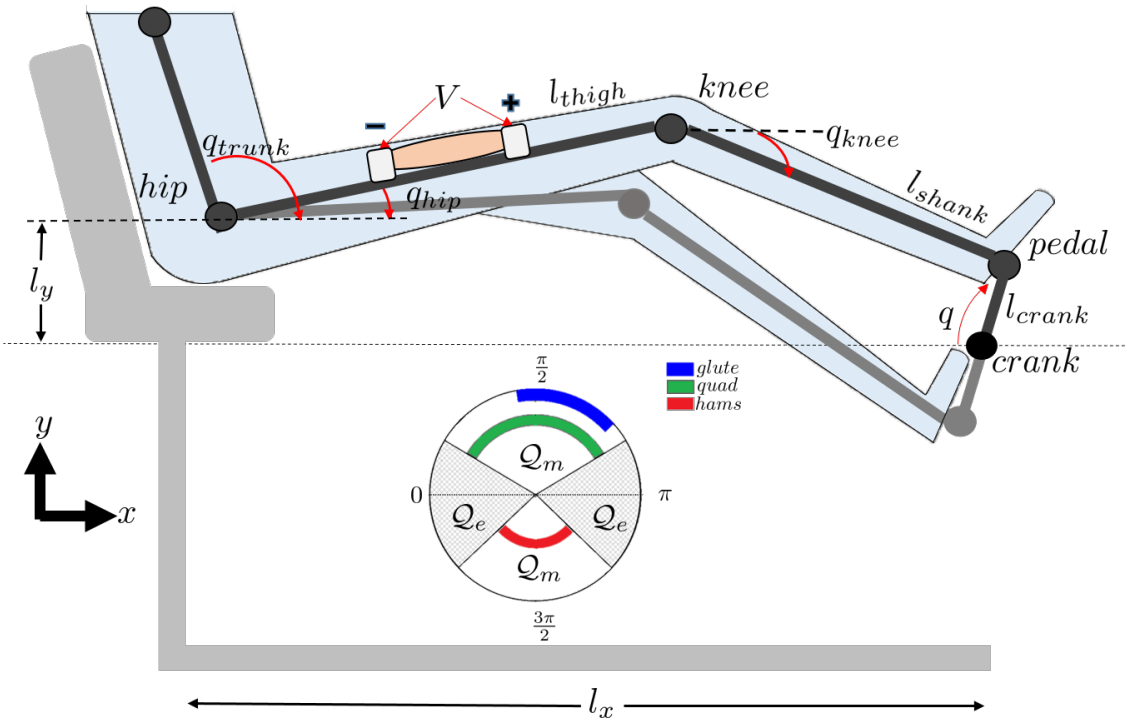


Figure 2-1. Schematic of the stationary cycle-rider system. The crank angle is denoted by $q$, while the knee, hip, and trunk angles are denoted by $q_{knee}$, $q_{hip}$, and $q_{trunk}$ respectively. The thigh length, shank length, cycle crank length, and the horizontal and vertical seat position are denoted by $l_{thigh}$, $l_{shank}$, $l_{crank}$, $l_x$, and $l_y$, respectively. The switching regions are depicted based on the crank angle to describe the regions of the crank cycle where the muscle groups ($\mathcal{Q}_m$) and the electric motor ($\mathcal{Q}_e$) are active. For visualization purposes in the schematic, electrical stimulation is only depicted for the right quadriceps muscle group of the rider.

where $\tau_c : \mathbb{R}^2 \to \mathbb{R}$ denotes the net cycle torque, and $\tau_r : \mathcal{Q} \times \mathbb{R}^2 \times \mathbb{R}_{\geq t_0} \to \mathbb{R}$ denotes the rider torque about the crank, both expressed as

$$\tau_c(\dot{q}, \ddot{q}) = J\ddot{q} + c_d\dot{q}, \tag{2-3}$$

$$\tau_r(q, \dot{q}, \ddot{q}, t) = \tau_p(q, \dot{q}, \ddot{q}, t) - \tau_a(q, \dot{q}, t), \tag{2-4}$$

where $\tau_p : \mathcal{Q} \times \mathbb{R}^2 \times \mathbb{R}_{\geq t_0} \to \mathbb{R}$ denotes the passive torque applied by the rider.

$$\tau_p = M_p(q)\ddot{q} + V(q, \dot{q}) + G(q) + P(q, \dot{q}) + d(t). \tag{2-5}$$

The torque applied by the electric motor about the crank axis is defined as

$$\tau_e(t) \triangleq B_e u_e(t), \tag{2-6}$$

where $B_e \in \mathbb{R}_{>0}$ is a positive torque constant such that $B_e \geq c_e$, where $c_e \in \mathbb{R}_{>0}$ is known, and $u_e : \mathbb{R}_{\geq t_0} \to \mathbb{R}$ is the motor current control input. The net active torque produced by the muscle contractions is

$$\tau_a(q, \dot{q}, t) \triangleq \sum_{m \in \mathcal{M}} B_m(q, \dot{q}) u_m(t), \tag{2-7}$$

where $B_m : \mathcal{Q} \times \mathbb{R} \to \mathbb{R}$ represents the uncertain, nonzero control effectiveness of the involved muscle groups with subscript $m$ indicating an element in the muscle set $\mathcal{M} \triangleq \{RQuad,\ RHam,\ RGlute,\ LQuad,\ LHam,\ LGlute\}$ that contains the right $(R)$ and left $(L)$ quadriceps femoris $(Quad)$, hamstrings $(Ham)$, and gluteal $(Glute)$ muscle groups, and $u_m : \mathbb{R}_{\geq t_0} \to \mathbb{R}$ denotes the stimulation intensity applied to each muscle group. The control effectiveness for each muscle group is defined as [12]

$$B_m(q, \dot{q}) \triangleq \Omega_m(q, \dot{q}) T_m(q),\ m \in \mathcal{M}, \tag{2-8}$$

where $\Omega_m : \mathcal{Q} \times \mathbb{R} \to \mathbb{R}$ denotes the uncertain relationship between stimulation intensity and the muscle group's evoked force which produces a resultant torque about the joint it spans, and $T_m : \mathcal{Q} \to \mathbb{R}$ denotes the relationship between a muscle's resultant torque about a joint to torque about the crank axis. Since most muscles cross multiple joints in the lower limbs, the ability of a muscle to actuate the limb in a certain direction (i.e., flexion or extension) depends on $T_m$. Even so, there are proportional values that relate the values of $T_m$ among muscles, which depend on muscle architecture, like cross sectional area, pennation angle, muscle fiber length, and flexion/extension velocity. These effects are captured in $\Omega_m$ which aids to create lower and upper bounds for

the control effectiveness $B_m$. The following assumption is exploited in the subsequent analysis.

**Assumption 2.1.** Muscles that span multiple joints such as the hamstrings and rectus femoris produce torque only about the knee joint (i.e., with negligible hip coactivation). The torque output is constrained to produce forward pedaling only based on the muscle activation switching law.

In (2-8), the uncertain function $\Omega_m$ is defined as [31]

$$\Omega_m(q, \dot{q}) \triangleq \zeta_m(q)\eta_m(q, \dot{q})cos(b_m(q)), \tag{2-9}$$

where $\zeta_m : \mathcal{Q} \to \mathbb{R}$ denotes the uncertain moment arm of a muscle's output force about the joint it spans, $\eta_m : \mathcal{Q} \times \mathbb{R} \to \mathbb{R}$ denotes the nonlinear function relating the stimulation intensity to muscle force, and $b_m : \mathcal{Q} \to \mathbb{R}$ denotes the uncertain pennation angle of the fibers. The following assumption and properties will be exploited in the subsequent analysis.

**Assumption 2.2.** The disturbance term $d$ is bounded as $|d| \leq \xi_d$, where $\xi_d \in \mathbb{R}_{>0}$ is a known constant.

**Property 1.** The moment arm $\zeta_m, \ \forall m \in \mathcal{M}$ is nonzero with a bounded first time derivative [79].

**Property 2.** The function $\eta_m, \forall m \in \mathcal{M}$ depends on the muscle force-length and muscle force-velocity relationships. The function $\eta_m$ is bounded [80] and is positive provided the muscle is not fully stretched or contracting concentrically at its maximum shortening velocity [81].

**Property 3.** The muscle fiber pennation angle $b_m, \forall m \in \mathcal{M}$ is non-constant [82] and bounded during muscle contractions, such that $cos(b_m) \neq 0$ [83, 84].

**Property 4.** Based on Assumption 2.1 and Properties 1-3, $\Omega_m$ is nonzero and bounded, i.e., $c_\omega < \Omega_m < c_\Omega, \ \forall m \in \mathcal{M}$, where $c_\omega, \ c_\Omega \in \mathbb{R}_{>0}$ are positive known constants.

### 2.1.2 Switched System Model

The rider-cycle model in (2-1) is further developed to account for switching between the lower-limb muscle groups and an electric motor. The stimulation intensities $u_m$, $\forall m \in \mathcal{M}$ are applied to the muscle groups in regions of the crank cycle where the torque transfer ratios $T_m$ are above a predefined threshold $\varepsilon_m \triangleq \Lambda_m max(T_m)$, $\forall m \in \mathcal{M}$, where $\Lambda_m \in [0, 1]$ is a selectable value. The muscle switching control design yields an autonomous, state-dependent, switched control system. The portion of the crank cycle over which a particular muscle group is stimulated is denoted by $\mathcal{Q}_m \subset \mathcal{Q}$, $\forall m \in \mathcal{M}$ , where the muscle groups are activated as described in [12] so that $\mathcal{Q}_M \triangleq \underset{m\in\mathcal{M}}{\cup} \mathcal{Q}_m$. The electric motor is activated as needed, especially in the regions where the FES-induced torque is small (i.e., during the rider's weakest torque production regions). The portions of the crank cycle over which the electric motor contributes to the torque production is denoted as $\mathcal{Q}_e \subset \mathcal{Q}$. In Chapters 3-4, $\mathcal{Q}_M \triangleq \underset{m\in\mathcal{M}}{\cup} \mathcal{Q}_m$ and $\mathcal{Q}_e \triangleq \mathcal{Q} \backslash \mathcal{Q}_M$. This implies that when no muscle group is stimulated, the electric motor is turned on. In this sense, muscle groups and the electric motor contribute independently to produce torque throughout the crank cycle. In Chapter 5, the muscle groups track a desired torque trajectory and the electric motor regulates cadence entirely throughout the crank cycle. A piecewise constant switching signal can be developed for each muscle group, $\sigma_m \in \{0,\ 1\}$, and for the electric motor, $\sigma_e \in \{0, 1\}$ as

$$\sigma_m(q) \triangleq \begin{cases} 1 & \text{if } q \in \mathcal{Q}_m \\ 0 & \text{if } q \notin \mathcal{Q}_m \end{cases}, \quad \sigma_e(q) \triangleq \begin{cases} 1 & \text{if } q \in \mathcal{Q}_e \\ 0 & \text{if } q \notin \mathcal{Q}_e \end{cases}. \tag{2-10}$$

Figure 2-1 denotes the switching regions (i.e., $\mathcal{Q}_m$ and $\mathcal{Q}_e$) where the muscle groups and the electric motor are activated based on the crank angle. Using these state-dependent switching signals, the stimulation inputs to the muscle groups and the motor input can be defined as

$$u_m(t) \triangleq k_m \sigma_m(q) u_{FES}(t), \ \ u_e(t) \triangleq k_e \sigma_e(q) u_{motor}(t), \tag{2-11}$$

where $k_m, k_e \in \mathbb{R}_{>0},\ m \in \mathcal{M}$ are positive, constant control gains, and $u_{FES},\ u_{motor} : \mathbb{R}_{\geq t_0} \to \mathbb{R}$ are the designed stimulation and electric motor current inputs, respectively. Further, for the development in Chapter 3, define $\nu(t) \triangleq u_{FES}(t) = u_{motor}(t)$, then substituting (2-11) into (2-1) and rearranging terms yields [11]

$$M(q)\ddot{q} + V(q,\dot{q})\dot{q} + G(q) + P(q,\dot{q}) + c_d\dot{q} + d(t) = B_\sigma(q,\dot{q})\nu(t), \tag{2-12}$$

where $B_\sigma \in \mathbb{R}_{>0}$ is a lumped, switched control effectiveness term defined as

$$B_\sigma(q,\dot{q}) \triangleq \sum_{m\in\mathcal{M}} B_m(q,\dot{q})k_m\sigma_m(q) + B_e k_e \sigma_e(q). \tag{2-13}$$

In Chapter 5, a dual objective of cadence and torque tracking is developed for which $u_{FES} \neq u_{motor}$. The electric motor is always turned on (i.e., $\sigma_e = 1,\ \forall q \in \mathcal{Q}$), while the muscle groups are activated based on $\sigma_m$ in (2-10). Then (2-12) can be rewritten as

$$M(q)\ddot{q} + V(q,\dot{q})\dot{q} + G(q) + P(q,\dot{q}) + c_d\dot{q} + d(t) = B_\sigma(q,\dot{q})u_{FES}(t) + B_e u_e. \tag{2-14}$$

The subscript $\sigma \in \mathcal{P} \triangleq \{1,2,3,...n\},\ \mathcal{P} \subset \mathbb{N},\ n \in \mathbb{R}_{>0}$ indicates the index of $B_\sigma$, which switches according to the crank position. There are a total of $n$ subsystems consisting of the activation of a combination of the muscle groups and the electric motor. The known sequence of switching states, which are the limit points of $\mathcal{Q}_m,\ \forall m \in \mathcal{M}$, is defined as $\{q_n\},\ n \in \{0,\ 1,\ 2,\ ...\}$, and the corresponding sequence of unknown switching times $\{t_n\}$ are defined such that each $t_n$ denotes the instant when $q$ reaches the corresponding switching state $q_n$. The switching signal $\sigma$ is assumed to be continuous from the right (i.e., $\sigma(q) = \lim_{q\to q_n^+}\sigma(q)$). The following properties from [11] of the switched system in (2-12) and (2-14) will be exploited in the subsequent chapters.

**Property 5.** $c_m \leq M \leq c_M$, where $c_m,\ c_M \in \mathbb{R}_{>0}$ are known constants.

**Property 6.** $|V| \leq c_V|\dot{q}|$, where $c_V \in \mathbb{R}_{>0}$ is a known constant.

**Property 7.** $|G| \leq c_G$, where $c_G \in \mathbb{R}_{>0}$ is a known constant.

**Property 8.** $|P| \leq c_{P1} + c_{P2}\,|\dot{q}|$, where $c_{P1},\ c_{P2} \in \mathbb{R}_{>0}$ are known constants.

**Property 9.** $\frac{1}{2}\dot{M} - V = 0$ by skew symmetry.

**Property 10.** Based on Properties 1-4, the lumped switching control effectiveness is bounded as $c_b \leq B_\sigma \leq c_B,\ \forall \sigma \in \mathcal{P}$, where $c_b, c_B \in \mathbb{R}_{>0}$ are known constants.

**Property 11.** The desired crank trajectory is periodic in the sense that $q_d(t) = q_d(t - T),\ \dot{q}_d(t) = \dot{q}_d(t - T),\ \ddot{q}_d(t) = \ddot{q}_d(t - T)$ with known period $T$.

# CHAPTER 3
# MOTORIZED AND FUNCTIONAL ELECTRICAL STIMULATION INDUCED CYCLING VIA SWITCHED REPETITIVE LEARNING CONTROL

In this chapter and in the work in [28, 60], a RLC is designed based on a saturated feedforward learning term developed in [44] to track a desired periodic cadence with known period on a stationary recumbent FES-cycle. The RLC is developed to deal with the periodic tracking control problem without the need to enforce a resetting condition. The nonlinear model of the motorized cycle-rider system presented in Chapter 2 is used for the design of a switching controller that activates lower-limb muscles based on a predetermined activation pattern, which exploits the kinematic effectiveness of the rider, and an electric motor coupled to the drive chain. The electric motor provides assistance as needed during the regions of the cycle crank where the muscle groups are not activated due to torque transfer inefficiencies.

Experimental results on five able-bodied individuals and three participants with neurological conditions (NCs) are presented in the experimental section proving the feasibility of the control technique. Comparative results of two trials with and without the learning feedforward term are presented. The results indicate that the inclusion of the RLC term in the switching controller yields a lower average root-mean-squared (RMS) cadence tracking error compared to the trial where the learning term was turned off. A common Lyapunov-like function is constructed by adding a Lyapunov-Krasovskii like term to account for the periodicity of the system's desired states. Although a negative semi-definite bound is obtained on the Lyapunov derivative, as opposed to the negative definite bound typically required for switched systems, asymptotic tracking over the time horizon of the overall switched system is ensured through the use of a corollary to the LaSalle-Yoshizawa theorem for nonsmooth systems [78, Corollary 2].

### 3.1 Control Development

The objective is to design a controller to track a desired crank cadence. The measurable crank position trajectory tracking error $e : \mathbb{R}_{\geq t_0} \to \mathbb{R}$ is defined as[1]

$$e(t) \triangleq q_d(t) - q(t), \tag{3-1}$$

where $q_d : \mathbb{R}_{\geq t_0} \to \mathbb{R}$ denotes the desired crank position, which satisfies Property 11, with bounded time derivatives such that $|\dot{q}_d(t)| \leq \xi_{d_1}$ and $|\ddot{q}_d(t)| \leq \xi_{d_2}$, where $\xi_{d_1}, \xi_{d_2} \in \mathbb{R}_{>0}$ are known positive constants.

*Remark* 3.1. The disturbance term $d(t)$ in (2-12) is set to zero in the subsequent analysis of this chapter.

To facilitate the subsequent control development and stability analysis, an auxiliary tracking error $r : \mathbb{R}_{\geq t_0} \to \mathbb{R}$ is defined as

$$r(t) \triangleq \dot{e}(t) + \alpha e(t), \tag{3-2}$$

where $\alpha \in \mathbb{R}_{>0}$ is a positive constant control gain. Taking the time derivative of (3-2) and premultiplying by $M$, substituting for (2-12) and (3-1), then performing some algebraic manipulation yields

$$M\dot{r} = -Vr + W_d + \chi - B_\sigma \nu + N_d, \tag{3-3}$$

where the auxiliary signals $W_d : \mathbb{R}_{\geq t_0} \to \mathbb{R}$, $\chi : \mathbb{R}_{\geq t_0} \to \mathbb{R}$, and $N_d : \mathbb{R}_{\geq t_0} \to \mathbb{R}$ are defined as

$$W_d \triangleq M(q_d)\ddot{q}_d + V(q_d, \dot{q}_d)\dot{q}_d + G(q_d) + c_d\dot{q}_d, \tag{3-4}$$

[1] The control objective can be quantified in terms of the first time derivative of $e(t)$.

$$\chi \triangleq M(q)(\ddot{q}_d + \alpha\dot{e}) + V(q,\dot{q})(\dot{q}_d + \alpha e) + G(q) + P(q,\dot{q}) + c_d\dot{q} - W_d - N_d, \quad (3\text{-}5)$$

$$N_d \triangleq c_{P1} + c_{P2}\dot{q}_d(t). \quad (3\text{-}6)$$

The auxiliary signal in (3-6) can be upper bounded as

$$|N_d| \leq \Theta, \quad (3\text{-}7)$$

where $\Theta \in \mathbb{R}$ is a known positive constant. By using Properties 5-9, (3-1) and (3-2), the Mean Value Theorem can be used to develop an upperbound for (3-5) as

$$\chi \leq \rho(\|z\|)\|z\|, \quad (3\text{-}8)$$

where $z : \mathbb{R}_{\geq 0} \to \mathbb{R}^2$ is a composite vector of error signals defined as

$$z \triangleq [e \ r]^T, \quad (3\text{-}9)$$

and $\rho(\cdot) \in \mathbb{R}$ is a known positive, radially unbounded, nondecreasing function. Based on (3-4) and the explicit boundedness of the periodic desired trajectory

$$|W_d(t)| \leq \beta_r, \quad (3\text{-}10)$$

where $\beta_r \in \mathbb{R}$ is a known positive bounding constant. Given the open-loop error system in (3-3), the control input is designed as

$$\nu = \hat{W}_d + k_1 r + k_2 sgn(r) + k_3\rho^2(\|z\|)r + k_4|\hat{W}_d|sgn(r), \quad (3\text{-}11)$$

where $k_1, k_2, k_3, k_4 \in \mathbb{R}_{>0}$ are control gains, $sgn(\cdot) : \mathbb{R} \to [-1,1]$ is the signum function, and $\hat{W}_d : \in \mathbb{R}_{\geq t_0} \to \mathbb{R}$ is the repetitive control law designed as

$$\hat{W}_d(t) = sat_{\beta_r}(\hat{W}_d(t-T)) + \mu r(t), \quad (3\text{-}12)$$

where $\mu \in \mathbb{R}_{>0}$ is a control gain, and $sat_{\beta_r}(\cdot)$ is defined as

$$sat_{\beta_r}(\Xi) \triangleq \begin{cases} \Xi & \text{for } |\Xi| \leq \beta_r \\ sgn(\Xi)\beta_r & \text{for } |\Xi| > \beta_r \end{cases}, \forall \Xi \in \mathbb{R}.$$

The closed-loop error system is obtained by substituting (3-11) into (3-3) to obtain

$$M\dot{r} = -Vr + \tilde{W}_d + \chi + N_d + \hat{W}_d - B_\sigma(\hat{W}_d + k_1 r + k_2 sgn(r) + k_3 \rho^2(\|z\|)r + k_4|\hat{W}_d|sgn(r)), \quad (3\text{-}13)$$

where $\tilde{W}_d : \mathbb{R}_{\geq t_0} \to \mathbb{R}$ is the learning estimation error defined as $\tilde{W}_d \triangleq W_d - \hat{W}_d$. Based on the periodicity and boundedness of $W_d$, $W_d(t) = sat_{\beta_r}(W_d(t)) = sat_{\beta_r}(W_d(t-T))$. Hence, by exploiting (3-12), the following expression can be developed for $\tilde{W}_d$

$$\tilde{W}_d = sat_{\beta_r}(W_d(t-T)) - sat_{\beta_r}(\hat{W}_d(t-T)) - \mu r(t). \quad (3\text{-}14)$$

### 3.2 Stability Analysis

**Theorem 3.1.** The controller in (3-11) with the repetitive learning law in (3-12), ensures global asymptotic cadence tracking in the sense that

$$\lim_{t\to\infty} \dot{e}(t) = 0, \quad (3\text{-}15)$$

provided the control gains are selected to satisfy the following sufficient conditions

$$\alpha > \frac{1}{2}, \quad \left(k_1 c_b + \frac{\mu}{2}\right) > \frac{1}{2}, \quad k_2 > \frac{\Theta}{c_b}, \quad k_4 > \frac{1 + c_B}{c_b},$$
$$\delta = min\left\{\left(\alpha - \frac{1}{2}\right), \left(k_1 c_b + \frac{\mu}{2} - \frac{1}{2}\right)\right\} > \frac{1}{2k_3 c_b}. \quad (3\text{-}16)$$

*Proof.* Let $V_c : \mathbb{R}^3 \times \mathbb{R}_{\geq t_0} \to \mathbb{R}$ be a positive-definite, continuously differentiable function defined as

$$V_c \triangleq \frac{1}{2}e^2 + \frac{1}{2}Mr^2 + \frac{1}{2\mu}\int_{t-T}^{t} (sat_{\beta_r}(W_d(\varphi)) - sat_{\beta_r}(\hat{W}_d(\varphi)))^2 d\varphi. \quad (3\text{-}17)$$

The function in (3-17) satisfies the following inequalities:

$$\lambda_1\|y\|^2 \leq V_c(y,t) \leq \lambda_2\|y\|^2, \tag{3-18}$$

where $\lambda_1 \triangleq min(\frac{1}{2}, \frac{c_m}{2}, \frac{1}{2\mu})$, $\lambda_2 \triangleq max(\frac{1}{2}, \frac{c_M}{2}, \frac{1}{2\mu})$ and $y \triangleq [z^T \ \sqrt{Q_L}]^T$ where $Q_L \triangleq \int_{t-T}^{t}(sat_{\beta_r}(W_d(\varphi)) - sat_{\beta_r}(\hat{W}_d(\varphi)))^2 d\varphi$. Let $y(t)$ be a Filippov solution to the differential inclusion $\dot{y} \in K[h](y)$, where $K[\cdot]$ is defined as [85], and $h$ is defined by using (3-2) and (3-13) as $h \triangleq [h_1 \ \ h_2 \ \ h_3]$, where

$$\begin{aligned}
h_1 &\triangleq r - \alpha e \\
h_2 &\triangleq M^{-1}\{-Vr + \tilde{W}_d + \chi + N_d - B_\sigma(k_1 r + k_2 sgn(r) \\
&\quad + \hat{W}_d + k_3\rho^2(\|z\|)r + k_4|\hat{W}_d|sgn(r)) + \hat{W}_d\} \\
h_3 &\triangleq \frac{1}{2\sqrt{Q_L}}\{(sat_{\beta_r}(W_d(t)) - sat_{\beta_r}(\hat{W}_d(t)))^2 \\
&\quad -(sat_{\beta_r}(W_d(t-T)) - sat_{\beta_r}(\hat{W}_d(t-T)))^2\}.
\end{aligned}$$

The control input in (3-11) has the signum function and the discontinuous lumped control effectiveness $B_\sigma$; hence, the time derivative of (3-17) exists almost everywhere (a.e.), i.e., for almost all $t$. Based on [78, Lemma 1], $\dot{V}_c(y(t),t) \overset{a.e.}{\in} \dot{\tilde{V}}_c(y(t),t)$, where $\dot{\tilde{V}}_c$ is the generalized time derivative of (3-17) along the Filippov trajectories of $\dot{y} = h(y)$ defined as in [78] as

$$\dot{\tilde{V}}_c \triangleq \bigcap_{\xi \in \partial V_c} \xi^T K \begin{bmatrix} \dot{e} \\ \dot{r} \\ \frac{\dot{Q}_L}{2\sqrt{Q_L}} \\ 1 \end{bmatrix} (e,\ r,\ 2\sqrt{Q_L},\ t),$$

where $\partial V_c(y,t)$ is the generalized gradient of $V$ at $(y,t)$ defined as $\partial V_c(y,t) = \overline{\text{co}}\{\lim \nabla V_c(y,t) | (y_i,t_i) \rightarrow (y,t), (y_i,t_i) \notin \Omega_{V_c}\}$, where $\Omega_{V_c}$ is the set of measure zero where the gradient of $V_c$ is not defined and $\overline{\text{co}}$ denotes convex closure [78, 86]. Since $V_c(y,t)$ is continuously differentiable in $y$,

$$\dot{\tilde{V}}_c \overset{a.e.}{\subset} [e,\ Mr,\ \left(\frac{1}{2\mu}\right) 2\sqrt{Q_L},\ \frac{1}{2}\dot{M}r^2]K \begin{bmatrix} \dot{e} \\ \dot{r} \\ \frac{\dot{Q}_L}{2\sqrt{Q_L}} \\ 1 \end{bmatrix}.$$

Therefore, after substituting for (3-2) and (3-13), and using Property 9, the generalized time derivative of (3-17) can be expressed as

$$\begin{aligned} \dot{\tilde{V}}_c \overset{a.e.}{\subset} & -\alpha e^2 + er + r(\tilde{W}_d + \hat{W}_d + \chi + N_d - K[B_\sigma]k_1 r - K[B_\sigma sgn(r)]k_2 - K[B_\sigma]\hat{W}_d \\ & -K[B_\sigma]k_3\rho^2(\|z\|)r - K[B_\sigma sgn(r)]k_4|\hat{W}_d|) - \frac{1}{2\mu}(sat_{\beta_r}(W_d(t-T)) \\ & -sat_{\beta_r}(\hat{W}_d(t-T)))^2 + \frac{1}{2\mu}(sat_{\beta_r}(W_d(t)) - sat_{\beta_r}(\hat{W}_d(t)))^2, \end{aligned} \tag{3-19}$$

where

$$\begin{aligned} K[sgn(r)] &= SGN(r), \\ K[B_\sigma] &\subset [c_b, c_B]. \end{aligned} \tag{3-20}$$

Substituting for (3-7), (3-8), and (3-14), using Property 10, and applying Young's inequality, the expression in (3-19) can be upper bounded as

$$\begin{aligned} \dot{\tilde{V}}_c \overset{a.e.}{\leq} & -\left(\alpha - \frac{1}{2}\right)e^2 - \left(k_1 c_b - \frac{1}{2}\right)r^2 - (k_2 c_b - \Theta)|r| - (k_4 c_b - 1 - c_B)|\hat{W}_d||r| \\ & +\tilde{W}_d r + \left[\rho(\|z\|)\|z\||r| - k_3 c_b \rho^2(\|z\|)|r|^2\right] - \frac{1}{2\mu}(\tilde{W}_d + \mu r)^2 \\ & +\frac{1}{2\mu}(sat_{\beta_r}(W_d(t)) - sat_{\beta_r}(\hat{W}_d(t)))^2. \end{aligned} \tag{3-21}$$

By completing the squares for the term in the bracket in (3-21), employing the property described in [44, Appendix I], and canceling terms, (3-21) can be rewritten as

$$\dot{\tilde{V}}_c \overset{a.e.}{\leq} -\left(\alpha - \frac{1}{2}\right) e^2 - \left(k_1 c_b + \frac{1}{2}\mu - \frac{1}{2}\right) r^2 + \frac{\|z\|^2}{4k_3 c_b} - \left(k_2 c_b - \Theta\right) |r| - \left(k_4 c_b - 1 - c_B\right) |\hat{W}_d||r|. \tag{3-22}$$

Provided the gain conditions in (3-16) are satisfied, the inequality in (3-22) can be further upper bounded as

$$\dot{\tilde{V}}_c \overset{a.e.}{\leq} -\left(\frac{\delta}{2} - \frac{1}{4k_3 c_b}\right) \|z\|^2 - \frac{\delta}{2}\|z\|^2.$$

By invoking [78, Corollary 2] $|e|, |r| \to 0$ as $t \to \infty$. Since $V_c > 0$ and $\dot{V}_c \overset{a.e.}{\leq} 0$, $V_c \in \mathcal{L}_\infty$. Hence, $e, r, Q_L \in \mathcal{L}_\infty$, which implies that $y \in \mathcal{L}_\infty$. From (3-12), $r \in \mathcal{L}_\infty$ implies that $\hat{W}_d \in \mathcal{L}_\infty$, which along with the fact that $W_d \in \mathcal{L}_\infty$ from (3-10) implies that $\tilde{W}_d \in \mathcal{L}_\infty$. From the fact that $e, r \in \mathcal{L}_\infty$ and $\hat{W}_d \in \mathcal{L}_\infty$ then $\nu \in \mathcal{L}_\infty$. Since $e, r \in \mathcal{L}_\infty$, then $\dot{e} \in \mathcal{L}_\infty$ from (3-2), and hence, $q, \dot{q} \in \mathcal{L}_\infty$ which implies $\ddot{q} \in \mathcal{L}_\infty$ from (2-12). □

## 3.3 Experiments

Experiments are provided to demonstrate the performance of the controller developed in (3-11) with (learning ON trial) and without (learning OFF trial) the learning feedforward control term $\hat{W}_d$ in (3-12). The switching control input was commanded as stimulation intensities to activate a total of six lower-limb muscle groups and as current to the electric motor.

### 3.3.1 Participants

Five able-bodied individuals (three male, two female) with ages ranging between 21 and 25 years participated in the FES-cycling protocol at the University of Florida. Three male individuals with NCs participated in the study at Brooks Rehabilitation in Jacksonville, FL. Demographics of the Brooks Rehabilitation participants are listed in Table 3-1. Prior to participation, written informed consent was obtained from all participants,

as approved by the Institutional Review Board at the University of Florida. The neurologically impaired individuals were medically stable, and a group of physical therapists was present during the study to monitor vital signs and provide assistance to the participants as needed. The participants with NCs self-reported their motor function and mobility status. Both able-bodied and neurologically impaired individuals were instructed and reminded through the experiments to avoid voluntarily contributing to the pedaling task. Able-bodied individuals were not informed of the desired trajectory and could not see the desired or actual trajectory. The neurologically impaired individuals were informed of the cycling cadence objective, but no feedback regarding the performance was provided throughout the experiments. Participant A exhibited a right side motor impairment, sensory deficit, and aphasia (language disorder). Participant A had good muscle tone and experience with strength training exercise, but not with FES-cycling. Participant B exhibited a left side impairment, was a part-time wheelchair user, and had previous experience with FES-cycling. Participant C is a quadriplegic due to a suffered spinal cord injury [lesion level C3 incomplete, American Spinal Injury Association (ASIA) Impairment Scale Grade A] with a limited range of motion for his left leg. Participant C had previous experience with FES-induced cycling. Participants A and B had reduced or disturbed sensitivity to electrical stimulation in the affected side. Despite the one-sided impairment demonstrated by the neurologically impaired participants, electrical stimulation was delivered to both lower extremities.

Table 3-1. Demographics of participants with a neurological condition.

| Participant | Age | Sex | Injury | Months Since Injury |
|---|---|---|---|---|
| A | 58 | M | Hemorrhagic Stroke | 60 |
| B | 56 | M | Ischemic Stroke | 16 |
| C | 32 | M | SCI C3 | 18 |

### 3.3.2 Experimental Setup

Testing was performed using a recumbent tricycle (TerraTrike Rover) mounted on an indoor trainer and adapted with orthotic boots, which constrained the rider's ankle to maintain the sagittal alignment of the lower legs. A brushed 24 VDC electric motor was mounted to the frame and coupled to the drive chain. An optical encoder (US Digital) was coupled to the cycle crank to measure the crank position. The controller was implemented on a personal computer (Windows 10 OS) running a real-time target (QUARC 2.5, Quanser) via MATLAB/Simulink 2015b (MathWorks Inc) with a sample rate of 500 Hz. The Quanser Q8-USB data acquisition board was used to read the encoder signal and to interface with an analog motor driver and a filter card (Advanced Motion Controls)[2] that commanded the current control to the electric motor. A current-controlled 8-channel stimulator (RehaStim, Hasomed GmbH) operating in Science Mode delivered biphasic, symmetric, rectangular pulses to the participant's muscle groups: quadriceps, hamstrings, and gluteal muscle groups[3] . Self-adhesive PALS® electrodes (3" by 5")[4] were placed on each muscle group in both extremities. The stimulation current amplitude was fixed at 90 mA for the quadriceps, 80 mA for the hamstrings, and 70 mA for the gluteal muscle groups. All able-bodied individuals and participants with NCs received the same current amplitudes across the lower-limb muscle groups.. The stimulation frequency was fixed at 60 Hz for all trials, and the pulsewidth was determined by $u_m$ in (2-11) and commanded to the stimulator. Figure 3-1 illustrates

[2] The servo drive and filter card were provided in part by the sponsorship of Advanced Motion Controls.

[3] All the healthy and neurologically impaired participants, except Participant C, were stimulated over all the six muscle groups. Participant C was stimulated only over his quadriceps and hamstrings due to time constraints and practical reasons.

[4] Surface electrodes for the study were provided compliments of Axelgaard Manufacturing Co., Ltd.

the motorized cycling test bed. As safety measures, participants had access to an emergency stop button and software stop conditions were implemented to limit the amount of motor current and stimulation intensity.

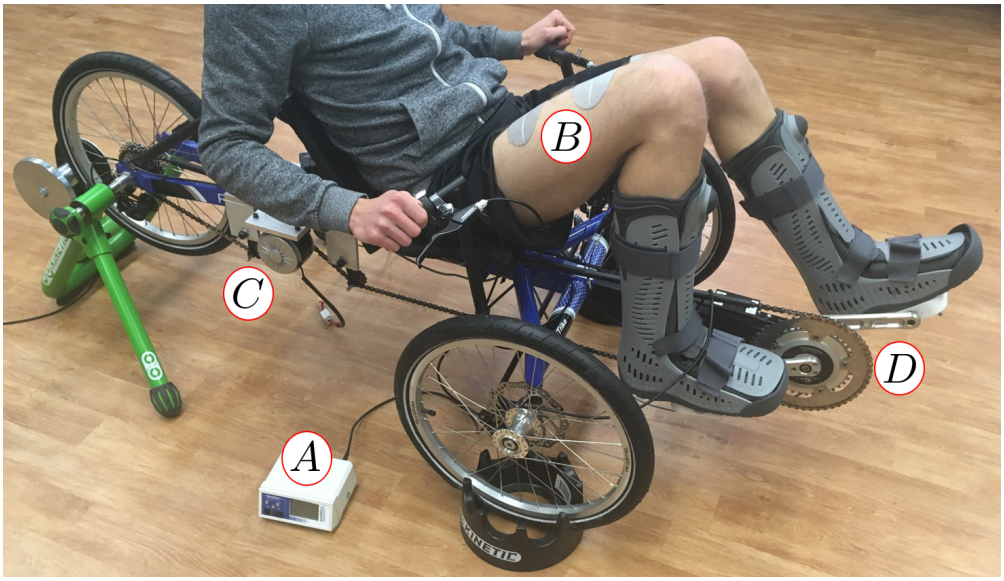


Figure 3-1. Motorized FES-cycling test bed. A) Current-controlled Rehastim stimulator. B) A pair of PALS electrodes. C) Brushed DC motor. D) Cycle crank fitted with sensors. Photo courtesy of the author.

Electrodes were placed over the participant's muscle groups according to the electrode's manufacturer manual[5] . Initial measurements of the participant's lower extremities were recorded to obtain necessary anatomical lengths using visible landmarks as in [12]. Participants were then seated on the tricycle, their feet were properly placed into the orthotic pedals, and necessary seat adjustments were made to prevent knee hyper-extension. The distance from the surface level to the greater trochanter and the distance from the greater trochanter to the cycle crank were measured. These measurements were used to calculate the torque transfer ratios $T_m$, and hence, to determine the stimulation pattern (i.e., regions of the crank cycle where the muscle groups were electrically stimulated).

[5] http://www.palsclinicalsupport.com/videoElements/videoPage.php

For the participants with NCs, trials where the electric motor was active at low speeds were conducted to familiarize the participants with the cadence. Afterwards, low intensity open loop stimulation trains were delivered to the targeted muscle groups to assess the level of response to electrical stimulation. Cadence tracking experiments were conducted for a duration $t_d$ between 2-5 minutes, $t_d \in [120, 300]$ seconds. All able-bodied individuals were able to cycle for 5 minutes. The desired cadence trajectory $\dot{q}_d$ smoothly approached a steady state value of 50 revolutions per minute (RPM)[6] during a time interval of 16 seconds, $t \in [0, t_1]$, $t_1 = 16$. During this interval, the switching controller only activated the motor (i.e., $\sigma_e = 1, \forall q \in \mathcal{Q}$). The cadence trajectory remained constant at 50 RPM for a transition time interval of 10 seconds, $t \in [t_1, t_1 + 10]$, where the width of the regions of the crank cycle at which electrical stimulation is delivered (i.e., $q \in \mathcal{Q}_m$) was gradually increased until it reached a steady state value. The width of the stimulation regions is determined by

$$\epsilon_m \triangleq \Lambda_m max(T_m), \forall m \in \mathcal{M} \tag{3-23}$$

where $\Lambda_m \in \mathbb{R}$ is a positive threshold designed as

$$\Lambda_m \triangleq \begin{cases} 1.4 - \frac{t}{40} & \text{if } t_1 \leq t < t_1 + 10 \\ 0.75 & \text{if } t \geq t_1 + 10 \end{cases}, \forall m \in \mathcal{M}. \tag{3-24}$$

Both (3-23) and (3-24) define how the switching controller gradually incorporates the activation of the lower limb muscles during the experiments. This implies that the stimulation regions (i.e., regions where $\sigma_m = 1$, $q \in \mathcal{Q}_m$) grow based on whether the transfer ratios $T_m \, \forall m \in \mathcal{M}$ at every crank angle are greater than the current value of $\epsilon_m, \forall m \in \mathcal{M}$ defined in (3-23). After the transition phase of 10 seconds, the stimulation

[6] For Participant C the desired cadence trajectory $\dot{q}_d$ approached a steady value of 40 RPM due to participant comfort.

regions reach a steady constant stimulation pattern (i.e., regions where $T_m$ is greater than the 75% of the maximum value of $T_m$). This mechanism to smoothly integrate electrical stimulation to the switching controller was selected because large muscle forces are needed to enable forward pedaling from rest until enough momentum has been achieved in the system. Then, the desired crank velocity $\dot{q}_d$ was designed to be a periodic function of time with an amplitude of $50 \pm 5$ RPM and a period of $T = 12$ seconds until the end of experiment, $t \in [t_1 + 10, t_d]$. This last section of the experiment where the cadence trajectory is periodic is called the steady state.

To compare the tracking performance of the RLC, two trials were developed for each enrolled participant. One trial implemented the control input designed in (3-11) with the learning feedforward term $\hat{W}_d$ in (3-12) (learning ON trial). For the other trial, $\hat{W}_d = 0$, which resulted in a control input only containing the middle three terms of $\nu$ in (3-11) (learning OFF trial). Based on the limited availability of the participants for multiple FES-cycling sessions, especially for the population with a neurological condition, both trials were completed in the same session. However, rest breaks were given between trials to avoid fatiguing the participant. The order of the two trials was randomized for each participant.

Figure 3-2 provides an example of the switching control inputs for both the muscle stimulation intensities and the motor current distributed over a single crank cycle. The control gains introduced in (2-11), (3-2), (3-11), and (3-12) were tuned to achieve appropriate tracking performance during preliminary testing and are defined as follows: $k_m \in [0.35, 0.6]$, $k_e \triangleq 1$, $\alpha \in [2, 3]$, $k_{1,m} \in [70, 265]$, $k_{2,m} \in [5, 7.5]$, $k_{3,m} = k_{4,m} \triangleq 0.001$, $k_{1,e} \triangleq 9$, $k_{2,e} \triangleq 4$, $k_{3,e} \triangleq 0.0009$, $k_{4,e} \triangleq 0.009$, and $\mu \in [2, 32]$, where the notation $k_{\psi,\varpi}$ is used to represent the gains used for the motor control input $u_e$ and the electrical stimulation inputs $u_m$ defined in (2-11), where $\psi \in \{1, 2, 3, 4\}$, $\varpi \in \{m, e\}$, the subscript $m$ denotes the muscle groups, and the subscript $e$ the electric motor. All the control gains were the same between the learning ON and OFF trials. However in some

OFF trials, $k_{1,m}$ was increased to achieve similar stimulation intensities for any given participant as for the ON trial.

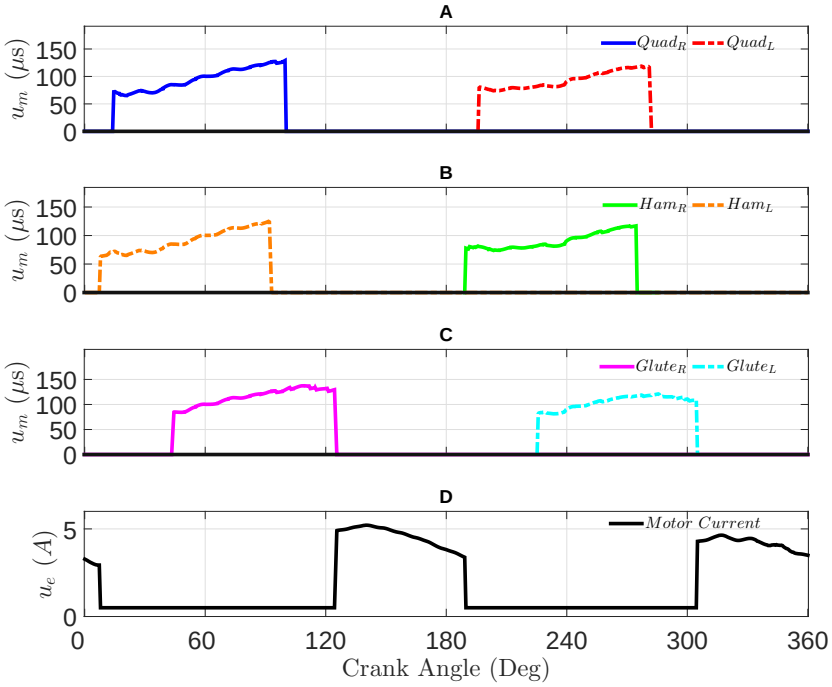


Figure 3-2. FES stimulation intensities and electric motor current input during a single crank cycle illustrating the switching controller in (2-11) with inputs $u_m$ and $u_e$. A) FES stimulation intensities commanded to the quadriceps. B) FES stimulation intensities commanded to the hamstrings. C) FES stimulation intensities commanded to the gluteal muscles. D) Motor current input commanded to the electric motor.

## 3.4 Results

The FES-cycling protocol with the two trials (learning ON and OFF) was completed by all the participants. Table 3-2 summarizes the cadence RMS error, the average of the cadence error $\dot{e}$, and percent error (% error) for the able-bodied individuals (S1-S5) and the participants with NCs (A-B) during steady state, $t \in [t_1 + 10, t_d]$ seconds, for both trials. The RMS error was calculated over moving time interval windows of 1.2 and 12 seconds (corresponding to the period of the desired trajectory). Figure 3-3 shows the cadence tracking performance of Participant S5, a typical result, for the learning ON trial, quantified by the RMS error and the instantaneous error $\dot{e}$. Figure 3-4 illustrates the

stimulation intensities $u_m$ delivered to the muscle groups, the electric motor current input $u_e$, and the learning feedforward term $\hat{W}_d$ for Participant S5 for the learning ON trial.

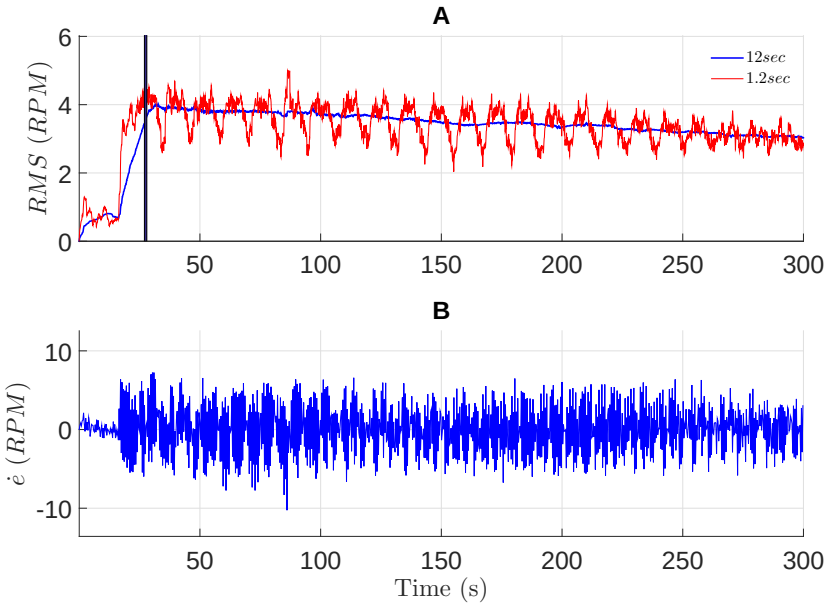


Figure 3-3. Tracking performance for Participant S5 during the learning ON trial. A) Cadence RMS error for two moving time interval windows. The vertical solid bar corresponds to the time when the learning is turned ON, that is when steady state is reached during the trial. B) Cadence instantaneous error $\dot{e}$. Instantaneous cadence is plotted by down sampling to 0.3 seconds.

Figure 3-5 shows the tracking performance of Participant S5 for the learning OFF trial. As an example of the tracking of the participants with NCs, Figure 3-6 shows the tracking performance of Participant A during the learning ON trial. Figure 3-7 illustrates the muscle stimulation intensities, the motor current input, the cadence tracking errors (RMS and $\dot{e}$), and the learning-based feedforward term $\hat{W}_d$ during several consecutive crank cycles at the beginning of the ON trial and then 100 crank cycles later for Participant S2. A Wilcoxon signed ranked test was performed at a significance level of $\alpha = 0.05$ to test for statistically significant differences between the RMS cadence tracking error between trials (learning ON versus learning OFF) for all participants ($N = 8$). The learning ON trial yielded a lower RMS cadence error than the learning OFF trial ($p - value = 0.0156$) with median values of 3.61 and 4.20, respectively.

Table 3-2. Cadence tracking results: RMS error (moving window of 1.2 s), average of the cadence error $\dot{e}$, and % error reported as mean $\pm$standard deviation (STD) during the steady state of the experiment for both trials with learning (ON column) and without learning (OFF column). STD* reports the mean over the standard deviations.

| Participant | RMS Error (RPM) | | $\dot{e}$ (RPM) | | % Error | |
|---|---|---|---|---|---|---|
| | ON | OFF | ON | OFF | ON | OFF |
| S1 | 3.31$\pm$0.53 | 3.94$\pm$0.56 | 0.04$\pm$3.34 | 0.03$\pm$3.98 | 0.03$\pm$6.82 | 0.05$\pm$8.07 |
| S2 | 3.61$\pm$0.42 | 4.20$\pm$0.51 | 0.03$\pm$3.61 | 0.01$\pm$4.23 | 0.06$\pm$7.35 | 0.05$\pm$8.56 |
| S3 | 4.16$\pm$0.64 | 4.70$\pm$0.77 | 0.02$\pm$4.16 | 0.05$\pm$4.76 | 0.06$\pm$8.59 | 0.17$\pm$9.70 |
| S4 | 3.85$\pm$0.41 | 4.33$\pm$0.55 | 0.03$\pm$3.85 | 0.02$\pm$4.36 | 0.05$\pm$7.85 | 0.04$\pm$8.86 |
| S5 | 3.45$\pm$0.49 | 3.81$\pm$0.39 | 0.03$\pm$3.47 | 0.01$\pm$3.83 | 0.03$\pm$7.09 | 0.02$\pm$7.78 |
| Mean (S1-S5) | 3.68 | 4.20 | 0.03 | 0.02 | 0.05 | 0.07 |
| STD* (S1-S5) | 0.51 | 0.57 | 3.70 | 4.24 | 7.57 | 8.62 |
| A | 2.14$\pm$0.45 | 2.85$\pm$0.40 | 0.01$\pm$2.19 | 0.01$\pm$2.92 | 0.02$\pm$4.33 | 0.02$\pm$5.82 |
| B | 4.21$\pm$1.04 | 4.26$\pm$1.21 | 0.09$\pm$4.21 | 0.35$\pm$4.31 | 0.17$\pm$8.73 | 0.55$\pm$8.82 |
| C | 3.15$\pm$0.63 | 3.37$\pm$0.72 | 0.02$\pm$3.23 | 0.01$\pm$3.42 | 0.00$\pm$8.06 | 0.11$\pm$8.72 |
| Mean (A-C) | 3.17 | 3.49 | 0.04 | 0.12 | 0.06 | 0.23 |
| STD* (A-C) | 0.75 | 0.85 | 3.31 | 3.60 | 7.30 | 7.91 |
| Combined Mean | 3.68 | 4.09 | 0.03 | 0.06 | 0.05 | 0.12 |
| Combined STD* | 0.58 | 0.64 | 3.56 | 4.01 | 7.35 | 8.29 |

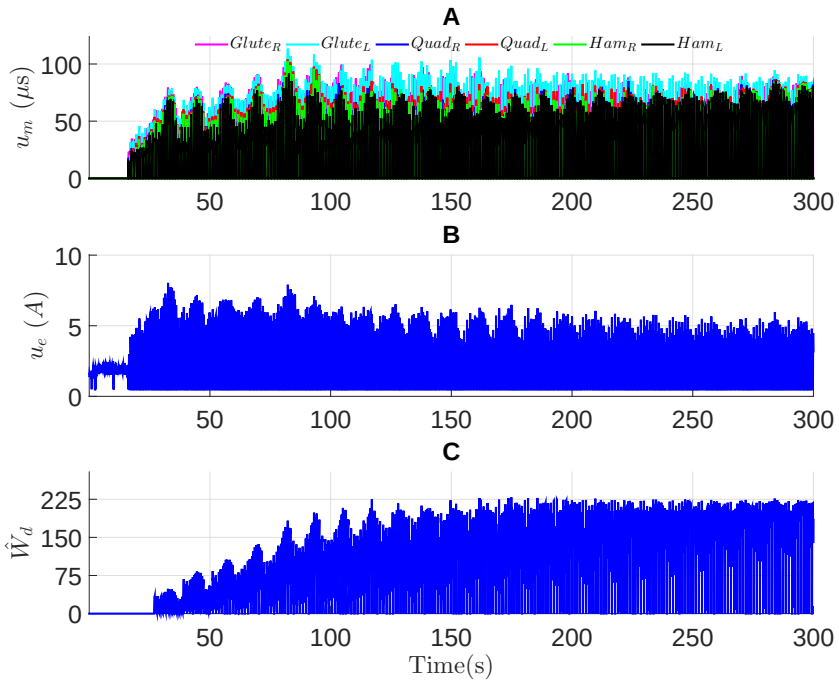


Figure 3-4. Control inputs for Participant S5 during the learning ON trial. A) Stimulation intensities $u_m$ for each muscle group. B) Electric motor current input $u_e$. C) Learning feedforward term $\hat{W}_d$.

## 3.5 Discussion

The experimental results demonstrate the feasibility of the controller in (3-11) to track a desired cadence with the combined contribution of FES activation of the lower limb muscles and motor assistance. The inclusion of the learning based feedforward term designed in (3-12) during the ON trial resulted in lower RMS cadence error and instantaneous tracking error $\dot{e}$ compared to the OFF trial, where the learning term was neglected for both able-bodied individuals and participants with NCs. The mean instantaneous cadence tracking error is $0.03 \pm 3.70$ RPM for the ON trial and $0.02 \pm 4.24$ RPM for the OFF trial across all healthy individuals. For people with NCs, the mean instantaneous cadence tracking error is $0.04 \pm 3.31$ RPM for the ON trial and $0.12 \pm 3.60$ RPM for the OFF trial.

Implementation of the RLC offers the advantage of adding a feedforward term to the control input by exploiting the system's periodic desired trajectories rather than

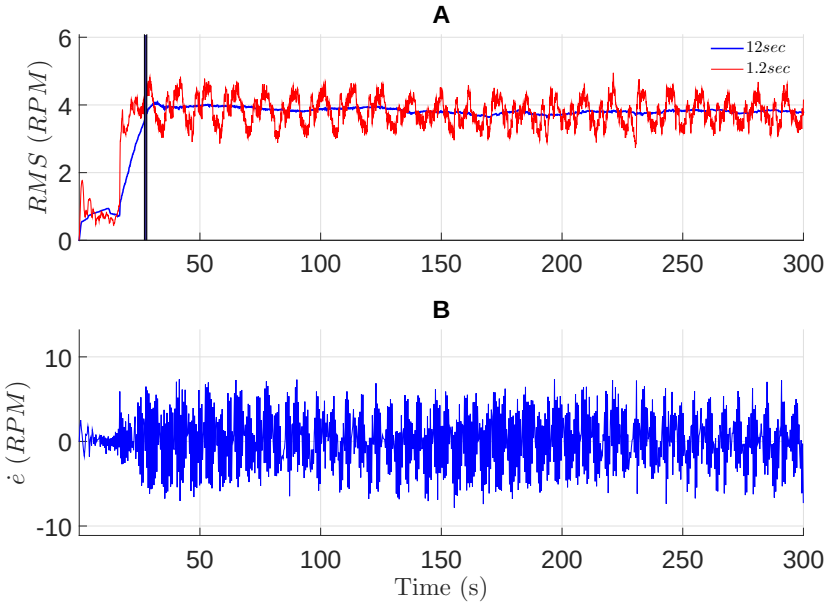


Figure 3-5. Tracking performance for Participant S5 during the learning OFF trial. A) Cadence RMS error for two moving time interval windows. The vertical solid bar corresponds to the time when the learning should have been turned ON, that is when steady state is reached during the trial. B) Cadence instantaneous error $\dot{e}$. Instantaneous cadence is plotted by down sampling to 0.3 seconds.

using a model-based control, such as in classical adaptive control where a regression matrix has to be known. In other words, the RLC is added to a robust controller aiming to improve the tracking performance as shown in Section 3.4.

Despite the fact that the stability analysis yields an asymptotic tracking result, there are factors in the experiment that could affect the steady-state tracking error, such as the inherent electromechanical delay that occurs between the input being delivered to the muscle and actual force production [87] or the effect of non-periodic disturbances such as muscle fatigue. Additional challenges were encountered while conducting experiments with participants possessing NCs such as observed intermittent muscle spasms, asymmetries between the lower extremities, and potential electrical stimulation sensitivity from residual sensory feedback. These challenges resulted in shorter experiment durations (e.g., $t_d < 300$ seconds) for the participants with NCs

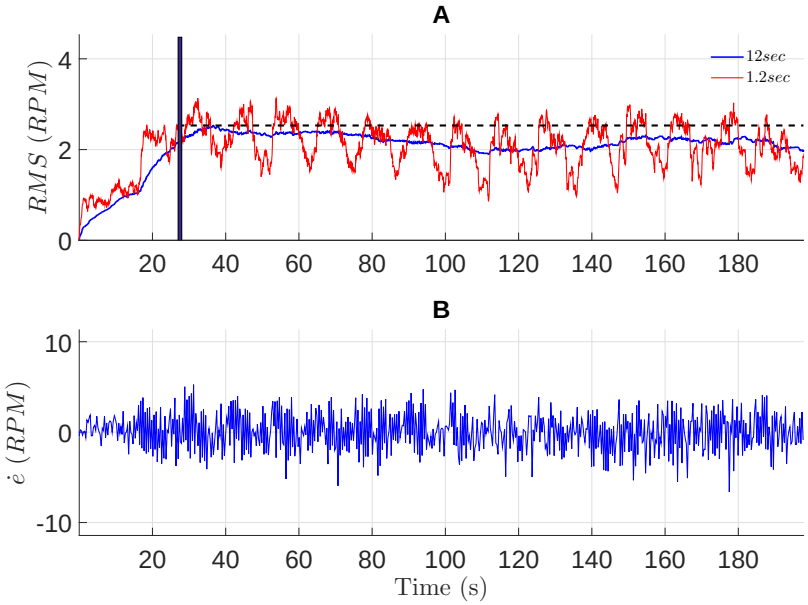


Figure 3-6. Tracking performance for Participant A during the learning ON trial. A) Cadence RMS error for two moving time interval windows. The vertical solid bar corresponds to the time when the learning is turned ON, that is when steady state is reached during the trial. The dashed black line depicts the maximum RMS error for the moving 12 seconds window. B) Cadence instantaneous error $\dot{e}$. Instantaneous cadence is plotted by down sampling to 0.3 seconds.

as compared to able-bodied individuals. Although Participants A and B had residual motor control on their affected side and full motor control in their contralateral side, no voluntary contribution to the pedaling task was provided (monitored by the consistent non-vanishing stimulation intensities delivered throughout the experiment) to compare their tracking performance with Participant C, who had no neurological motor control. The results reported in Table 3-2 are representative of typical performance during FES-cycling tasks.

The results show that by switching the control effort between muscle activation via FES and the electric motor, the participants with NCs were capable of producing smooth cadence without any voluntary contribution. This relevant observation demonstrates the efficacy of the control technique, since it has been reported that the intact leg of participants with hemiparesis provides enough muscle force without FES (i.e., voluntary

contribution only) to complete the pedaling task and to compensate for the affected leg [88, 89]. However, this inherent compensation by the healthy leg diminishes the potential FES benefits during cycling. Moreover in [88], 90% of the stroke participants were unable to increase crank contribution when receiving open-loop stimulation on their affected limb. In [89], a post-training voluntary pedaling test was conducted where FES was also delivered open-loop to both the affected and intact lower-limbs of participants with postacute hemiparesis which showed improved motion symmetry and activation timing of the impaired muscles. For spinal cord injured populations, power output, metabolic rate, and muscle strength increased after FES-cycling training using fixed stimulation parameters [90]. Clinical trials with larger neurologically impaired populations are required to investigate the impact of the control method developed in the present study. Ultimately, a cycling protocol that adopts closed-loop FES and learning control for the affected limb and motivates voluntary intent for the intact limb while using a split crank cycle may result in a more suitable rehabilitation approach for people with stroke.

### 3.6 Concluding Remarks

A switched controller with a learning based feedforward term was designed to activate the lower limb muscles and an electric motor to yield asymptotic cadence tracking. The switching signal commands stimulation intensities to the muscle groups when they can contribute efficiently to the pedaling task and activates the electric motor in regions of the crank cycle where muscles have low torque efficiency. The developed controller compensates for periodic dynamics (based on the desired periodic reference trajectory) using a repetitive learning feedforward term combined with robust feedback terms. Global asymptotic tracking is achieved with the aid of a corollary to the LaSalle-Yoshizawa theorem for nonsmooth systems in [78].

The RLC was successfully tested in experiments conducted on five able-bodied individuals and three participants with NCs. The added value of the RLC (e.g., against a pure robust controller) for cadence tracking was illustrated by comparing the tracking

performance during two trials with and without learning (ON and OFF trials respectively). For the healthy control group, a mean RMS cadence error of $3.68 \pm 0.51$ RPM $(0.05 \pm$7.57% error$)$ was obtained for the ON trial compared to the RMS cadence error of $4.20 \pm 0.57$ RPM ($0.07 \pm$8.62% error) for the OFF trial. For the patient population, a mean RMS cadence error of $3.17 \pm 0.75$ RPM ($0.06 \pm 7.30\%$ error) was obtained for the ON trial compared to the RMS cadence error of $3.49 \pm 0.85$ RPM ($0.23 \pm 7.91\%$ error) for the OFF trial. The results on the participants with NCs demonstrate the ability to yield repetitive cycling despite lower-limb motion asymmetries, sensitivity to electrical stimulation, constrained range of motion, and lack of neurological motor control.

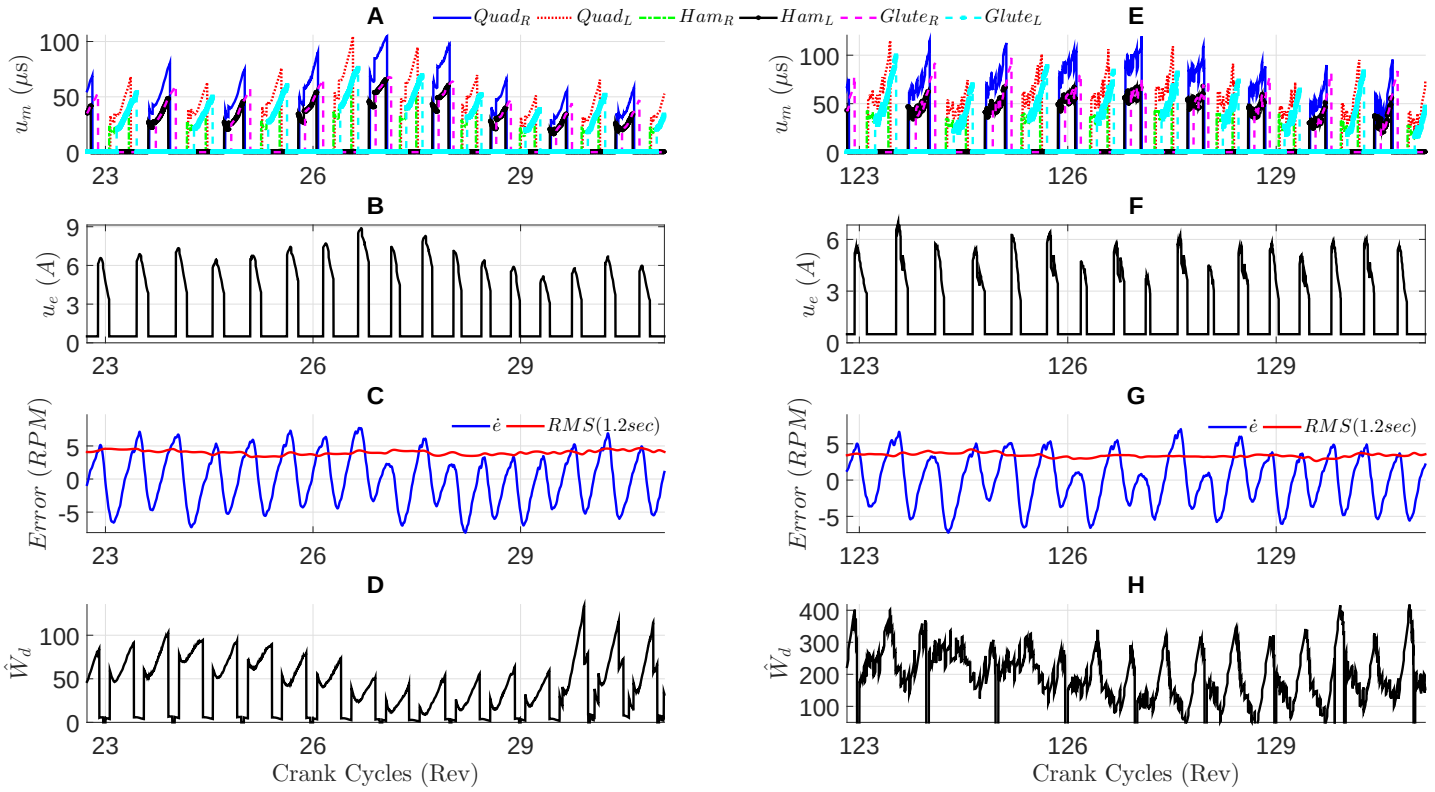


Figure 3-7. Control inputs and cadence performance during the ON trial for Participant S2. A) FES control inputs during the beginning of the trial. B) Motor current input during the beginning of the trial. C) Cadence tracking error (RMS and instantaneous error) during the beginning of the trial. D) Learning-based feedforward term $\hat{W}_d$ during the beginning of the trial. E) FES control inputs 100 crank cycles later in the same trial. F) Motor current input 100 crank cycles later in the same trial. G) Cadence tracking error (RMS and instantaneous error $\dot{e}$) 100 crank cycles later in the same trial. H) Learning-based feedforward term $\hat{W}_d$ 100 crank cycles later in the same trial.

# CHAPTER 4
# DISTRIBUTED REPETITIVE LEARNING CONTROL FOR COOPERATIVE CADENCE TRACKING IN FUNCTIONAL ELECTRICAL STIMULATION CYCLING

In this chapter, a switched controller with distributed RLC (i.e., an independent learning feedforward input is designed for each actuator) is developed to achieve cadence tracking through the cooperation of lower-limb muscles and an electric motor coupled to the cycle. The distributed feedforward learning terms compensate for the periodic dynamics based on the desired cadence tracking trajectory. The switched controller is designed using a nonlinear cycle-rider dynamic model and it is implemented without the requirement of any identification procedure despite the parametric uncertainty present in the system. The robust feedback terms aid in the rejection of disturbances present in the cycle and in the lower-limbs of the rider. Due to the construction of a filtered tracking error, the distributed RLC affects both cadence and position tracking. Global asymptotic tracking is achieved via a Lyapunov-based stability analysis using a common Lyapunov function that accounts for the periodicity of the system, and by invoking a corollary to the LaSalle-Yoshizawa theorem for nonsmooth systems [78, Corollary 2]. Experimental results are reported for seven able-bodied individuals and five participants with different NCs during a 3 minute cycling protocol.

## 4.1 Switched Dynamics and Inputs

In this chapter, the stimulation intensities delivered to the muscle groups and the motor input are defined as

$$u_m(t) \triangleq k_m \sigma_m(q) \left( \nu(t) + \hat{W}_{d,m}(t) \right), \tag{4-1}$$

$$u_e(t) \triangleq k_e \sigma_e(q) \left( \nu(t) + \hat{W}_{d,e}(t) \right), \tag{4-2}$$

respectively, where $k_m, k_e \in \mathbb{R}_{>0}$, $\forall m \in \mathcal{M}$ are positive, constant control gains, $\nu : \mathbb{R}_{\geq t_0} \to \mathbb{R}$ is a subsequently designed control input, and $\hat{W}_{d,m}, \hat{W}_{d,e} : \mathbb{R}_{\geq t_0} \to \mathbb{R}$, $\forall m \in \mathcal{M}$ are the repetitive learning control laws designed for each muscle and the electric motor,

respectively. Substituting (2-6), (2-7), (4-1), and (4-2) into (2-1) and rearranging terms yields

$$M(q)\ddot{q} + V(q,\dot{q})\dot{q} + G(q) + P(q,\dot{q}) + c_d\dot{q} + d = B_\sigma\left(\nu + \hat{W}_d\right), \tag{4-3}$$

where $B_\sigma \in \mathbb{R}_{\geq 0}$ is the lumped switched control effectiveness term defined in 2-13 and $\hat{W}_d : \mathbb{R}_{\geq t_0} \to \mathbb{R}$ is the lumped feedforward learning term.

### 4.2 Control Development

The objective is to design a controller to track a desired crank cadence. A measurable auxiliary tracking error, denoted by $e_1 : \mathbb{R}_{\geq t_0} \to \mathbb{R}$ is defined as[1]

$$e_1 \triangleq \int_{t_0}^{t} \left(q_d(\varphi) - q(\varphi)\right) d\varphi, \tag{4-4}$$

where $q_d : \mathbb{R}_{\geq t_0} \to \mathbb{R}$ denotes the desired crank position, which satisfies Property 11, and its first two time derivatives are bounded such that $|\dot{q}_d(t)| \leq \xi_1$ and $|\ddot{q}_d(t)| \leq \xi_2$, where $\xi_1, \xi_2 \in \mathbb{R}_{>0}$ are known positive constants. To facilitate the subsequent control development, filtered tracking errors $e_2 : \mathbb{R}_{\geq t_0} \to \mathbb{R}$ and $r : \mathbb{R}_{\geq t_0} \to \mathbb{R}$ are defined as

$$e_2 \triangleq \dot{e}_1 + \alpha_1 e_1 \tag{4-5}$$

$$r \triangleq \dot{e}_2 + \alpha_2 e_2 \tag{4-6}$$

where $\alpha_1, \alpha_2 \in \mathbb{R}_{>0}$ are positive, constant control gains. Taking the time derivative of (4-6) and premultiplying by $M$, substituting for (4-3), using the second time derivative of (4-5) and then performing some algebraic manipulation yields

$$M\dot{r} = -Vr + W_d + \chi + N_d - B_\sigma\left(\nu + \hat{W}_d\right) - e_2, \tag{4-7}$$

[1] The control objective is quantified using the second time derivative of $e_1(t)$. Functional dependencies are omitted henceforth, unless they add clarity.

where the auxiliary signals $W_d : \mathbb{R}_{\geq t_0} \to \mathbb{R}$, $\chi : \mathbb{R}_{\geq t_0} \to \mathbb{R}$, and $N_d : \mathbb{R}_{\geq t_0} \to \mathbb{R}$ are defined as

$$W_d \triangleq = \sum_{i \in \mathcal{A}} W_{d,i} = \sum_{i \in \mathcal{A}} \left( M_i(q_d)\ddot{q}_d + V_i(q_d, \dot{q}_d)\dot{q}_d + G_i(q_d) \right), \tag{4-8}$$

$$\begin{aligned} \chi \triangleq\ & M(q)(\ddot{q}_d + (\alpha_1 + \alpha_2)\,\dot{e}_2) + V(q, \dot{q})(\dot{q}_d - \alpha_1^2 e_1 + (\alpha_1 + \alpha_2)\,e_2) \\ & + G(q) + P(q, \dot{q}) + c_d\dot{q} - W_d - N_d + e_2, \end{aligned} \tag{4-9}$$

$$N_d \triangleq c_{P1} + (c_{P2} + c_d)\,\dot{q}_d + d. \tag{4-10}$$

for $i \in \mathcal{A}$, where $\mathcal{A} \triangleq \{\mathcal{M}, \text{Motor}\}$. The auxiliary signal in (4-10) can be upper bounded as

$$N_d \leq \Theta, \tag{4-11}$$

where $\Theta \in \mathbb{R}_{>0}$ is a known positive constant. By using Properties 5-9, (4-5), and (4-6), the Mean Value Theorem can be used to develop an upper bound for (4-9) as

$$\chi \leq \rho(\|z\|)\|z\|, \tag{4-12}$$

where $z : \mathbb{R}_{\geq t_0} \to \mathbb{R}^3$ is a composite vector of error signals defined as

$$z \triangleq \begin{bmatrix} e_1 & e_2 & r \end{bmatrix}^T, \tag{4-13}$$

and $\rho(\cdot) \in \mathbb{R}$ is a known positive, radially unbounded, nondecreasing function. Based on (4-8) and the explicit boundedness of the periodic desired trajectory

$$\|W_d(t)\| \leq \beta_r, \tag{4-14}$$

where $\beta_r \in \mathbb{R}$ is a known positive bounding constant. Given the cadence open-loop error system in (4-7), the control input is designed as

$$\nu \triangleq k_1 r + \left( k_2 + k_3\rho(\|z\|)\|z\| + k_4\|\hat{W}_d\| \right) sgn(r), \tag{4-15}$$

where $k_1, k_2, k_3, k_4 \in \mathbb{R}_{>0}$ are selectable positive gain constants, $sgn(\cdot) : \mathbb{R} \to [-1, 1]$ is the signum function, and $\hat{W}_d : \mathbb{R}_{\geq t_0} \to \mathbb{R}$ is the distributed repetitive learning control law designed as

$$\hat{W}_d(t) \triangleq \sum_{i \in \mathcal{A}} \hat{W}_{d,i}(t) = \sum_{m \in \mathcal{M}} \hat{W}_{d,m} + \hat{W}_{d,e}, \tag{4-16}$$

$$\hat{W}_{d,m} \triangleq \sigma_m \left( sat_{\beta_m} \left( \hat{W}_{d,m}(t - T) \right) + k_{L,m} r \right), \tag{4-17}$$

$$\hat{W}_{d,e} \triangleq \sigma_e \left( sat_{\beta_e} \left( \hat{W}_{d,e}(t - T) \right) + k_{L,e} r \right), \tag{4-18}$$

where $k_{L,i} \in \mathbb{R}_{>0}$, $\forall i \in \mathcal{A}$ are learning control gains, and $sat_{\beta_i}(\cdot)$ is defined as

$$sat_{\beta_i}(\Xi_i) \triangleq \begin{cases} \Xi_i & \text{for } |\Xi_i| \leq \beta_i \\ sgn(\Xi_i)\beta_i & \text{for } |\Xi_i| > \beta_i \end{cases}, \forall i \in \mathcal{A}.$$

The closed-loop error system is obtained by substituting (4-15) into (4-7) which yields

$$\begin{aligned} M\dot{r} &= -Vr + \chi + N_d + \tilde{W}_d + \hat{W}_d - e_2 - B_\sigma(\hat{W}_d + k_1 r \\ &\quad + \left( k_2 + k_3 \rho(\|z\|)\|z\| + k_4 \|\hat{W}_d\| \right) sgn(r)), \end{aligned} \tag{4-19}$$

where $\tilde{W}_d \in \mathbb{R}$ is the learning estimation error defined as $\tilde{W}_d = \sum_{i \in \mathcal{A}} \tilde{W}_{d,i} \triangleq \sum_{i \in \mathcal{A}} \left( W_{d,i} - \hat{W}_{d,i} \right) = W_d - \hat{W}_d$. Based on the periodicity and boundedness of $W_d$, $W_d(t) = \sum_{i \in \mathcal{A}} sat_{\beta_i}(W_{d,i}(t)) = \sum_{i \in \mathcal{A}} sat_{\beta_i}(W_{d,i}(t - T))$. Hence, by exploiting (4-16), the following expression can be developed for $\tilde{W}_d$

$$\begin{aligned} \tilde{W}_d &= \sum_{i \in \mathcal{A}} \tilde{W}_{d,i} \\ &= \sum_{i \in \mathcal{A}} sat_{\beta_i}(W_{d,i}(t - T)) - \sum_{m \in \mathcal{M}} \sigma_m \left( sat_{\beta_m}(\hat{W}_{d,m}(t - T)) + k_{L,m} r \right) \\ &\quad - \sigma_e \left( sat_{\beta_e} \left( \hat{W}_{d,e}(t - T) \right) + k_{L,e} r \right). \end{aligned} \tag{4-20}$$

To incorporate the repetitive learning error term in the subsequent stability analysis, an auxiliary function $Q_L : \mathbb{R}_{\geq t_0} \to \mathbb{R}$ is defined as

$$Q \triangleq \sum_{i \in \mathcal{A}} \frac{1}{2k_{L,i}} \int_{t-T}^{t} (sat_{\beta_i}(W_{d,i}(\varphi)) - sat_{\beta_i}(\hat{W}_{d,i}(\varphi)))^2 d\varphi. \tag{4-21}$$

### 4.3 Stability Analysis

**Theorem 4.1.** *The controller in (4-15) with the repetitive learning law in (4-16) ensures global asymptotic cadence tracking provided the control gains are selected to satisfy the following sufficient conditions*

$$\alpha_1,\ \alpha_2 > \frac{1}{2}, \quad k_2 > \frac{\Theta}{c_b}, \quad k_3 > \frac{1}{c_b}, \quad k_4 > \frac{1 + c_B}{c_b}. \tag{4-22}$$

*Proof.* Let $V_1 : \mathbb{R}^4 \times \mathbb{R}_{\geq t_0} \to \mathbb{R}$ be a nonnegative, continuously differentiable, function defined as

$$V_1 \triangleq \frac{1}{2}e_1^2 + \frac{1}{2}e_2^2 + \frac{1}{2}Mr^2 + Q_L. \tag{4-23}$$

The function in (4-23) satisfies the following inequalities:

$$\lambda_1 \|y\|^2 \leq V_1(y,t) \leq \lambda_2 \|y\|^2,$$

where $\lambda_1 \triangleq min(\frac{1}{2}, \frac{1}{2}c_m, \frac{1}{2k_{L,i}})$, $\lambda_2 \triangleq max(\frac{1}{2}, \frac{1}{2}c_M, \frac{1}{2k_{L,i}})$, $\forall i \in \mathcal{A}$ and $y \triangleq [z^T \ \sqrt{Q_L}]^T$ where $Q_L \triangleq \sum_{i \in \mathcal{A}} \int_{t-T}^{t} (sat_{\beta_i}(W_{d,i}(\varphi)) - sat_{\beta_i}(\hat{W}_{d,i}(\varphi)))^2 d\varphi$. Let $y(t)$ be a Filippov solution to the differential inclusion $\dot{y} \in K[h](y)$, where $K[\cdot]$ is defined as in [85], and $h$ is defined by using (4-5), (4-6) and (4-19) as $h \triangleq [h_1 \ \ h_2 \ \ h_3 \ \ h_4]$, where $h_1 \triangleq e_2 - \alpha_1 e_1$, $h_2 \triangleq r - \alpha_2 e_2$, $h_3 \triangleq M^{-1}\{-Vr + \chi + N_d + \tilde{W}_d + \hat{W}_d - e_2 - B_\sigma(\hat{W}_d + k_1 r + (k_2 + k_3\rho(\|z\|)\|z\| + k_4\|\hat{W}_d\|)sgn(r)\}$, $h_4 \triangleq \frac{1}{2\sqrt{Q_L}} \sum_{i \in \mathcal{A}} \{(sat_{\beta_i}(W_{d,i}(t)) - sat_{\beta_i}(\hat{W}_{d,i}(t)))^2 - (sat_{\beta_i}(W_{d,i}(t-T)) - sat_{\beta_i}(\hat{W}_{d,i}(t-T)))^2\}$. The control input in (4-15) includes the signum function and the discontinuous lumped control effectiveness $B_\sigma$; hence, the

time derivative of (4-23) exists almost everywhere (a.e.), i.e., for almost all $t$. Based on [78, Lemma 1], the time derivative of (4-23), $\dot{V}_1(y(t),t) \overset{a.e.}{\in} \dot{\tilde{V}}_1(y(t),t)$, where $\dot{\tilde{V}}_1$ is the generalized time derivative of (4-23) along the Filippov trajectories of $\dot{y} = h(y)$ is defined as $\dot{\tilde{V}}_1 \triangleq \bigcap_{\xi \in \partial V_1} \xi^T K \left[\dot{e}_1 \; \dot{e}_2 \; \dot{r} \; \frac{\dot{Q}_L}{2\sqrt{Q_L}} \; 1\right]^T (e_1,\, e_2,\, r,\, 2\sqrt{Q_L},\, t)$. Since $V_1(y,t)$ is continuously differentiable in $y$, $\partial V_1 = \{\nabla V_1\}$, thus

$$\dot{\tilde{V}}_1 \overset{a.e.}{\subset} [e_1,\, e_2,\, Mr,\, \sum_{i \in \mathcal{A}} \left(\frac{1}{2k_{L,i}}\right) 2\sqrt{Q_L},\, \frac{1}{2}\dot{M}r^2] K \begin{bmatrix} \dot{e}_1 \\ \dot{e}_2 \\ \dot{r} \\ \frac{\dot{Q}_L}{2\sqrt{Q_L}} \\ 1 \end{bmatrix}.$$

Therefore, after substituting for (4-5), (4-6) and (4-19), and using Property 9, the generalized time derivative of (4-23) can be expressed as

$$\begin{aligned} \dot{\tilde{V}}_1 \overset{a.e.}{\subset}\; & e_1 e_2 - \alpha_1 e_1^2 - \alpha_2 e_2^2 + r\Big(\tilde{W}_d + \hat{W}_d + \chi + N_d + K[B_\sigma]\hat{W}_d - K[B_\sigma]k_1 r \\ & - K[B_\sigma sgn(r)]\left(k_2 + k_3\rho(\|z\|)\|z\| + k_4\|\hat{W}_d\|\right)\Big) \\ & + \sum_{i \in \mathcal{A}} \frac{1}{2k_{L,i}} (sat_{\beta_i}(W_{d,i}(t)) - sat_{\beta_i}(\hat{W}_{d,i}(t)))^2 \\ & - \sum_{i \in \mathcal{A}} \frac{1}{2k_{L,i}} (sat_{\beta_i}(W_{d,i}(t-T)) - sat_{\beta_i}(\hat{W}_{d,i}(t-T)))^2, \end{aligned} \tag{4-24}$$

Substituting for (4-11), (4-12), (4-20), (3-20) and using Property 10 and Young's inequality, an upper bound for (4-24) can be developed as

$$\begin{aligned} \dot{\tilde{V}}_1 \overset{a.e.}{\leq}\; & -\left(\alpha_1 - \frac{1}{2}\right) e_1^2 - \left(\alpha_2 - \frac{1}{2}\right) e_2^2 - k_1 c_b r^2 - (k_2 c_b - \Theta)\,|r| - (k_3 c_b - 1)\,\rho(\|z\|)\|z\||r| \\ & - (k_4 c_b - 1 - c_B)\,\|\hat{W}_d\||r| + \sum_{i \in \mathcal{A}} \frac{1}{2k_{L,i}} (sat_{\beta_i}(W_{d,i}(t)) - sat_{\beta_i}(\hat{W}_{d,i}(t)))^2 \\ & + \tilde{W}_d r - \sum_{i \in \mathcal{A}} \frac{1}{2k_{L,i}} (\tilde{W}_{d,i} + k_{L,i} r)^2. \end{aligned} \tag{4-25}$$

By employing the following property

$$\left(W_{d,i}(t) - \hat{W}_{d,i}(t)\right)^2 \geq \left(sat_{\beta_i}(W_{d,i}(t)) - sat_{\beta_i}(\hat{W}_{d,i}(t))\right)^2,$$

as proven in [44, Appendix I], and canceling terms, (4-25) can be rewritten as

$$\begin{aligned}\dot{\tilde{V}}_1 \overset{a.e.}{\leq} & -\left(\alpha_1 - \frac{1}{2}\right)e_1^2 - \left(\alpha_2 - \frac{1}{2}\right)e_2^2 - \left(k_1 c_b + \frac{k_{L,min}}{2}\right)r^2 - (k_2 c_b - \Theta)|r| \\ & - (k_3 c_b \rho(\|z\|)\|z\| - \rho(\|z\|)\|z\|)|r| - (k_4 c_b - 1 - c_B)\|\hat{W}_d\||r|, \end{aligned} \tag{4-26}$$

where the minimum learning gain $k_{L,min} \in \mathbb{R}_{>0}$ is defined as $k_{L,min} \triangleq min\{k_{L,i}\}, \forall i \in \mathcal{A}$. Provided the gain conditions in (4-22) are satisfied, the inequality in (4-26) can be further upper bounded as

$$\dot{\tilde{V}}_1 \overset{a.e.}{\leq} -\delta\|z\|^2, \tag{4-27}$$

where $\delta \in \mathbb{R}$ is defined as

$$\delta \triangleq min\left\{\left(\alpha_1 - \frac{1}{2}\right), \left(\alpha_2 - \frac{1}{2}\right), \left(k_1 c_b + \frac{k_{L,min}}{2}\right)\right\}.$$

By invoking [78, Corollary 2], $|e_1|, |e_2|, |r| \to 0$ as $t \to \infty$. Since $V_1 > 0$ and $\dot{V}_1 \overset{a.e.}{\leq} 0$, $V_1 \in \mathcal{L}_\infty$, hence, $e_1, e_2, r, Q_L \in \mathcal{L}_\infty$. From (4-16), $\hat{W}_d \in \mathcal{L}_\infty$, which along with the fact that $W_d \in \mathcal{L}_\infty$ from (4-14), implies that $\tilde{W}_d \in \mathcal{L}_\infty$. Then from (4-15), $\nu \in \mathcal{L}_\infty$, and from (4-1) and (4-2), $u_m, u_e \in \mathcal{L}_\infty$, which implies $\tau_a, \tau_e \in \mathcal{L}_\infty$. Since $e_1, e_2, r \in \mathcal{L}_\infty$, then $\dot{e}_1, \dot{e}_2 \in \mathcal{L}_\infty$ from (4-5) and (4-6), and hence, $q, \dot{q} \in \mathcal{L}_\infty$, which implies $\ddot{q} \in \mathcal{L}_\infty$ from (2-12). □

### 4.4 Experiments

The cadence controller developed in (4-15) with the distributed repetitive learning-based feedforward control in (4-16) was implemented on both able-bodied individuals and people with NCs to quantify the performance. The switched control input was

commanded as stimulation intensities $u_m$ in (4-1) to activate the right and left quadriceps (RQ, LQ), hamstrings (RH, LH), and gluteal (RG, LG) muscle groups, and as current $u_e$ in (4-2) to the electric motor.

### 4.4.1 Participants

Seven able-bodied individuals (5 male, 2 female) with ages ranging between 22 and 43 years old participated in the FES-cycling protocol at the University of Florida. Five participants with NCs (2 male, 3 female) were either recruited through the UF Health Integrated Data Repository (UF Consent2Share project) and completed the FES-cycling protocol at the University of Florida or were enrolled at Brooks Rehabilitation in Jacksonville, FL. Demographics of the participants with NCs are listed in Table 4-1. The enrollment of the participants for the experiments of this chapter followed the same procedure as in Section 3.3.1. Also the same instructions were given during experiments to the healthy individuals and the participants with NCs as in Section 3.3.1. Participant A is a paraplegic due to SCI (lesion level T8-T9 complete) with previous limited experience with FES technologies. Participant A used a wheelchair full-time for mobility. Participant B is a participant with Spina Bifida (SB) (level L5-S1) and Arnold Chiari malformation. Participant B used a wheelchair part-time for mobility and a walker for ambulation at home. Participant C is a participant with relapsing remitting MS and used a single point cane for ambulation. Participant C presented tremor in her lower extremities during ambulation. Participant D is a quadriplegic due to a SCI (lesion level C5-C7, and incomplete T12) with previous experience with upper- and lower-limb cycling and used an electric-powered wheelchair for mobility. Participant E is a post hemorrhagic stroke participant with left side impairment and minor loss of sensory perception. Participant E used a single point cane for ambulation and had an ankle foot orthosis.

Table 4-1. Demographics of participants with a neurological condition.

| Participant | Age | Sex | Injury | Months Since Injury |
|---|---|---|---|---|
| A | 28 | F | SCI T8-T9 | 135 |
| B | 25 | M | SB L5-S1 | Since Birth |
| C | 28 | F | MS | 96 |
| D | 32 | M | SCI C5-C7, T12 | 76 |
| E | 48 | F | Hemorrhagic Stroke | 16 |

### 4.4.2 Experimental Setup

The experimental testbed for the work developed in this chapter is the same as previously described in 3.3.2. The pulsewidth for each muscle group was computed by $u_m$ in (4-1) and (4-15)-(4-17) and commanded to the stimulator via serial port communication. Anatomical lengths of the participant's lower extremities were recorded utilizing visible landmarks as in [12]. These measurements were used to determine the stimulation pattern (i.e., the crank angles where the muscle groups were electrically stimulated).

Cadence trials with only the motor being activated were implemented to familiarize the participants with NCs with different operating speeds. Afterwards, open-loop stimulation pulse trains were delivered to the participants with NCs to determine the minimum threshold that elicits visible muscle contractions. The experiment duration $t_d$ was 3 minutes. The desired cadence trajectory $\dot{q}_d$ smoothly approached a steady state value of 50 RPM during the time interval, $t \in [0, t_1]$, $t_1 = 16$ seconds, during which, only the motor was activated (i.e., $\sigma_e = 1$, $q \in \mathcal{Q}_e$ for the whole crank cycle). The cadence trajectory remained constant at 50 RPM for a transition time interval of 10 seconds, $t \in [t_1, t_1 + 10]$, where the regions of the crank cycle for which electrical stimulation was delivered (i.e., $q \in \mathcal{Q}_m$) increased until it reached a steady state value. After the transition interval, the desired cadence began its periodic trajectory as described below.

The width of the stimulation regions is determined by a time-varying positive threshold $\Lambda_m \in [0, 1]$, $\forall m \in \mathcal{M}$ that reaches a constant value at the end of the transition interval and remains invariant until the end of the experiment (i.e., $t \in [t_1 + 10, t_d]$). The design of $\Lambda_m$ smoothly integrates electrical stimulation at the beginning of the experiment to avoid demanding high stimulation intensities.

The periodic crank velocity tracked by the learning controller in (4-16) had an amplitude of $50 \pm 5$ RPM and a period of $T = 12$ seconds and was commanded for $t \in [t_1 + 10, t_d]$. To facilitate the selection of gains in (4-1), (4-2), (4-15), (4-17), and (4-18), separate gains were selected for each muscle group and the electric motor, without loss of generality. The control gains introduced in (4-1), (4-2), (4-5), (4-6), (4-15), (4-17), and (4-18) were tuned to yield appropriate tracking performance and selected as follows: $k_m \in [0.45, 0.5]$, $k_e \triangleq 10$, $\alpha_1 \in [0.625, 0.75]$, $\alpha_2 \in [1.5, 1.75]$, $k_{1,m} \in [65, 520]$, $k_{2,m} \in [5, 28]$, $k_{3,m} \in [0.01, 0.08]$, $k_{4,m} \in [0.5, 1.5]$, $k_{1,e} \triangleq 1$, $k_{2,e} \triangleq 0.3$, $k_{3,e} \triangleq 0.001$, $k_{4,e} \triangleq 0.001$, $k_{L,m} = [k_{L,RQ},\ k_{L,LQ},\ k_{L,RH},\ k_{L,LH},\ k_{L,RG},\ k_{L,LG}] \in [[15, 90],\ [15, 90],\ [12, 80],\ [16, 80],\ [12, 75],\ [14, 75]]$, and $k_{L,e} \in [0.15, 0.18]$. Moreover, the learning gains $k_{L,m}$ were selected to obtain a high contribution of the learning inputs $\hat{W}_{d,m}$ in the calculation of the stimulation intensities $u_m$.

### 4.5 Results

The FES-cycling experiments were successfully completed by all the enrolled participants. Table 4-2 summarizes the average cadence tracking error $\ddot{e}_1$, the average position tracking error $\dot{e}_1$, the cadence RMS error, and the cadence percent error (% error) during $t \in [t_1, t_d]$ seconds for the healthy individuals (S1-S7). Table 4-3 reports the results for the participants with NCs (A-E). The cadence RMS error was calculated over a moving time interval window corresponding to the period of the desired trajectory, i.e., 12 seconds. Figure 4-1 shows the switching of the stimulation intensities $u_m$, the muscle learning feedforward inputs $\hat{W}_{d,m}$, the motor current input $u_e$, and the electric motor learning feedforward input $\hat{W}_{d,e}$ over a single crank cycle for Participant S4 after

2 minutes of cadence tracking. Figure 4-2 shows the cadence tracking performance quantified by the cadence RMS error, the cadence tracking error $\ddot{e}_1$, and the position tracking error $\dot{e}_1$ for Participant A. Figure 4-3 illustrates the stimulation intensities delivered to the muscle groups $u_m$ and the electric motor current input $u_e$ for the entire experiment duration for Participant A.

Table 4-2. Tracking results for healthy participants: average cadence tracking error $\ddot{e}_1$, average position tracking error $\dot{e}_1$, cadence RMS error (moving window of 12 s), and cadence percent error reported as mean value $\pm$ standard deviation (STD)

| Participant | $\ddot{e}_1$ (RPM) | $\dot{e}_1$ (deg) | RMS (RPM) | % Error |
|---|---|---|---|---|
| S1 | 0.04$\pm$3.57 | 0.01$\pm$3.28 | 3.57$\pm$0.30 | 0.06$\pm$7.26 |
| S2 | 0.05$\pm$3.76 | 0.00$\pm$4.35 | 3.75$\pm$0.27 | 0.08$\pm$7.61 |
| S3 | 0.07$\pm$3.57 | 0.25$\pm$11.65 | 3.55$\pm$0.39 | 0.08$\pm$7.22 |
| S4 | 0.04$\pm$4.04 | 0.02$\pm$9.24 | 4.01$\pm$0.55 | 0.05$\pm$8.26 |
| S5 | 0.07$\pm$3.22 | 0.02$\pm$3.84 | 3.23$\pm$0.20 | 0.12$\pm$6.52 |
| S6 | 0.06$\pm$3.44 | 0.02$\pm$3.24 | 3.43$\pm$0.45 | 0.11$\pm$7.04 |
| S7 | 0.00$\pm$3.63 | 0.76$\pm$14.90 | 3.57$\pm$0.64 | 0.01$\pm$7.40 |
| Mean | 0.03$\pm$3.61 | 0.15$\pm$8.43 | 3.58$\pm$0.43 | 0.07$\pm$7.35 |

Table 4-3. Tracking results for participants with NCs: average cadence tracking error $\ddot{e}_1$, average position tracking error $\dot{e}_1$, cadence RMS error (moving window of 12 s), and cadence percent error reported as mean value $\pm$ standard deviation (STD)

| Participant | $\ddot{e}_1$ (RPM) | $\dot{e}_1$ (deg) | RMS (RPM) | % Error |
|---|---|---|---|---|
| A | 0.04$\pm$3.90 | 0.02$\pm$6.57 | 3.89$\pm$0.30 | 0.05$\pm$7.93 |
| B | 0.02$\pm$4.53 | 0.04$\pm$4.93 | 4.48$\pm$0.77 | 0.03$\pm$9.35 |
| C | 0.06$\pm$3.89 | 0.05$\pm$16.40 | 3.80$\pm$0.81 | 0.15$\pm$8.00 |
| D | 0.02$\pm$5.24 | 0.88$\pm$33.55 | 5.07$\pm$1.34 | 0.21$\pm$10.96 |
| E | 0.03$\pm$4.08 | 0.08$\pm$4.95 | 4.06$\pm$0.64 | 0.06$\pm$8.37 |
| Mean | 0.03$\pm$4.36 | 0.21$\pm$17.24 | 4.26$\pm$0.84 | 0.1$\pm$8.99 |

To assess the effect of the distributed feedforward repetitive learning control component, two trials with different learning gains were performed for Participant S5 (selected randomly from the healthy individuals). Figure 4-4 depicts the distributed muscle and electric motor learning feedforward terms (i.e., $\hat{W}_{d,m}$ and $\hat{W}_{d,e}$) for the two trials. Figure 4-4 illustrates the first trial where the muscle learning gains were set to

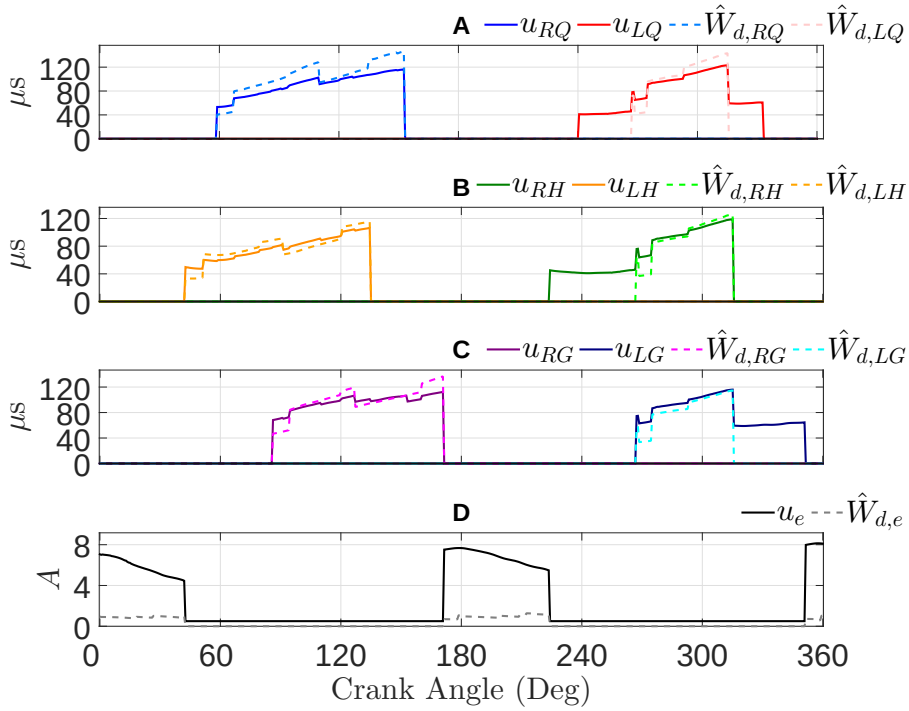


Figure 4-1. FES stimulation intensities, electric motor current input, and the muscle and motor learning feedforward terms over one crank cycle for Participant S4. The stimulation inputs $u_m$ correspond to the solid lines and the muscle learning feedforward terms $\hat{W}_{d,m}$ correspond to the dashed lines. A) FES stimulation intensities and learning feedforwad terms delivered to the quadriceps. B) FES stimulation intensities and learning feedforwad terms delivered to the hamstrings. C) FES stimulation intensities and learning feedforwad terms delivered to the gluteal muscle groups. D) The current input $u_e$ (solid line) and motor learning feedforward term $\hat{W}_{d,e}$ (dashed line) delivered to the electric motor. This figure illustrates the switching of the control inputs designed in (4-1)-(4-2).

$k_{L,m} = [20; 20; 18; 18; 15; 15]$ and $k_{1,m} = 85$. Figure 4-4 also depicts the second trial where the muscle learning gains were doubled compared to the first trial and $k_{1,m} = 65$. For both trials the electric motor learning gain was set to $k_{L,e} = 0.18$. Figure 4-5 shows the corresponding tracking performance of the two trials quantified by the cadence RMS error and the position tracking error $\dot{e}_1$.

Figure 4-6 illustrates the muscle and electric motor learning feedforward terms $\hat{W}_{d,m}$ and $\hat{W}_{d,e}$ for Participant A and Participant S3. The differences in amplitude, symmetry,

and duration of the learning feedforward inputs can be contrasted for a participant with a movement disorder (Participant A) and an able-bodied individual (Participant S3).

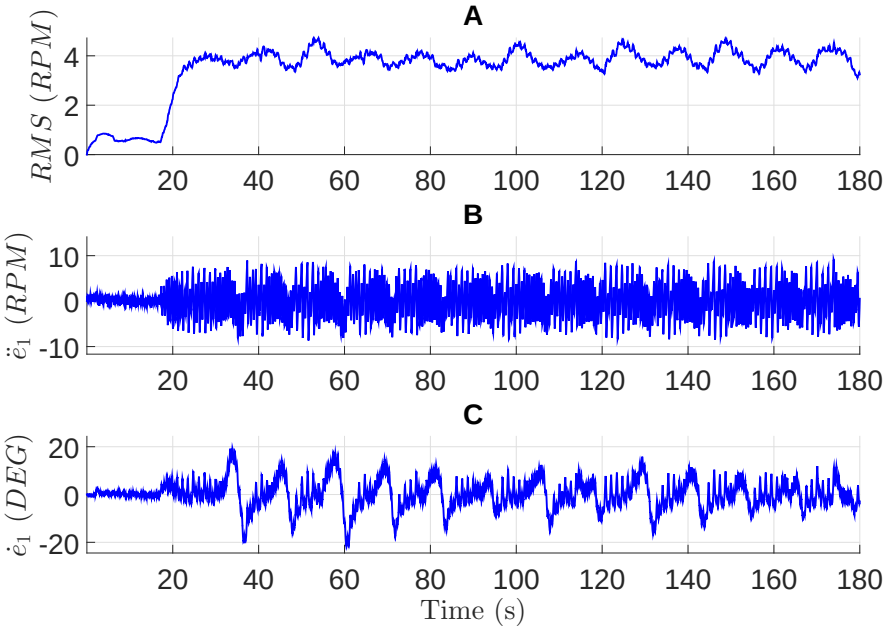


Figure 4-2. Tracking performance for Participant A. A) Cadence RMS error with a moving time interval window of 12 seconds (same as the period $T$ of $\dot{q}_d$ for $t \in [t_1 + 10, t_d]$). B) Average cadence tracking error $\ddot{e}_1$. C) Average position error $\dot{e}_1$.

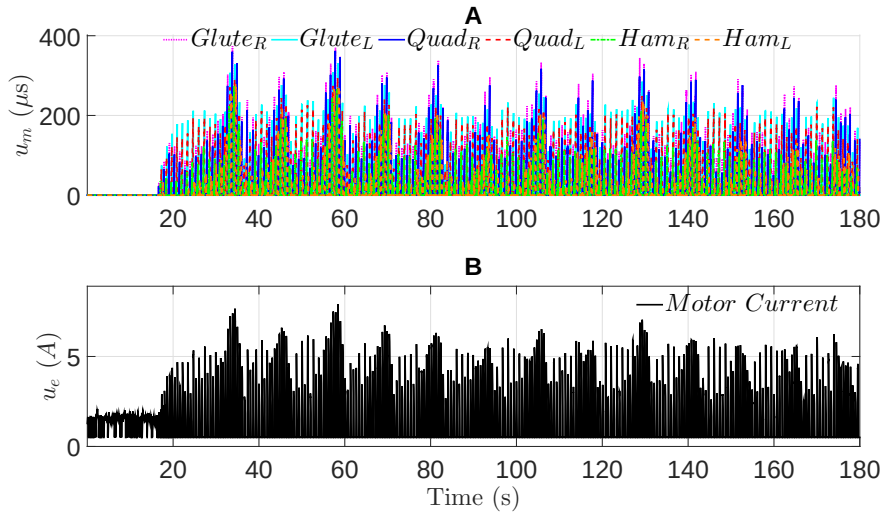


Figure 4-3. Control inputs for Participant A. A) Stimulation intensities delivered to the muscle groups. B) Electric motor current input.

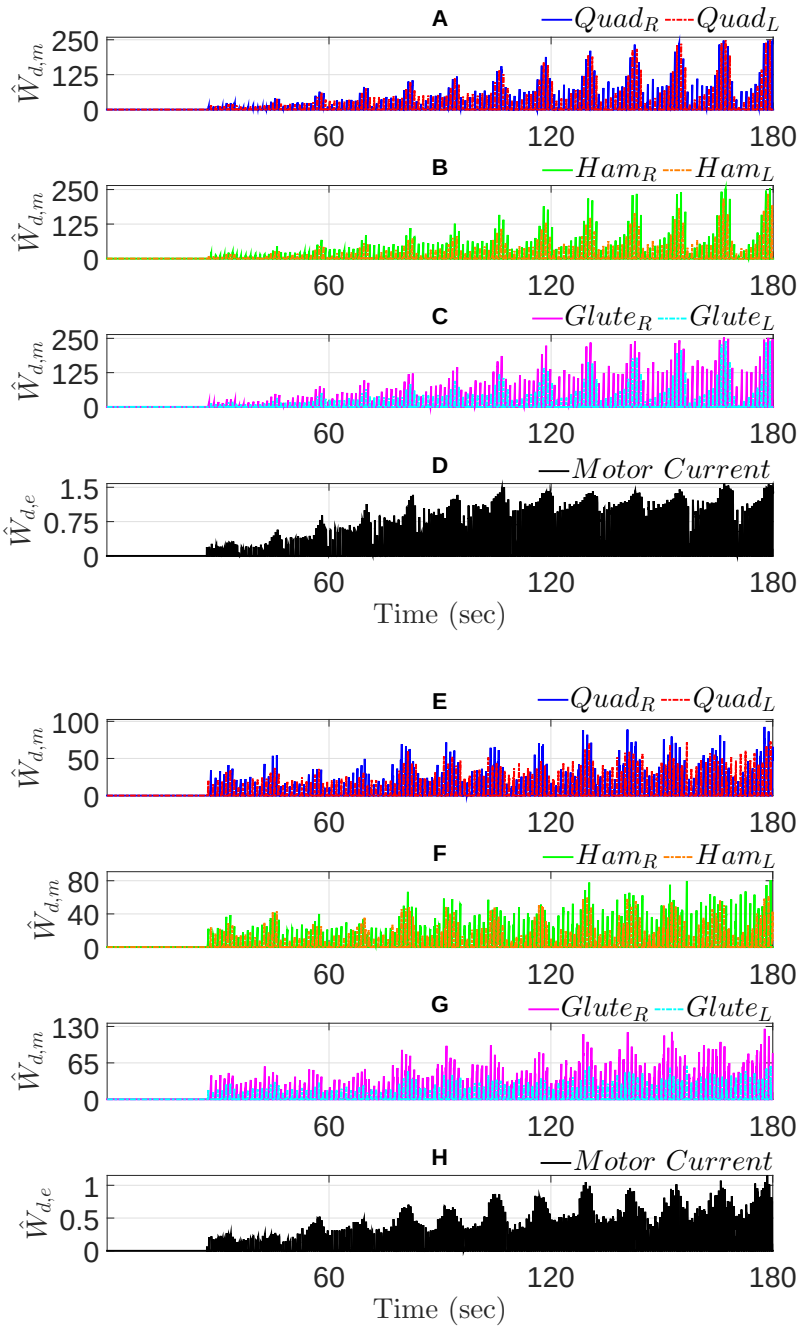


Figure 4-4. Effect of modifying muscle learning gains $k_{L,m}$ on the muscle feedforward learning terms $\hat{W}_{d,m}$ and electric motor learning feedforward term $\hat{W}_{d,e}$ during two different trials for Participant S5. A) Quadriceps learning feedforward terms in the first trial. B) Hamstrings learning feedforward terms in the first trial. C) Gluteal muscle groups learning feedforward terms in the first trial. D) Electric motor learning feedforward term in the first trial. E) Quadriceps learning feedforward terms in the second trial. F) Hamstrings learning feedforward terms in the second trial. G) Gluteal muscle groups learning feedforward terms in the second trial. H) Electric motor learning feedforward term in the second trial.

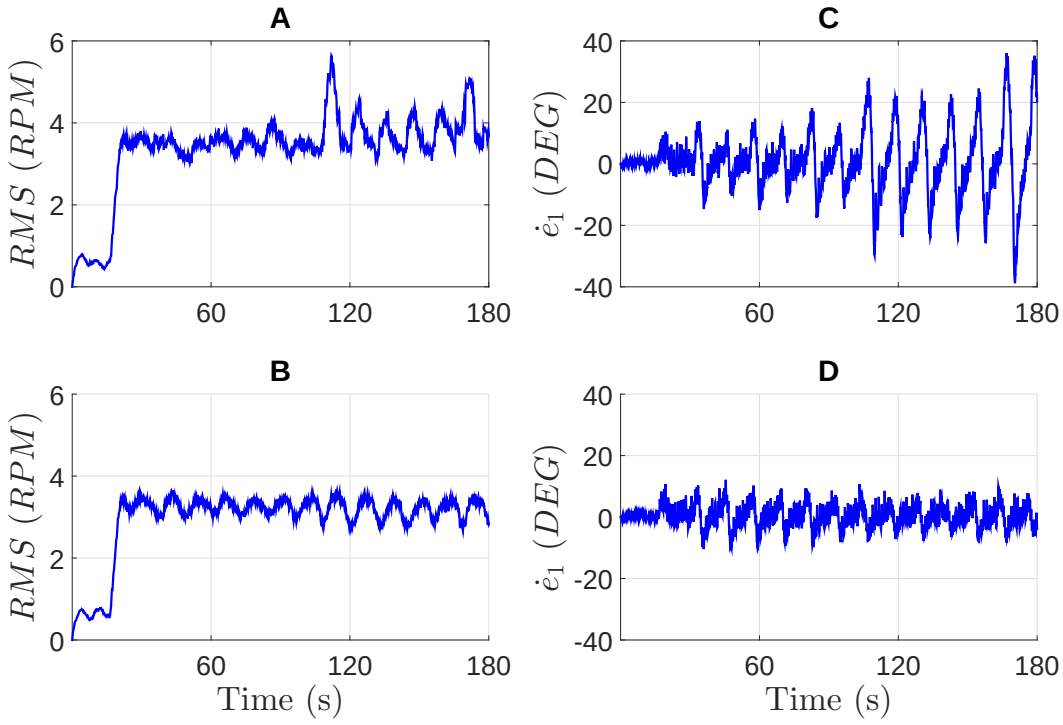


Figure 4-5. Tracking performance for Participant S5 during two trials with different muscle learning gains $k_{L,m}$. A) Cadence RMS error in the first trial. B) Cadence RMS error in the second trial. C) Position tracking error $\dot{e}_1$ in the first trial. D) Position tracking error $\dot{e}_1$ in the second trial.

### 4.6 Discussion

The experimental results conducted in healthy individuals and participants with NCs demonstrate the feasibility of the controllers developed in (4-1) and (4-2) with distributed repetitive learning inputs designed in (4-17) and (4-18) to cooperatively track a desired cadence trajectory. The average cadence tracking error $\ddot{e}_1$ is $0.03 \pm 3.61$ RPM for seven able-bodied individuals and $0.03 \pm 4.36$ RPM for five participants with NCs. The average position tracking error $\dot{e}_1$ is $0.15 \pm 8.43^{\circ}$ for able-bodied individuals and $0.21 \pm 17.24^{\circ}$ for the participants with NCs (see Tables 4-2-4-3).

The average cadence and position tracking errors are similar to the results reported in FES-cycling literature such as [11, 12, 34, 91]. The cadence tracking performance for both healthy and neurologically impaired individuals in this study is consistent with the cadence performance reported in [11], where a robust approach was employed, and

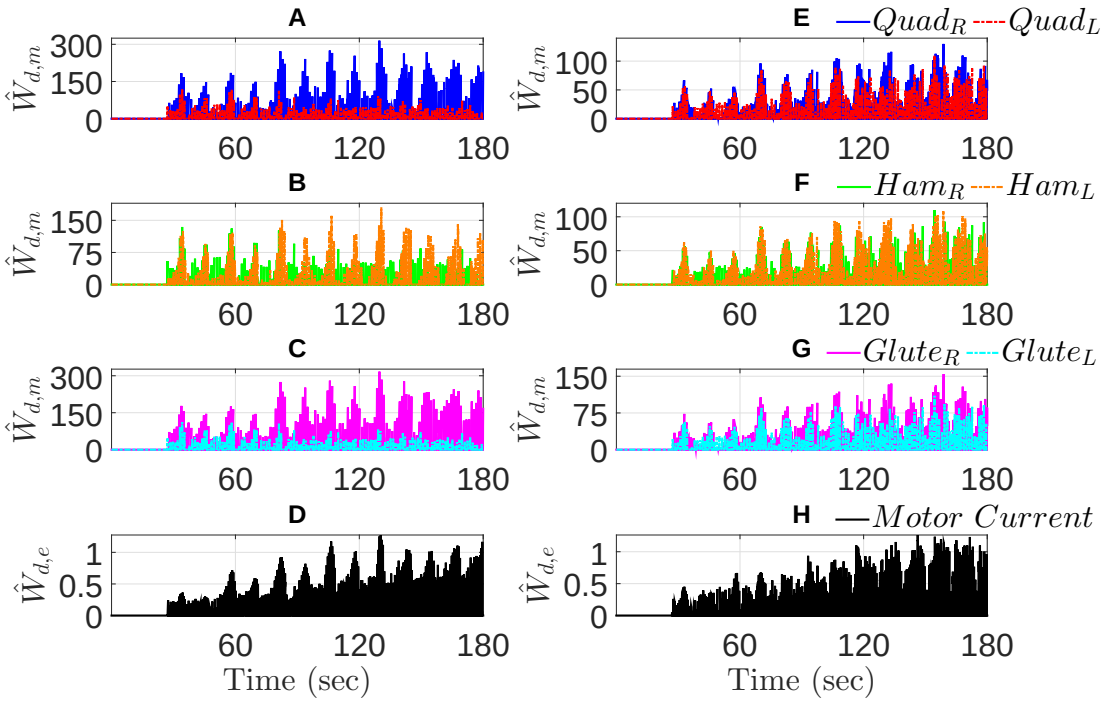


Figure 4-6. Comparison of muscle and electric motor learning feedforward terms for Participant A and Participant S3. Muscle learning feedforward terms $\hat{W}_{d,m}$ are illustrated for the right $(R)$ and left $(L)$ leg. A) Quadriceps learning feedforward terms for Participant A. B) Hamstrings learning feedforward learning terms for Participant A. C) Gluteal muscle groups learning feedforward terms for Participant A. D) Electric motor learning feedforward term $\hat{W}_{d,e}$ for Participant A. E) Quadriceps learning feedforward terms for Participant S3. F) Hamstrings learning feedforward learning terms for Participant S3. G) Gluteal muscle groups learning feedforward terms for Subject S3. H) Electric motor learning feedforward term $\hat{W}_{d,e}$ for Participant S3 .

with [91], where a RISE-based approach was implemented, exploiting the stimulation of antagonistic biarticular muscles. The position tracking performance obtained from healthy and neurologically impaired participants using the distributed learning approach in this chapter is better (quantified by smaller mean and standard deviation of the position error) than the performance obtained in [11, 91]. The cycling experiments performed in [11] included healthy individuals only and in [91] several able-bodied participants and one participant with Parkinson's disease. Therefore another important

contribution of this chapter is the suitable position and cadence tracking obtained with people with different NCs. The implementation of the distributed repetitive learning control adds a feedforward term to each of the lower-limb muscle groups stimulation intensities and electric motor current based on its past inputs. By the construction of $r$ in (4-6), the muscle and electric motor learning feedforward terms have a proportional-integral-derivative (PID) form and affect both cadence and position tracking.

The feedforward repetitive learning control term has a significant effect in the tracking performance as depicted in the two trials (using different muscle learning gains $k_{L,m}$) for Participant S5 in Figure 4-5. The cadence RMS error and position error in Figure 4-5A-C, respectively, depicts the tracking performance of the first trial. After 100 seconds, oscillations of both the cadence RMS error (Figure 4-5A) and position tracking error (Figure 4-5C) occur due to the high robust gain $k_{1,m}$ which results in higher stimulation intensities. The muscle learning feedforward terms $\hat{W}_{d,m}$ in Figure 4-4A-C grew consistently reaching a maximum of 225 $\mu s$ at the end of the first trial. The first trial resulted in increased stimulation intensities $u_m$ that induced discomfort, which may potentially result in early experiment termination particularly for participants with greater sensitivity to the stimulation. Also, it is well known that higher stimulation intensities result in increased muscle fatigue which inherently limits the experiment duration due to the rapid decay of muscle force. The cadence tracking percent error during the first trial shown in Figure 4-5A is $0.03 \pm 7.52\%$. Alternatively, the cadence RMS error and position tracking error in Figure 4-5B-D, respectively, illustrate a steady tracking performance during the second trial. In the second trial the muscle learning gains $k_{L,m}$ were doubled compared to the first trial. The cadence RMS error in Figure 4-5B drops below 3 RPM intermittently and never crosses 4 RPM. The position tracking error $\dot{e}_1$ in Figure 4-5D decreases in amplitude from period to period. Consistently, the muscle learning feedforward terms $\hat{W}_{d,m}$ in Figure 4-4E-G illustrate steady learning inputs across all muscle groups reaching maximums of 90 $\mu s$ for the quadriceps, 80 $\mu s$ for the

hamstrings, and 100 $\mu s$ for the gluteal muscle groups. Steady stimulation inputs result in smoother cadence tracking and prevents over-stimulation of the muscles, potentially enabling longer cycling sessions. The cadence tracking percent error during the second trial shown in Figure 4-5B is $0.12 \pm 6.52\%$.

The distributed repetitive learning control is able to adapt for participants with NCs. In Figure 4-6A and Figure 4-6C, the quadriceps and gluteal learning feedforward terms $\hat{W}_{d,m}$ illustrate high amplitude and asymmetric profiles. These learning inputs may be representative of the lack of neurological motor control and muscle weakness of Participant A (SCI participant). The learning feedforward terms for the right quadriceps ($\hat{W}_{d,RQ}$) and glutes ($\hat{W}_{d,RG}$) had higher magnitudes with mean values of 82 $\mu s$ and 89 $\mu s$ than their left counterparts. In Figure 4-6E-H, the muscle and electric motor learning feedforward terms $\hat{W}_{d,m}$ and $\hat{W}_{d,e}$ denote steady and more symmetric profiles for Participant S3 (able-bodied participant) with mean magnitudes for all muscle groups between 40-50 $\mu s$. These learning inputs may be representative of adequate muscle strength and symmetry between both participant's legs.

The stability analysis ensures asymptotic tracking, however there are factors during experiments such as muscle fatigue, disturbances in the cycle, and electromechanical delay, which degrade the tracking performance for both able-bodied individuals and participants with NCs. Nevertheless, the switched controller was able to accommodate for participants with movement disorders as a result of neurological conditions such as SCI, SB, MS, and post stroke. For the SCI participants, Participants A (paraplegic) and D (quadriplegic), the lack of muscle mass and strength, intermittent spasms, and the lack of neurological motor control resulted in increased stimulation intensities with a mean value across all muscle groups of 105 $\mu s$ and 135 $\mu s$, respectively. The percentage of time during which Participants A and D were actively stimulated was 34% and 31%, respectively, to achieve a balance between the muscles' contribution and the motorized assistance. The kinematics of the participants also determines

the stimulation pattern, thus affecting the muscle activation times. Participant B, a participant with SB, evoked visible active contractions with 30% of the stimulation intensities required for the SCI participants. The percentage of time during which Participant B was actively stimulated was 32%. Participant C, a participant with MS, required 25% of the stimulation intensities required for the SCI participants. Participant C was actively stimulated 45% of the time. Participant E, a post stroke participant, had residual motor control on her left affected side and full neurological motor control in her contralateral side; however, the participant was asked to not contribute voluntarily during the cadence experiments. Participant E was actively stimulated for 46% of the time with 20% of the stimulation intensities delivered to the SCI participants. The percentage of time during which the participants with NCs were actively stimulated suggests an adequate balance between the FES and motorized contributions to maintain the desired cadence. Moreover, stimulation times have a high impact in the rate of muscle fatigue, which affects cycling duration and thus the amount of dose of rehabilitative stimulation. Furthermore, experiments in a longitudinal study can help to elucidate the clinical significance of longer stimulation times in people with different conditions.

The results for able-bodied individuals and participants with NCs show that by switching the control effort between the stimulation intensities delivered to the six muscle groups and the electric motor, desirable cadence and position tracking was achieved. The developed controller showed robustness and appropriate tracking performance despite the challenges faced during experiments. Clinical trials with a larger population of participants with NCs are required to investigate the long-term impact of the control methodology developed in this chapter. For example, in [18] a FES-cycling study with 25 SCI participants found important gains in neurological, motor, and sensory function and increased muscle volume and strength during 29.1 months. A cycling protocol that adopts the distributed repetitive learning approach for power

tracking to monitor the torque contribution of the muscles may lead to a more suitable rehabilitation approach like in strength training.

## 4.7 Concluding Remarks

A nonlinear controller that switches among lower-limb muscles and an electric motor with distributed learning feedforward inputs was designed to yield global asymptotic cadence tracking. The switched muscle and electric motor distributed learning compensates for the periodic dynamics of the desired cadence trajectory. The robust feedback terms in the switched controller aid in rejecting disturbances present in the motorized cycle and rider. The controller is implemented on a nonlinear rider-cycle system with parametric uncertainties and without the need to perform any identification procedures despite the wide range of participants enrolled in the experiments. Global asymptotic tracking was achieved with the aid of a corollary to the LaSalle-Yoshizawa theorem for nonsmooth systems in [78].

The distributed repetitive learning switched controller was tested in experiments with seven able-bodied individuals and five participants with NCs such as SCI, SB, MS, and post stroke. For the healthy control group and for the neurologically impaired population, a mean RMS (computed over a time window equal to the period $T = 12$ seconds) cadence error of $3.58 \pm 0.43$ RPM (0.06$\pm$7.35 % average error) and $4.26 \pm 0.84$ RPM (0.1$\pm$8.99 % average error) was obtained, respectively. The results obtained in people with NCs demonstrate the ability of the switched controller to yield consistent repetitive cadence despite lower-limb asymmetries, muscle spasticity, muscle atrophy, tremor, muscle weakness, hypersensitivity, and absence of neurological motor control.

# CHAPTER 5
# TORQUE AND CADENCE TRACKING IN FUNCTIONAL ELECTRICAL STIMULATION INDUCED CYCLING USING PASSIVITY-BASED AND SPATIAL REPETITIVE LEARNING CONTROL

In Chapters 3-4, learning controllers were developed for cadence tracking by switching between muscle groups and motor. However, motivation also exists to maximize the torque output produced by the activation of lower-limb muscles for strength training and building muscle mass [35]. The simultaneous control of cadence and torque is task specific to cycling, where the purpose is to achieve a desired power. The dual objective of torque and cadence tracking, i.e., power tracking, has been studied in several FES-cycling protocols [34, 61]. However, no previous result has exploited the repetitive/periodic nature of cycling during power tracking. Hence, the development of learning control algorithms that can take advantage of the periodicity of FES-cycling while guaranteeing stability of the human-machine closed-loop system is desired.

In this chapter and in the work in [92], a novel switched muscle controller, leveraging the idea of spatial learning control, is designed for torque tracking of a spatially periodic function of the crank position. The periodic desired torque trajectory is designed based on the knee kinematic effectiveness of the rider, which varies as a function of the crank angle. In parallel, a robust sliding-mode controller is designed for the electric motor to achieve cadence tracking. Because every crank cycle (i.e., a full revolution) is completed within different time periods, the spatial periodicity of the torque trajectory is leveraged to update the learning controller based on the crank position. A passivity-based analysis is developed to ensure stability of the torque (muscle control) and cadence (motor control) subsystems. Experimental testing was conducted on five able-bodied individuals for control validation and three participants with NCs to assess the feasibility of the control technique applied to people with movement disorders. The combined average cadence

tracking error was $0.01 \pm 1.20$ RPM for a 50 RPM trajectory and the combined average power tracking error is $1.78 \pm 1.25$ W for a peak power of 10 W.

## 5.1 Control Development

### 5.1.1 Cadence Control

The first objective is to design a motor controller that tracks a target cadence. The measurable angular crank position tracking error $e : \mathbb{R}_{\geq t_0} \to \mathbb{R}$ is defined as

$$e \triangleq q - q_d, \tag{5-1}$$

where $q_d : \mathbb{R}_{\geq t_0} \to \mathbb{R}$ denotes the desired crank position, and its first two time derivatives are bounded such that $|\dot{q}_d(t)| \leq \xi_1$ and $|\ddot{q}_d(t)| \leq \xi_2$, where $\xi_1, \xi_2 \in \mathbb{R}_{>0}$ are known positive constants. The cadence control objective is quantified using the first time derivative of (5-1). To facilitate the subsequent control development, an auxiliary tracking error $r : \mathbb{R}_{\geq t_0} \to \mathbb{R}$ is defined as[1]

$$r \triangleq \dot{e} + \alpha e, \tag{5-2}$$

where $\alpha \in \mathbb{R}_{>0}$ is a constant control gain. After taking the time derivative of (5-2) and premultiplying by $M$, substituting for (2-12) and (5-1) and then performing some algebraic manipulation

$$M\dot{r} = -Vr + \chi + \tilde{N} + B_\sigma u_{FES} + B_e u_e - e, \tag{5-3}$$

where the auxiliary signals $\chi : \mathbb{R}_{\geq t_0} \to \mathbb{R}$ and $\tilde{N} : \mathbb{R}_{\geq t_0} \to \mathbb{R}$ are defined as

$$\chi \triangleq W_d - M(q)(\ddot{q}_d - \alpha\dot{e}) - V(q,\dot{q})(\dot{q}_d - \alpha e) - G(q) - P(q,\dot{q}) - c_d\dot{q} + N_d + e, \tag{5-4}$$

[1] Functional dependencies are removed henceforth unless they add clarity to the exposition.

$$\tilde{N} \triangleq -(W_d + N_d + d), \tag{5-5}$$

and the signals $W_d : \mathbb{R}_{\geq t_0} \to \mathbb{R}$ and $N_d : \mathbb{R}_{\geq t_0} \to \mathbb{R}_{>0}$ are defined as

$$W_d \triangleq M(q_d)\ddot{q}_d + V(q_d, \dot{q}_d)\dot{q}_d + G(q_d) + c_d\dot{q}_d, \tag{5-6}$$

$$N_d \triangleq c_{P1} + c_{P2}\dot{q}_d. \tag{5-7}$$

The auxiliary signal in (5-5) can be upper bounded as

$$|\tilde{N}| \leq \Theta_1, \tag{5-8}$$

where $\Theta_1 \in \mathbb{R}_{>0}$ is a known positive constant. By using Properties 5-9, (5-1) and (5-2), the Mean Value Theorem can be used to develop an upper bound for (5-4) as

$$\chi \leq \rho(\|z\|)\|z\|, \tag{5-9}$$

where $z : \mathbb{R}_{\geq t_0} \to \mathbb{R}^2$ is a composite vector of error signals defined as

$$z \triangleq [e \;\; r]^T, \tag{5-10}$$

and $\rho(\cdot) \in \mathbb{R}$ is a known positive, radially unbounded, nondecreasing function. Given the cadence open-loop error system in (5-3), the control input to the motor is designed as

$$u_e = -k_1 r - (k_2 + k_3\rho(\|z\|)\|z\|)\, sgn(r) + \nu_p, \tag{5-11}$$

where $k_1, k_2, k_3 \in \mathbb{R}_{>0}$ are selectable positive gain constants, $sgn(\cdot) : \mathbb{R} \to [-1, 1]$ is the signum function, and $\nu_p : \mathbb{R}_{\geq t_0} \to \mathbb{R}$ is a subsequently designed control. The cadence closed-loop error system is obtained by substituting (5-11) into (5-3)

$$M\dot{r} = -Vr + \chi + \tilde{N} + B_\sigma u_{FES} - e - B_e(k_1 r - \nu_p + (k_2 + k_3\rho(\|z\|)\|z\|)\, sgn(r)). \tag{5-12}$$

### 5.1.2 Spatial Learning Control for Torque Tracking

The second objective is to track a desired torque trajectory in the muscle stimulation regions (i.e., $q \in \mathcal{Q}_M$, see Figure 5-1). The torque tracking error signal is designed based on the difference between the desired torque and the torque produced by the muscle contractions defined in (2-7). Torque sensors are commonly included on rehabilitation cycles which provide a measurement of the net torque contributions about the crank. Direct measurement of muscle force requires real-time invasive sensing which is not practical as discussed in [9]. Similar to previous FES experiments (cf. [9, 62]), a baseline measurement of the required torque to drive the cycle-rider system at a desired speed is obtained a priori where no electrical stimulation is applied to the lower-limb muscles (i.e., $\tau_a = 0$ such that $\tau_r = \tau_p$) under the assumption that the disturbances $d$ by the rider and the cycle are sufficiently small. Setting $\tau_a = 0$ in (2-4), a nominal torque measurement $\tau_n : \mathbb{R}_{\geq t_0} \to \mathbb{R}$ of (2-2) can be obtained as

$$\tau_n = \tau_e = \tau_c + \tau_p. \tag{5-13}$$

An estimate of the nominal torque measurement $\hat{\tau}_n : \mathbb{R}_{\geq t_0} \to \mathbb{R}$ (i.e., $\hat{\tau}_n = \hat{\tau}_c + \hat{\tau}_p$) can be obtained by using fitting techniques such as Fourier series using torque measurements [62]. The mismatch between the nominal torque and the nominal torque estimate $\tilde{\tau}_n : \mathbb{R}_{\geq t_0} \to \mathbb{R}$ is obtained as

$$\tilde{\tau}_n = \tau_n - \hat{\tau}_n \leq \epsilon_n, \tag{5-14}$$

where $\epsilon_n \in \mathbb{R}_{>0}$ is an upper bound in the estimation error. The net active muscle torque $\tau_a$ is obtained by subtracting the nominal torque estimate $\hat{\tau}_n$ from the continuous time torque measurement $\tau_M : \mathbb{R}_{\geq t_0} \to \mathbb{R}$ (i.e., the net torque contributions about the crank) such that

$$\tau_a = \tau_M - \hat{\tau}_n. \tag{5-15}$$

To quantify the torque control objective, a torque tracking error-like term $e_\tau : \mathbb{R}_{\geq t_0} \to \mathbb{R}$ is defined as [93]

$$e_\tau = \int_{t_0}^{t} (\tau_d(\varphi) - \tau_a(\varphi))\, d\varphi, \tag{5-16}$$

where $\tau_d : \mathbb{R}_{\geq t_0} \to \mathbb{R}$ denotes a bounded periodic desired torque trajectory.

*Remark* 5.1. In (5-16), the desired torque trajectory $\tau_d$ is a function of time. However in the experiments in Section 5.3, the desired torque trajectory $\tau_d$ is a bounded and periodic function of the crank angle $q \in [0, 2\pi)$. Hence, a mapping between time and space is needed. This mapping is feasible since there exists a relationship between time and the crank position. The angular speed (cadence) of the system is defined as $\dot{q} \triangleq dq/dt$, which can be integrated to yield $q = \int_0^t \dot{q}(\varphi) d\varphi \triangleq f(t)$. This relationship between temporal and spatial coordinates is common for rotary machine systems as explained in [75]. For the cycle-rider system, only forward pedaling is allowed (no change of direction) and the desired cadence $\dot{q}_d$ is positive. Moreover, the cadence controller in (5-11) is designed and proven to achieve $\dot{q} > 0$ (i.e., the actual cadence is nonzero) based on the stability proof in Section 5.2. Hence, $q$ is a strictly increasing function of $t$, (i.e., the relationship between $t$ and $q$ is bijective [75]). Thus the function $q = f(t)$ is analytic and the inverse function $t = f^{-1}(q)$ exists globally. Therefore, any function of $t$ can also be expressed as a spatial function of $q$ (e.g., $\tau_d(t)$ can be expressed as $\tau_d(f^{-1}(q))$).

The torque open-loop error system is obtained by taking the time derivative of (5-16) and using (2-7), $u_m$ in (2-11), and (2-13) yields

$$\dot{e}_\tau = \tau_d - B_\sigma u_{FES}. \tag{5-17}$$

Given the open-loop error system in (5-17), the muscle control input is designed as

$$u_{FES} = \hat{W}_d + k_4 e_\tau - \nu_{FES}, \tag{5-18}$$

where $k_4 \in \mathbb{R}_{>0}$ is a positive constant control gain, $\nu_{FES} : \mathbb{R}_{\geq t_0} \to \mathbb{R}$ is a subsequently designed control term, and $\hat{W}_d : \mathbb{R}_{\geq t_0} \to \mathbb{R}$ is the subsequently designed repetitive learning control law.

*Remark* 5.2. The repetitive learning control law $\hat{W}_d(t)$ is typically designed based on the knowledge of the time period $T$ of a periodic process [44, 46]. However, for the current development the implementable repetitive learning control law is designed based on the state periodicity of the desired torque trajectory $\tau_d$ (e.g., designed based on the crank position). According to the mapping between time and space described in Remark 5.1, an implementable spatial repetitive learning law is denoted as $\hat{W}_d(t) = \hat{W}_d(f^{-1}(q))$. The map $q - 2\pi \triangleq f(t - T)$ is necessary for the subsequent construction of the learning control law. Using Remark 5.1, the map $t - T = f^{-1}(q - 2\pi)$ is also obtained. Knowledge of the period $T$ (i.e., the time to complete a revolution) is not necessary for the later implementation of $\hat{W}_d$, nevertheless it can be computed from $T = \int_{q-2\pi}^{q} dt = \frac{1}{\dot{q}} \int_{q-2\pi}^{q} dq$. Because the time period T depends on the cadence tracking of the electric motor, the time period T is expected to vary across crank cycles, since it will depend on the cadence tracking by the electric motor.

Based on the subsequent stability analysis, the repetitive learning control law in (5-18) is defined as

$$\begin{aligned} \hat{W}_d &\triangleq \Gamma sat_{\beta_r}\left(\hat{W}_d(t-T)\right) + k_L e_\tau, \\ &= \Gamma sat_{\beta_r}\left(\hat{W}_d\left(f^{-1}(q-2\pi)\right)\right) + k_L e_\tau. \end{aligned} \tag{5-19}$$

where $\Gamma \in (0, 1]$ is a selectable constant, $k_L \in \mathbb{R}_{>0}$ is a positive constant learning control gain, and $sat_{\beta_r}(\cdot)$ is defined as

$$sat_{\beta_r}(\Xi) \triangleq \begin{cases} \Xi & \text{for } |\Xi| \leq \beta_r \\ sgn(\Xi)\beta_r & \text{for } |\Xi| > \beta_r \end{cases}, \forall \Xi \in \mathbb{R}. \tag{5-20}$$

where $\beta_r \in \mathbb{R}_{>0}$ is a selectable constant. The closed-loop error system is obtained by substituting (5-18) into (5-17) as

$$\dot{e}_\tau = \tilde{W}_d + \hat{W}_d - B_\sigma(\hat{W}_d + k_4 e_\tau - \nu_{FES}), \tag{5-21}$$

where $\tilde{W}_d : \mathbb{R}_{\geq t_0} \to \mathbb{R}$ is the learning estimation error defined as $\tilde{W}_d \triangleq \tau_d - \hat{W}_d$. Based on the periodicity and boundedness of $\tau_d$, $\tau_d(t) = sat_{\beta_r}(\tau_d(t)) = sat_{\beta_r}(\tau_d(t-T))$. Hence, by exploiting (5-19), the following expression can be developed

$$\tilde{W}_d = sat_{\beta_r}(\tau_d(t-T)) - \Gamma sat_{\beta_r}(\hat{W}_d(t-T)) - k_L e_\tau(t). \tag{5-22}$$

## 5.2 Stability Analysis

The stability of the learning controller for torque tracking and robust sliding-mode controller for cadence tracking can be examined independently through the following two theorems. Theorem 5.1 shows that the closed-loop torque error system is output strictly passive ( [94, Definition 6.3]) and asymptotic tracking is achieved, thus ensuring passivity of the switched system with respect to the muscle control input. Theorem 5.2 shows that the closed-loop cadence error system is output strictly passive and exponential tracking is achieved, which ensures passivity of the switched system with respect to the motor control input. In addition, Lemma 5.1 is included to prove that the time derivative of the torque tracking error in (5-16) is uniformly bounded.

**Theorem 5.1.** *Given the closed-loop error system in (5-21), the system is output strictly passive (OSP) from input* $v_1 = \gamma_1 \hat{W}_d + c_b \nu_{FES}$ *to output* $e_\tau$ *in* $q \in \mathcal{Q}_M$ *and the controller designed in (5-18) and repetitive learning law in (5-19) ensures asymptotic tracking*[2] *in the sense that*

$$\lim_{t \to \infty} e_\tau(t) = 0. \tag{5-23}$$

[2] For $q \notin \mathcal{Q}_M$ the torque controller in (5-18) and desired torque trajectory $\tau_d$ are zero.

*Proof.* Let $V_1 : \mathbb{R}^2 \times \mathbb{R}_{\geq t_0} \to \mathbb{R}$ be a nonnegative, continuously differentiable, storage function defined as

$$V_1 \triangleq \frac{1}{2}e_\tau^2 + \frac{1}{2k_L}\int_{t-T}^{t}(sat_{\beta_r}(\tau_d(\varphi)) - \Gamma sat_{\beta_r}(\hat{W}_d(\varphi)))^2 d\varphi. \tag{5-24}$$

The storage function in (5-24) satisfies the following inequalities:

$$\lambda_1\|w\|^2 \leq V_1(w,t) \leq \lambda_2\|w\|^2,$$

where $\lambda_1 \triangleq min(\frac{1}{2}, \frac{1}{2k_L})$, $\lambda_2 \triangleq max(\frac{1}{2}, \frac{1}{2k_L})$ and $w \triangleq [e_\tau \ \sqrt{Q_L}]^T$ where $Q_L \triangleq \int_{t-T}^{t}(sat_{\beta_r}(\tau_d(\varphi)) - sat_{\beta_r}(\hat{W}_d(\varphi)))^2 d\varphi$. Let $w(t)$ be a Filippov solution to the differential inclusion $\dot{w} \in K[h](w)$, where $K[\cdot]$ is defined as [85] and $h$ is defined by using (5-21) as $h \triangleq [h_1 \quad h_2]$, where $h_1 \triangleq \tilde{W}_d + \hat{W}_d - B_\sigma(\hat{W}_d + k_4 e_\tau - \nu_{FES})$, $h_2 \triangleq \frac{1}{2\sqrt{Q_L}}\{(sat_{\beta_r}(\tau_d(t)) - sat_{\beta_r}(\hat{W}_d(t)))^2 - (sat_{\beta_r}(\tau_d(t-T)) - sat_{\beta_r}(\hat{W}_d(t-T)))^2\}$. The control input in (5-18) has the discontinuous lumped control effectiveness $B_\sigma$; hence the time derivative of (5-24) exists almost everywhere (a.e.), i.e., for almost all $t$. Based on [78, Lemma 1], $\dot{V}_1(w(t),t) \overset{a.e.}{\in} \dot{\tilde{V}}_1(w(t),t)$, where $\dot{\tilde{V}}_1$ is the generalized time derivative of (5-24) along the Filippov trajectories of $\dot{w} = h(w)$ and is defined as $\dot{\tilde{V}}_1 \triangleq \bigcap_{\xi \in \partial V_1} \xi^T K \begin{bmatrix} \dot{e}_\tau & \frac{\dot{Q}_L}{2\sqrt{Q_L}} & 1 \end{bmatrix}^T (e_\tau,\ 2\sqrt{Q_L},\ t)$. Since $V_1(w,t)$ is continuously differentiable in $w$, $\partial V_1 = \{\nabla V_1\}$, thus

$$\dot{\tilde{V}}_1 \overset{a.e.}{\subset} [e_\tau,\ \left(\frac{1}{2k_L}\right) 2\sqrt{Q_L}] K \begin{bmatrix} \dot{e}_\tau & \frac{\dot{Q}_L}{2\sqrt{Q_L}} \end{bmatrix}^T. \tag{5-25}$$

Therefore, after substituting for (5-21), the generalized time derivative of (5-24) can be expressed as

$$\begin{aligned}\dot{\tilde{V}}_1 \overset{a.e.}{\subset}\ & e_\tau\left(\tilde{W}_d + \hat{W}_d - K[B_\sigma](k_4 e_\tau + \hat{W}_d - \nu_{FES})\right) \\ & -\frac{1}{2k_L}(sat_{\beta_r}(\tau_d(t-T)) - sat_{\beta_r}(\hat{W}_d(t-T)))^2\end{aligned}$$

$$+\frac{1}{2k_L}(sat_{\beta_r}(\tau_d(t)) - sat_{\beta_r}(\hat{W}_d(t)))^2. \tag{5-26}$$

By employing the following property [44]

$$\left(\tau_d(t) - \hat{W}_d(t)\right)^2 \geq \left(sat_{\beta_r}(\tau_d(t)) - \Gamma sat_{\beta_r}(\hat{W}_d(t))\right)^2,$$

using a similar proof as developed in [44, Appendix I], using Property 10 to lower bound $K[B_\sigma]$, and canceling terms, an upper bound for (5-26) can be developed as

$$\dot{\tilde{V}}_1 \overset{a.e.}{\leq} -\delta_1 e_\tau^2 + v_1 e_\tau, \tag{5-27}$$

where $v_1 = \gamma_1 \hat{W}_d + c_b \nu_{FES}$, $\gamma_1 = 1 + c_B$, and $\delta_1 \triangleq c_b k_4 + \frac{k_L}{2}$, $\delta_1 > 0$. Integrating (5-27) yields

$$\int_{t_0}^{t} v_1(\varphi) e_\tau(\varphi) d\varphi \overset{a.e.}{\geq} \left(\tilde{V}_1(t) - \tilde{V}_1(t_0) + \int_{t_0}^{t} \delta_1 e_\tau^2(\varphi) d\varphi\right). \tag{5-28}$$

Hence from (5-28), the system is output strictly passive (OSP) from the input $v_1$ to the output $e_\tau$. Therefore, the closed-loop system in (5-21) is passive with a radially unbounded positive definite storage function. From [95, Theorem 2.28], to prove asymptotic tracking, the zero-state observability condition has to be satisfied[3] . By designing $\nu_{FES}$ in (5-18) as $\nu_{FES} \triangleq -k_5 \hat{W}_d$, where $k_5 \triangleq \frac{\gamma_1}{c_b}$, and substituting it into (5-27), $\dot{\tilde{V}}_1 \overset{a.e.}{\leq} -\delta_1 e_\tau^2 \leq 0$. By invoking [78, Corollary 2] and since $\dot{\tilde{V}}_1(w,t) \overset{a.e.}{\leq} -W(w)$, where $W$ is a continuous positive semi-definite function, $|e_\tau| \to 0$ as $t \to \infty$. Since $V_1 \geq 0$ and $\dot{V}_1 \overset{a.e.}{\leq} 0$, $V_1 \in \mathcal{L}_\infty$, hence, $e_\tau, Q_L \in \mathcal{L}_\infty$. From (5-19), $\hat{W}_d \in \mathcal{L}_\infty$, which along with the fact that $\tau_d \in \mathcal{L}_\infty$ implies that $\tilde{W}_d \in \mathcal{L}_\infty$. From (5-18), $u_{FES} \in \mathcal{L}_\infty$, and from (2-11), $u_m \in \mathcal{L}_\infty$. Hence the closed-loop system in (5-21) is passive and asymptotic tracking is achieved. □

[3] In [96], the definition of zero-state observability is described for Filippov solutions.

Theorem 5.1 was used to ensure asymptotic torque tracking. However, to prove that the time derivative of the torque tracking error in (5-16) is bounded, a separate analysis needs to be developed to establish a bound for the closed-loop torque error system in (5-21). The following lemma establishes a bound for $\dot{e}_\tau$.

**Lemma 5.1.** *The torque tracking error $\dot{e}_\tau$ in (5-21) is uniformly bounded for $q \in \mathcal{Q}_M$ in the sense that*

$$|\dot{e}_\tau| \leq \left(2 + c_B\left(1 + \frac{k_4}{k_L} + k_5\right)\right) k_L |e_\tau| + \left(2 + \frac{1}{\Gamma} + c_B\left(1 + k_5\right)\right) \Gamma \beta_r. \tag{5-29}$$

*Proof.* The integral torque tracking error $e_\tau$ can be rewritten as

$$e_\tau = \int_{t_0}^{t} \frac{de_\tau(\varphi)}{d\varphi} d\varphi + C, \tag{5-30}$$

where $C \in \mathbb{R}$ is an integration constant. Based on (5-23), the expression in (5-30) can be used to prove that $\lim_{t\to\infty} \frac{de_\tau(\varphi)}{d\varphi} d\varphi$ exists and is finite. Moreover, based on the development in Theorem 1, $e_\tau, \hat{W}_d, \tilde{W}_d \in \mathcal{L}_\infty$, and hence $\dot{e}_\tau \in \mathcal{L}_\infty$. Using (5-20), (5-21), and (5-22), the upperbound for $|\dot{e}_\tau|$ in (5-29) can be obtained. □

Theorem 5.1 and Lemma 5.1 address the torque tracking objective. The following theorem examines the stability of the closed-loop cadence error system.

**Theorem 5.2.** *Given the closed-loop error system in (5-12), the system is output strictly passive (OSP) from input $v_2 = B_\sigma u_{FES} + c_e \nu_p$ to output $r$ and achieves exponential tracking when $u_m = 0$, provided the following sufficient gain conditions are satisfied*

$$k_2 > \frac{\Theta_1}{c_e}, \quad k_3 > \frac{1}{c_e}. \tag{5-31}$$

*Proof.* Let $V_2 : \mathbb{R}^2 \times \mathbb{R}_{\geq t_0} \to \mathbb{R}$ be a nonnegative, continuously differentiable, storage function defined as

$$V_2 = \frac{1}{2}e^2 + \frac{1}{2}Mr^2. \tag{5-32}$$

The storage function in (5-32) satisfies the following inequalities:

$$\lambda_3\|z\|^2 \leq V_2(z,t) \leq \lambda_4\|z\|^2,$$

where $\lambda_3 \triangleq min(\frac{1}{2}, \frac{c_m}{2})$, $\lambda_4 \triangleq max(\frac{1}{2}, \frac{c_M}{2})$ and $z$ was defined in (5-10). Let $z(t)$ be a Filippov solution to the differential inclusion $\dot{z} \in K[h](z)$, where $K[\cdot]$ is defined as in [78], and $h$ is defined by using (5-1) and (5-2) as $h \triangleq [h_3 \;\; h_4]$, where $h_3 \triangleq r - \alpha e$ and $h_4 \triangleq M^{-1}\{-Vr + \chi + \tilde{N} + B_\sigma u_{FES} - e - B_e(k_1 r - \nu_p + (k_2 + k_3\rho(\|z\|)\|z\|)\, sgn(r))\}$. Using similar arguments as in the proof of Theorem 1, using (5-8), (5-9), (5-12), and Properties 5 and 6, the generalized time derivative of (5-32) can be upper bounded as

$$\dot{\tilde{V}}_2 \overset{a.e.}{\leq} -\alpha e^2 - k_1 c_e r^2 - (k_2 c_e - \Theta_1)\,|r| - (k_3 c_e - 1)\,\rho(\|z\|)\|z\||r| + (B_\sigma u_{FES} + c_e\nu_p)\,r. \tag{5-33}$$

Integrating (5-33) yields

$$\int_{t_0}^{t} v_2(\varphi)r(\varphi)d\varphi \overset{a.e.}{\geq} (\tilde{V}_2(t) - \tilde{V}_2(t_0) + \int_{t_0}^{t} \delta_2\|z(\varphi)\|^2 d\varphi), \tag{5-34}$$

where $\delta_2 = min\{\alpha, k_1 c_e\}$, and $v_2 = B_\sigma u_{FES} + c_e\nu_p$, which can be used to prove that the closed-loop system in (5-12) is output strictly passive (OSP) from input $v_2$ to output $r$, provided the sufficient gain conditions in (5-31) are satisfied. In fact, the system is strictly passive [94] since the integral term in the right-hand side of (5-34) is a positive definite function of the state $z$. Moreover, by setting $\nu_p \triangleq -k_p r$, $k_p \in \mathbb{R}_{>0}$ in (5-33), $\dot{V}_2 \overset{a.e.}{\leq} -\delta_3 V_2$ where $\delta_3 = \frac{min\{\delta_2, k_p\}}{\lambda_4}$, during $q \notin \mathcal{Q}_M$ since $\sigma_m = 0 \implies B_\sigma = 0, \forall m \in \mathcal{M}$, provided the gain conditions in (5-31) are satisfied. Hence, exponential cadence tracking is obtained in the sense that

$$\|z(t)\| \leq \sqrt{\frac{\lambda_4}{\lambda_3}}\|z(t_n)\| exp\left(-\frac{\delta_3}{2}(t-t_n)\right), \forall q \notin \mathcal{Q}_M.$$

□

## 5.3 Experiments

The cadence controller designed in (5-11) and torque controller developed in (5-18) with the learning-based feedforward control term in (5-19) were tested in experiments on both healthy individuals and people with NCs. The switched muscle control input was commanded as stimulation intensities $u_m$ to activate the right and left quadriceps (RQ, LQ), hamstrings (RH, LH), and gluteal (RG, LG) muscle groups for torque (power) tracking, and as current input $u_e$ to the electric motor, which tracked a steady cadence throughout the crank cycle.

### 5.3.1 Participants

Five able-bodied individuals labeled as S1-S5 (three male and two female with age range of 22-26 years) participated in the FES-cycling protocol at the University of Florida. Three participants with NCs (one female, two male) were recruited in the same way as in Section 4.4.1. The same instructions were given during experiments to the healthy individuals and the participants with NCs as in Section 3.3.1. Participant A is a participant with Spina Bifida (SB) and corresponds to Participant B in Section 4.4.1. Participant B has quadriplegia due to spinal cord injury (SCI) and corresponds to Participant D in Section 4.4.1. Participant C is a participant with relapsing remitting multiple sclerosis (MS) and corresponds to Participant C in Section 4.4.1.

### 5.3.2 Experimental Setup

The motorized recumbent tricycle described in Section 3.3.2 with crank position and torque (using a SRM Science Road Wireless Power Meter) feedback was used for the FES-cycling experiments. The cadence and torque controllers were implemented using the same hardware and software as discussed in Section 3.3.2. The stimulation

current amplitudes and frequency were selected as in previous chapters and in [28]. Warm up trials at different operating speeds with and without open-loop stimulation pulse trains were conducted for the participants with NCs to acclimate them to the cycle. An estimate of the nominal torque $\hat{\tau}_n$ was obtained in a separate trial where the muscles were not stimulated and the electric motor was used to passively rotate the participant's legs. The FES-cycling trial had a duration of $t_d = 180$ seconds. The electric motor tracked a time-varying cadence that reached a steady state value of 50 RPM after $t_1 = 16$ seconds. When the experiment duration reached $t_2 = 21$ seconds, the torque controller in (5-18) with learning control designed in (5-19) was activated and hence torque tracking started (i.e., the lower-limb muscles were stimulated).

In cycling, the torque produced about the knee joint contributes significantly to the crank propulsion during the top and bottom portions of the crank cycle (i.e., regions where $q \in \mathcal{Q}_M$, see Figure 5-1) [67, 68]. Due to the importance of the knee joint torque for energy generation to the crank [67], the desired torque trajectory was designed to be a modified function of the knee joint torque transfer ratio, (which can be computed as a function of the crank angle and anatomical lengths of the rider). Hence, the desired torque trajectory is periodic based on the crank angle and nonzero during the stimulation regions (i.e., for $q \in \mathcal{Q}_M$) defined as

$$\tau_d(q) \triangleq \begin{cases} A_d \sin\left(2\frac{q-q_1}{\frac{1}{2}q_2-q_1}\pi\right) & q_1 < q \leq \frac{1}{2}q_2 \\ \frac{A_d}{2}\cos\left(\frac{q-\frac{1}{2}q_2}{\frac{1}{2}q_2}\pi\right) + \frac{A_d}{2} & \frac{1}{2}q_2 < q \leq q_2 \\ 0 & q_2 < q \leq q_3 \\ A_d \sin\left(\frac{q-q_3}{q_4-q_3}\pi\right) & q_3 < q \leq \frac{q_4+q_3}{2} \\ \frac{A_d}{2}\cos\left(\frac{q-\frac{1}{2}(q_4-q_3)+q_3}{\frac{1}{2}(q_4-q_3)}\pi\right) + \frac{A_d}{2} & \frac{q_3+q_4}{2} < q \leq q_4 \\ 0 & q_4 < q \leq q_1 \end{cases},$$

where $q_1, q_2, q_3, q_4 \in \mathbb{R}_{>0}$ are constant predefined crank angles within $q \in \mathcal{Q}_M$ (i.e., related to the start and end of the stimulation regions, see Figure 5-1) of each rider, and the peak torque amplitude $A_d \in \mathbb{R}_{\geq 0}$ is defined as $A_d \triangleq \frac{P_d}{\dot{q}_d}$, where $P_d \triangleq 10$ W, is the maximum desired power demand (unless stated otherwise), and $\dot{q}_d$ is the desired cadence. The generated desired torque trajectory leverages the approach of commanding a desired torque based on a phase-variable (i.e., modified knee kinematic efficiency) in [64, 65, 97] rather than designing the desired torque as an explicit function of time for experiments. The crank position is measured continuously, which ensures that the start and end points of torque tracking regions (i.e., $q \in \mathcal{Q}_M$) are always known. Since the electric motor tracks cadence throughout the entire crank cycle (i.e., inherently advancing the cycle in and out of the torque tracking regions), the spatial feedforward learning input can be applied for torque tracking without requiring the typical resetting assumption before the start of a new period (i.e., crank cycle). The control gains introduced in (2-11), (5-11), (5-18), and (5-19) were selected as follows: $k_m \in [4.5, 5]$, $\alpha \triangleq 2.5$, $k_1 \triangleq 9$, $k_2 \triangleq 0.1$, $k_3 \triangleq 0.01$, $k_4 \in [60, 250]$, $k_5 \triangleq 0.5$, $k_p \triangleq 0.001$, $\Gamma \in [0.95, 1]$, and $k_L \in [25, 45]$.

### 5.4 Results

The FES-cycling protocol with cadence and torque tracking objectives was completed by all participants. Table 5-1 summarizes the average of the cadence error (i.e., the time derivative of (5-1)), the average of the torque tracking error $e_\tau$ in (5-16), the average of the time derivative of (5-16), and its respective average power output tracking error from the start of torque tracking until the end of the experiment (i.e., during $t \in [t_2, t_d]$ seconds). The power output tracking error can be computed as the difference between the active power output $P_a = \tau_a \dot{q}$ and the desired power output $P_D = \tau_d \dot{q}_d$. For post-processing purposes and to account for the time-delayed nature of muscle activation, the actual torque error $\dot{e}_\tau$ was computed by averaging the active torque output $\tau_a$ within a time window of 0.1 s after the stimulation inputs were applied and withdrawn

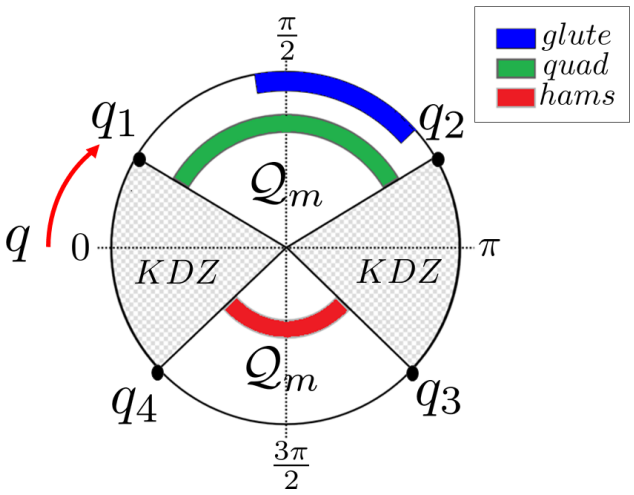


Figure 5-1. Schematic of the crank angles where the lower-limb muscles are activated and where the desired torque trajectory $\tau_d$ is nonzero ($q \in \mathcal{Q}_M$). The constant predetermined crank angles $q_1$ and $q_3$ determine the start of the stimulation regions, while $q_2$ and $q_4$ define the end of those stimulation regions. Hence the gray areas labeled as $KDZ$ denote the crank angles where muscles are not activated, i.e., $q \notin \mathcal{Q}_M$.

(see Discussion section for more details). Figure 5-2 shows the root-mean-squared error (RMS) of the cadence tracking error calculated over a moving time interval window of 12 seconds, and the RMS of the torque tracking error calculated over a moving time interval window of 1.2 seconds of Participant B. Figure 5-3 depicts the stimulation intensities delivered to the muscle groups $u_m$, the electric motor current input $u_e$, and the feedforward learning term $\hat{W}_d$ for Participant B. Figure 5-4 illustrates the switched muscle control inputs, the desired and actual torque output, and the feedforward learning control input for healthy Participant S3 (as a common example) after 2 minutes of cycling.

To assess the effect of the cadence and peak power output demands, four trials were conducted for Participant S3. Table 5-2 summarizes the results of four cycling experiments for Participant S3 using $\dot{q}_d = 40$ RPM and $\dot{q}_d = 50$ RPM paired with $P_d = 5$ W and $P_d = 10$ W. Figure 5-5 illustrates the actual power output $P_a$ elicited by Participant S3 compared to the desired power $P_D$ for an entire cycling protocol. Figure 5-6 depicts

the actual power output $P_a$ as a function of the crank angle obtained from Participant S3 during the first 50 crank cycles and the subsequent 50 crank cycles.

Table 5-1. Tracking results for all participants: average cadence tracking error $\dot{e}$, average torque error $e_\tau$, average actual torque error $\dot{e}_\tau$ and its corresponding average power error reported as mean value $\pm$ standard deviation (STD).

| Participant | $\dot{e}$ (RPM) | $e_\tau$ (N·m·s ) | $\dot{e}_\tau$ (N·m) | Power Error (W) |
|---|---|---|---|---|
| S1 | 0.03±1.07 | 0.08±0.08 | 0.65±0.24 | 3.41±1.27 |
| S2 | 0.01±1.58 | 0.05±0.12 | 0.24±0.51 | 1.26±2.56 |
| S3 | 0.02±0.85 | 0.10±0.12 | 0.41±0.30 | 2.15±1.55 |
| S4 | 0.02±1.27 | 0.13±0.18 | 0.31±0.06 | 1.61±0.32 |
| S5 | 0.00±0.96 | 0.12±0.14 | 0.47±0.18 | 2.45±0.94 |
| Mean (S1-S5) | 0.02±1.17 | 0.10±0.13 | 0.42±0.30 | 2.18±1.52 |
| A# | 0.02±0.68 | 0.04±0.06 | 0.06±0.03 | 0.30±0.14 |
| B | 0.00±1.78 | 0.06±0.09 | 0.39±0.19 | 2.11±0.99 |
| C# | 0.01±0.96 | 0.06±0.10 | 0.18±0.02 | 0.91±0.13 |
| Mean (A-C) | 0.01±1.23 | 0.05±0.09 | 0.21±0.11 | 1.11±0.58 |
| Combined Mean | 0.01±1.20 | 0.08±0.12 | 0.34±0.25 | 1.78±1.25 |

# Participants A and C tracked a peak power demand of $P_d = 5$ W

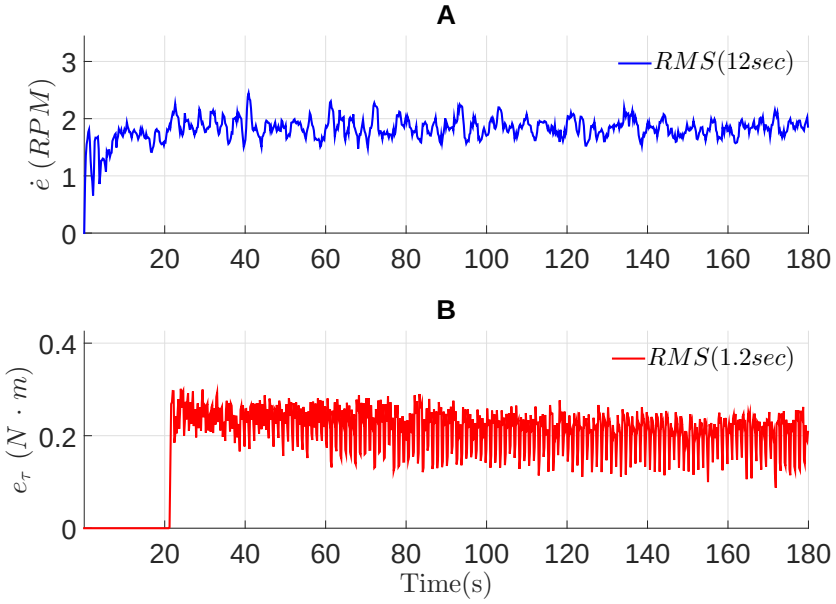


Figure 5-2. Tracking performance for Participant B. A) RMS of the cadence tracking error $\dot{e}$ computed with a moving time interval window of 12 seconds. B) RMS of the torque tracking error $e_\tau$ computed with a moving time interval window of 1.2 seconds.

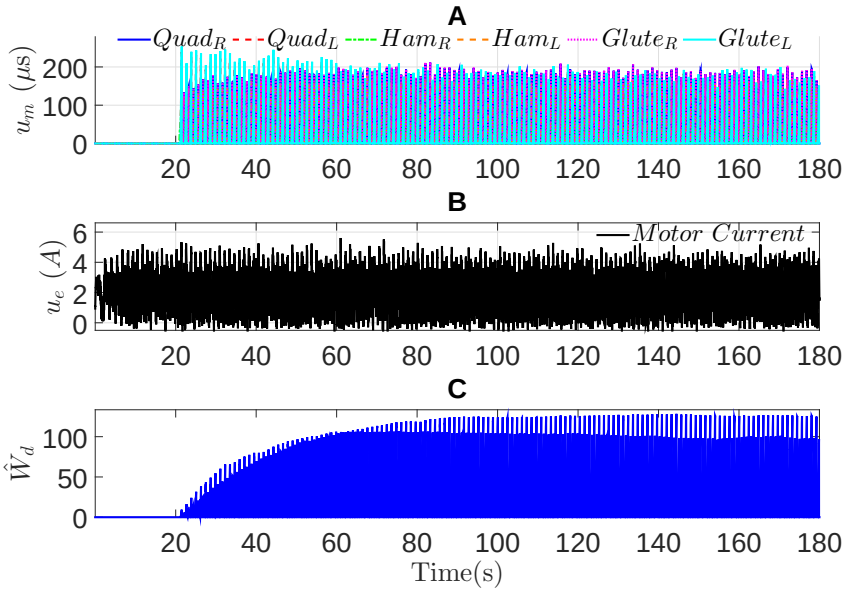


Figure 5-3. Control inputs for Participant B. A) Stimulation intensities delivered to the six muscle groups denoted by $u_m$ for each muscle. B) Electric motor current input $u_e$. C) Learning feedforward term $\hat{W}_d$.

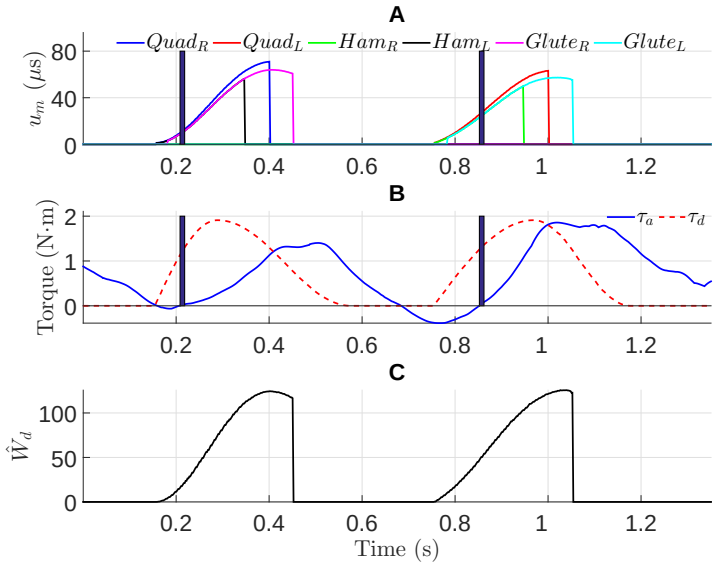


Figure 5-4. FES stimulation intensities, torque performance, and learning feedforward input during a single crank cycle for Participant S3 after 2 minutes of cycling. A) FES stimulation intensities. B) Active torque output $\tau_a$ and desired torque $\tau_d$. The vertical solid bars correspond to the time where the torque output rises above zero, which illustrates the variability in muscle torque output is greatly affected by the electromechanical delay (EMD) in the muscle activation dynamics [87, 98, 99]. C) Learning feedforward input.

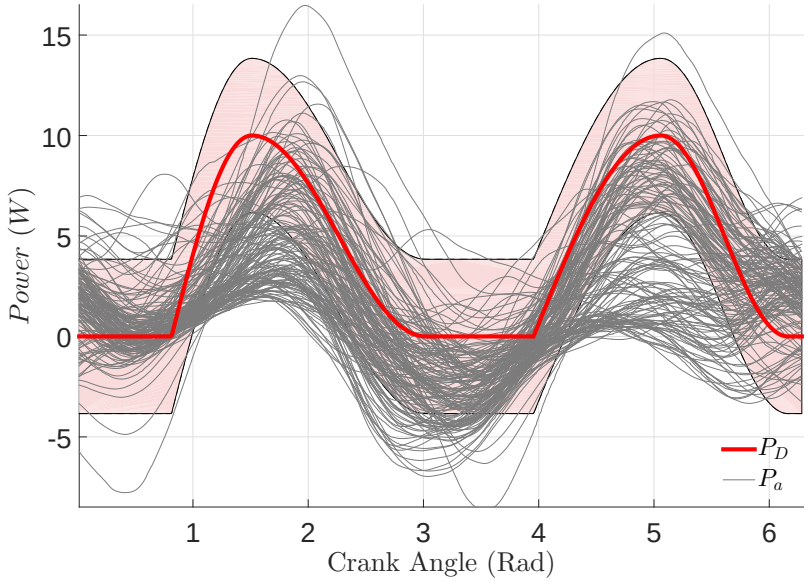


Figure 5-5. Active power $P_a$ elicited by Participant S3 as a function of the crank angle during a cycling experiment with peak power of $P_d = 10$ W and $\dot{q}_d = 50$ RPM. The light red area delineates $\pm 1$ standard deviation from the desired power $P_D$.

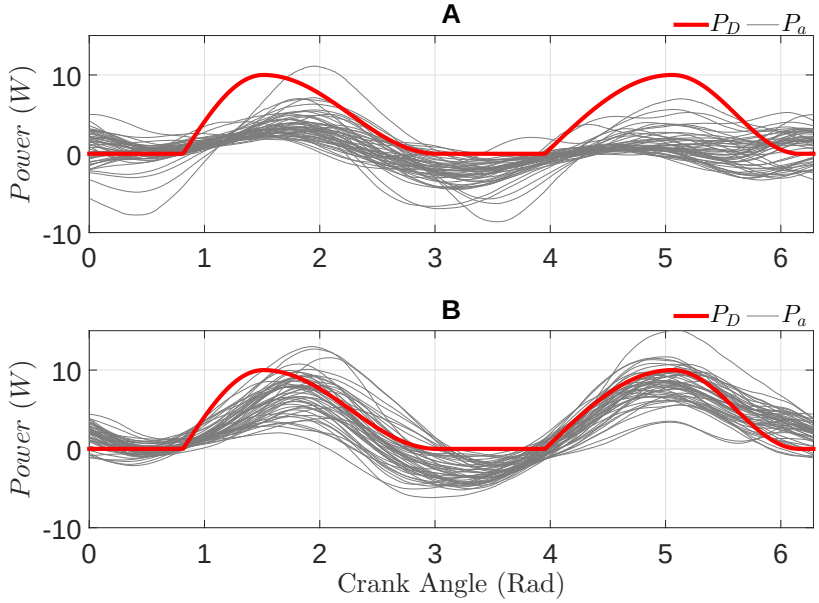


Figure 5-6. Active power $P_a$ comparison of Participant S3 during a cycling experiment with peak power of $P_d = 10$ W and $\dot{q}_d = 50$ RPM. A) Active power $P_a$ elicited during the first 50 crank cycles of the experiment. B) Active power $P_a$ elicited during the subsequent 50 crank cycles.

Table 5-2. Tracking results using different peak power $P_d$ and cadence $\dot{q}_d$ demands for Participant S3: average cadence tracking error $\dot{e}$, average torque error $e_\tau$, average actual torque error $\dot{e}_\tau$ and its corresponding average power error reported as mean value $\pm$ standard deviation (STD).

| Cadence (RPM) | $\dot{e}$ (RPM) | | $e_\tau$ (N·m·s) | | $\dot{e}_\tau$(N·m) | | Power Error (W) | |
|---|---|---|---|---|---|---|---|---|
| | Peak Power (W) | | Peak Power (W) | | Peak Power (W) | | Peak Power (W) | |
| | $P_d = 5$ | $P_d = 10$ | $P_d = 5$ | $P_d = 10$ | $P_d = 5$ | $P_d = 10$ | $P_d = 5$ | $P_d = 10$ |
| $\dot{q}_d$ =40 | 0.00$\pm$0.69 | 0.01$\pm$0.99 | 0.09$\pm$0.10 | 0.11$\pm$0.17 | 0.25$\pm$0.19 | 0.02$\pm$0.25 | 1.54$\pm$1.29 | 0.88$\pm$1.97 |
| $\dot{q}_d$ =50 | 0.02$\pm$0.91 | 0.02$\pm$0.85 | 0.06$\pm$0.06 | 0.10$\pm$0.12 | 0.32$\pm$0.18 | 0.41$\pm$0.30 | 1.67$\pm$0.95 | 2.15$\pm$1.55 |
| Mean | 0.01$\pm$0.81 | 0.02$\pm$0.92 | 0.08$\pm$0.08 | 0.11$\pm$0.15 | 0.29$\pm$0.19 | 0.22$\pm$0.28 | 1.61$\pm$1.13 | 1.52$\pm$1.77 |

## 5.5 Discussion

The goal of this chapter was to demonstrate the feasibility of the torque controller developed in (5-18) with learning control $\hat{W}_d$ in (5-19) to track a desired torque trajectory by the stimulation of lower-limb muscles and to regulate cadence by the controller in (5-11). The experimental results demonstrated an average cadence tracking error $\dot{e}$ of $0.02 \pm 1.17$ RPM for the healthy individuals and $0.01 \pm 1.23$ RPM for the participants with NCs. The average power tracking error is $2.18 \pm 1.52$ W for the able-bodied individuals and $1.11 \pm 0.58$ W for the participants with NCs (see Table 5-1). The feedforward learning control exploited the periodicity of the desired torque trajectory designed as a function of the crank angle. Hence, by leveraging past control inputs the torque controller showed robustness and displayed power tracking improvements as depicted in Figure 5-6 for Participant S3. In Figure 5-6, the crank angles where the power drops below zero describe the regions where the muscles were not stimulated and only the motor tracked cadence or where despite the fact the muscles were stimulated not enough contraction was built to evoke positive active power. In addition, the learning controller was able to compensate for different power demands while the motor regulated different cadences as reported for the four trials in Table 5-2 for Participant S3.

The results presented in this study align with previous FES literature where the focus is to investigate how the lower-limb muscles activated via FES and motorized assistance cooperate to achieve power control objectives. In [62], lower-limb muscles were stimulated in a FES-cycling protocol to track power discretely (i.e., the power reading was averaged over a full crank cycle and the controller was updated only at the beginning of the crank cycle) and experimental results were presented for three healthy participants. In [61], the control design and stability analysis was presented for an FES-cycling system where the muscle groups are stimulated to achieve a desired cadence while the electric motor tracks a resistive torque. However no experimental results were reported in [61]. A closed-loop control strategy with motor assistance was

reported in [34], where power output (stimulation of muscles) and cadence (electric motor control) were monitored simultaneously for a paraplegic. Two major cycling protocols were conducted in [34]; in the first protocol, the cadence reference changed in steps while the muscles tracked a constant 10 W power reference, and in the second protocol a constant cadence was tracked by the motor while the power tracked by the muscles varied between 10 and 15 W. However, the tracking performance was not quantitatively reported in [34]. In [29], a power control FES-cycling objective with varying amplitudes between 5 and 10 W was implemented in three paraplegics via sliding mode control achieving tracking performance of $7.4 \pm 1.4$ % error. In [9], the stimulation of the quadriceps and hamstrings was used to reduce the torque contribution of a powered exoskeleton during locomotion for three paraplegics. Despite the existing results in the FES community to address power tracking, the lack of homogeneity in calculating and reporting the power tracking performance complicates the cross comparison among the published results (i.e., some studies isolate the torque contribution by the muscles while others do not). Hence, there is motivation to develop an extensive power tracking FES-cycling study to compare the performance of closed-loop controllers using a large number of participants with NCs.

In this study, the active torque elicited by the participants was obtained by subtracting the estimate of the nominal torque of the system from the continuous torque measurements. However, the inherent noise in the nominal torque estimate of the rider's passive dynamics obtained in a separate trial, when no electrical stimulation was present, may have affected the torque tracking error in the FES-cycling experiments. Future efforts will focus on eliminating the requirement of estimating the passive dynamics of the rider.

Muscle fatigue and electromechanical delay (EMD) are factors that likely played a role in degrading the torque tracking performance during experiments for both healthy individuals and participants with NCs. Muscle fatigue is a well known issue in FES

applications and potential alternatives have been developed such as the example in [100]. However, the complexity in the muscle response to electrical stimulation depends on the muscle activation dynamics, which is affected by the EMD. As depicted in Figure 5-4, there exists a muscle contraction delay illustrated by the time difference between the onset of the stimulation and the point where the active torque elicited by the participant rises above baseline (zero torque line). Also, there exists a muscle relaxation delay illustrated by the fact that when the stimulation intensities are set to zero (e.g., right after the end of a stimulation region), the muscles continue eliciting torque for hundreds of milliseconds. Recently in [87], a comprehensive protocol that electrically stimulated the quadriceps muscle groups under isometric conditions concluded that the EMD increases (i.e., varies with time) as the number of muscle contraction increases. The dual effect of muscle contraction and relaxation delay is an important challenge in the development of rehabilitative treatments using FES, as noted in the present study. It was further demonstrated in [87], that each muscle control effectiveness, denoted in the present work as $B_\sigma$, decays with muscle fatigue. In [34], a practical alternative was recommended to compensate for the muscle delay dynamics by advancing (i.e., shift forward) the muscle stimulation pattern (i.e., switching signals) proportional to the rider's cadence. The results of the present study motivate the further development of a FES-cycling learning controller that constructively compensates for the muscle EMD with guarantee of stability.

Additional challenges were present in the experiments with participants with NCs. Participant B (quadriplegic) required high stimulation intensities throughout the entire experiment, as illustrated in Figure 5-3, due to the lack of muscle strength and mass. Also, Participant B suffered from intermittent spasms during the experiment, which acted as disturbances to the cycle-rider system. Participants A and C elicited asymmetric torque profiles during the upstroke and downstroke portions of the crank cycle. Nevertheless, the torque controller was able to modify the stimulation intensities

to allow the participants to complete the tracking task during the experiment duration. However for Participants A and C, due to the lack of muscle strength, the peak power demand $P_d$ was set to 5 W in contrast to the 10 W required for the healthy individuals and Participant B. For participants with asymmetries in their ability to elicit torque, a split-crank bicycle is an ideal testbed for further experiments. A split-crank bicycle allows decoupling of the limb trajectories, thus granting different torque and cadence objectives for each leg.

The results of the able-bodied individuals and participants with NCs show that by switching across different muscles torque/power tracking was achieved. Clinical trials with a larger population of participants with NCs such as individuals with traumatic brain injury, hemiplegia, Parkinson's disease, cerebral palsy, etc., are required to investigate the long-term impact of the control methodology developed in this chapter.

## 5.6 Concluding Remarks

A cadence controller that commanded current to the electric motor and a torque controller that commanded stimulation intensities to six muscle groups were implemented in this chapter to achieve cadence and torque tracking in a FES-cycling protocol. The switched muscle torque controller included a feedforward learning input that compensated for the periodic dynamics of the desired torque trajectory. A passivity-based analysis was developed to ensure stability of the torque and cadence closed-loop systems. For both healthy individuals and people with NCs, the combined average cadence tracking error is $0.01 \pm 1.20$ RPM and the combined average power tracking error is $1.78 \pm 1.25$ W.

The experimental results in people with NCs demonstrate the ability of the switched learning controller to elicit active torque output in participants demonstrating varied motor impairments as a result of spinal cord injury, spina bifida, and multiple sclerosis. However, based on the tracking performance, muscle fatigue and the effect of EMD are important factors that degrade the efficacy of the developed control methodology.

# CHAPTER 6
# CONCLUSIONS

Learning control methods, such as RLC, are powerful tools to yield suitable tracking performance during time or state periodic tasks, where continuous operation without resetting of the system is satisfied. As a result, asymptotic tracking (i.e., precise trajectory tracking) is achieved by the learning controllers despite uncertainty in the plant dynamics. Cycling is naturally a periodic/repetitive process where cadence and torque tracking have been the primary objectives. The focus of this dissertation was to leverage the time or spatial periodicities of the desired tracking objectives for the cycle-rider system to design learning controllers in the context of FES-cycling. The switched control authorities by the lower-limb muscle groups and the electric motor present the benefits of coupling the physiological and functional benefits of FES with the continuous, consistent and repeatable operation of the electric motor. Also, learning control offers the advantage to design a feedforward input added to the controller to rely less on high gain/ high frequency feedback such as sliding mode control. The implications of reducing high gain/frequency content in the muscle stimulation inputs can aid to extend the cycling duration and reduce muscle fatigue. In addition, passivity is a suitable tool to ensure safe human-robot interaction as demonstrated during power tracking in FES-cycling.

The results of this dissertation address the design of switched learning controllers and its stability analysis through Lyapunov- and passivity- based methods. Experimental validation of the learning controllers was performed in healthy individuals and people with NCs. The relevance of the experimental results in able-bodied individuals is twofold. First, experiments involving healthy individuals helps with the validation of the control technique and tests its feasibility and efficacy before its translation to more complex and challenging experiments with persons with NCs. And second, an ideal performance of the controller can be obtained and cross-comparisons with other control techniques can be made. The development of experiments with NCs seeks to bridge the gap between

the contributions of the control system community and clinical practice. Ultimately, the benefits of FES technologies have to be concluded from longitudinal studies with large population and broad range of movement disorders. However, relevant insights are obtained by interacting with participants with NCs regarding the practical value of a particular cycling protocol (including the implemented controller) and the faced challenges in experiments inspire new technical contributions for future control design.

In Chapter 3, a switched RLC method was found to be more effective than a pure robust controller (i.e., without feedforward control) in the tracking of a time periodic cadence trajectory. The implementation of the RLC offers the advantage to add a feedforward term to the control input by exploiting the periodicity of the desired trajectory. Compared to classical adaptive control, learning control does not rely on the knowledge of a regression matrix of the dynamics. The experimental results, more evident in healthy subjects, demonstrate the typical error minimization from period to period that is unique to the performance obtained from learning controllers in literature. However, there are challenges ubiquitous to FES such as muscle fatigue, the potential destabilizing effect of electromechanical delay (EMD) and other factors related to the neurological motor control of an individual that degrade tracking performance.

In Chapter 4, the development of a distributed repetitive learning control strategy was formulated to add a feedforward input to each of the lower-limb muscle groups and electric motor current based on past inputs. By the construction of the filtered tracking error, the switched learning controller affects both cadence and position tracking. Chapter 4 was inspired by the advances of distributed learning in network control and other applications where multiple agents or actuators are used to cooperatively perform a tracking problem. The tuning of the learning controllers was proven to affect the tracking performance, where bigger learning gains resulted in better position and cadence tracking performance as illustrated for a healthy individual. An interesting remark is that bigger learning gains results in steady (low amplitude) stimulation intensities compared

to its counterpart (small learning gains) resulting in higher stimulation intensities. This observation can be explained by the fact that for small learning gains, the robust part of the switching controller has to compensate for the most part of the uncertainties and disturbances of the system. Higher stimulation intensities during cycling represent an important factor that leads to accelerated fatigue or even experiment termination for people with hypersensitivity (e.g., individuals post-stroke). The distributed learning control approach was able to adapt for participants with NCs. The amplitude of the learning inputs may be representative of the muscle strength and tone, and the level of asymmetries between the legs as illustrated with the comparison between a healthy individual and a participant with movement disorders. The percentage of time during which the participants with NCs were actively stimulated suggests an adequate balance between the FES and motorized contributions to maintain the desired cadence. Moreover, stimulation times have a high impact in the rate of muscle fatigue, which affects cycling duration and thus the amount of dose of rehabilitative stimulation.

In Chapter 5, the dual objective of torque and cadence tracking was accomplished by designing a novel spatial learning controller for the muscles and a robust sliding-mode controller for the electric motor. Due to the importance of the knee joint torque for energy generation to the crank, the desired torque trajectory was designed to be a modified function of the knee torque transfer ratio (which can be computed as a function of the crank angle). Hence, Chapter 5 leverages the idea of spatial learning control to investigate the torque tracking defined by a periodic function of the crank position. The electric motor provided steady cadence throughout the entire crank cycle. The feedforward learning control exploited the periodicity of the desired torque trajectory designed as a function of the crank angle. Hence, by leveraging past control inputs the torque controller showed robustness and displayed power tracking improvements during the experiments. A passivity-based analysis was developed to ensure safe interaction

between the human and the machine. Moreover, asymptotic and exponential tracking were obtained for the torque and cadence tracking objectives, respectively.

Switching control is inherent in FES-cycling since multiple lower limb muscles are needed to produce a coordinated movement. Switching between multiple muscle groups and the electric motor makes the overall system a switched system. Most results for switched systems, including the ones for FES-cycling [11, 12], have relied on robust control methods to ensure exponential tracking by virtue of a negative definite Lyapunov function derivative. Dwell time conditions have been developed when switching between controlled (stabilizable) and uncontrolled subsystems based on the subsystems decay or growth rates. However, in the control developments of Chapters 3-5 the use of learning control yields a negative semi-definite Lyapunov function derivative. Hence, a generalization of the LaSalle-Yoshizawa for nonsmooth analysis in [78] was invoked for the present work in the context of switched systems to ensure asymptotic tracking. Moreover, the recent contribution in [101] for switched systems theory presents strong analytical tools to design adaptive and learning controllers and ensure stability of complex systems such as in human-machine interaction applications.

During experiments muscle fatigue, EMD, disturbances in the cycle, and other factors related to the neurological motor control of the participants contributed to tracking performance degradation. Participants with movement disorders as a result of neurological conditions such as spinal cord injury (SCI), spina bifida, multiple sclerosis, and post stroke displayed intermittent muscle spasms, asymmetries between the lower extremities, and potential electrical stimulation sensitivity from residual sensory feedback. For SCI participants, the lack of muscle mass and strength, intermittent spasms (acting as external disturbances), and the lack of neurological motor control resulted in increased stimulation intensities in most cycling protocols. Asymmetries between legs while eliciting active torque was a major impediment to achieve higher power outputs in Chapter 5 added to the fact that most participants with NCs have low muscle mass and tone in

their lower-limb muscle groups. An extension of the developed control techniques to the case where participants with residual neurological motor control (e.g., post stroke individuals) are allowed and encouraged to participate in cycling performance is the focus of future research. For participants with asymmetries in their ability to elicit torque, a split-crank bicycle is an ideal testbed for further experiments. A split-crank bicycle allows decoupling of the limb trajectories, thus granting different torque and cadence objectives for each leg. Long-term clinical trials with a larger and broader population are needed to expand the findings of this dissertation while implementing switched learning controllers. The future development of FES closed-loop controllers have to take into account target populations to improve the efficacy of the control methodology and boost the potential for clinical adoption. For example, the design of FES controllers for adults with neural disorders such as stroke and Parkinson's diseases should be different compared to the studies involving participants with pediatric disorders such as cerebral palsy, spina bifida, etc. In addition, future FES-cycling studies should focus on analyzing standard clinical outcome measures resulting from the implementation of closed-loop learning controllers for FES-cycling and the challenges related to clinical adoption.

The experimental results presented in this dissertation quantify the cycling performance using position, cadence, and torque from the sensors fitted in the cycle. Future work may focus on implementing FES-cycling protocols that exploit sensory feedback from the rider using wearable sensors that measure muscle activation via electromyography (EMG). The use of sensory feedback enables the development of closed-loop controllers that take into account the muscle activation and human intent such as in myoelectric control. Despite the recent advances in human sensing and motorized devices, a major problem to be solved in the context of human-machine interaction while developing neuroprostheses is how to appropriately share the control between the robotic device and the human. Particularly, the development of a framework for shared autonomy is fundamental to achieve predictable autonomous behavior, providing

assistance to the human when needed, but also adapting to the time varying human's abilities and preferences.

The performance of FES controllers is affected by a time-varying muscle effectiveness (decreasing with muscle fatigue) and EMD (increasing with muscle fatigue). The results of the present dissertation, particularly the results in Chapter 5, motivate the further development of a FES-cycling learning controller that compensates for the muscle EMD. Additionally, adaptive techniques such as Concurrent Learning (CL) and Integral Concurrent Learning (ICL) [102] are promising methodologies to be applied for FES-cycling, or for applications involving human-machine interaction, from a stability analysis perspective and the potential tracking performance advantages. The concept of sparsity design for learning controllers in resource-constrained systems provides an interesting topic of research in the context of human cyper-physical systems, such as the FES-cycling problem. Besides the implementation of learning controllers in this dissertation to FES-cycling, the fields of adaptive/learning control and switched systems present endless opportunities to advance human rehabilitation engineering, an exciting field that seeks to enhance the quality of lives of people with NCs.

# REFERENCES


[1] P. H. Peckham and J. S. Knutson, "Functional electrical stimulation for neuromuscular applications," *Annu. Rev. Biomed. Eng.*, vol. 7, pp. 327–360, Mar. 2005.

[2] P. J. Cienfuegos, A. Shoemaker, R. W. Grange, N. Abaid, and A. Leonessa, "Classical and adaptive control of ex vivo skeletal muscle contractions using Functional Electrical Stimulation (FES)," *PLOS ONE*, vol. 12, no. 3, pp. 1–29, March 2017.

[3] C. Rouse, V. H. Duenas, C.Cousin, A. Parikh, and W. E. Dixon, "A switched systems approach based on changing muscle geometry of the biceps brachii during functional electrical stimulation," *IEEE Control Syst. Lett.*, vol. 2, no. 1, pp. 73–78, 2018.

[4] B. Lew, N. Alavi, B. K. Randhawa, and C. Menon, "An exploratory investigation on the use of closed-loop electrical stimulation to assist individuals with stroke to perform fine movements with their hemiparetic arm," *Front. Bioeng. Biotechnol.*, vol. 4, p. 20, 2016.

[5] J. McCabe, M. Monkiewicz, J. Holcomb, S. Pundik, and J. J. Daly, "Comparison of robotics, functional electrical stimulation, and motor learning methods for treatment of persistent upper extremity dysfunction after stroke: A randomized controlled trial," *Arch. Phys. Med. Rehabil.*, vol. 96, no. 6, pp. 981 – 990, 2015.

[6] R. Nataraj, M. L. Audu, and R. J. Triolo, "Restoring standing capabilities with feedback control of functional neuromuscular stimulation following spinal cord injury," *Med. Eng. Phys.*, vol. 42, pp. 13–25, April 2017.

[7] A. J. Hunt, B. M. Odle, L. M. Lombardo, M. L. Audu, and R. J. Triolo, "Reactive stepping with functional neuromuscular stimulation in response to forward-directed perturbations," *J Neuroeng Rehabil*, vol. 14, no. 1, pp. 1–12, June 2017.

[8] N. A. Alibeji, N. A. Kirsch, and N. Sharma, "An adaptive low-dimensional control to compensate for actuator redundancy and FES-induced muscle fatigue in a hybrid neuroprosthesis," *Control Eng. Pract.*, vol. 59, pp. 204–219, 2017.

[9] K. H. Ha, S. A. Murray, and M. Goldfarb, "An approach for the cooperative control of FES with a powered exoskeleton during level walking for persons with paraplegia," *IEEE Trans. Neural Syst. Rehabil. Eng.*, vol. 24, no. 4, pp. 455–466, 2016.

[10] N. A. Alibeji, N. A. Kirsch, and N. Sharma, "A muscle synergy-inspire adaptive control scheme for a hybrid walking neuroprosthesis," *Front. Bioeng. Biotechnol.*, vol. 3, no. 203, pp. 1–13, Dec. 2015.

[11] M. J. Bellman, R. J. Downey, A. Parikh, and W. E. Dixon, “Automatic control of cycling induced by functional electrical stimulation with electric motor assistance,” *IEEE Trans. Autom. Science Eng.*, vol. 14, no. 2, pp. 1225–1234, April 2017.

[12] M. J. Bellman, T. H. Cheng, R. J. Downey, C. J. Hass, and W. E. Dixon, “Switched control of cadence during stationary cycling induced by functional electrical stimulation,” *IEEE Trans. Neural Syst. Rehabil. Eng.*, vol. 24, no. 12, pp. 1373–1383, 2016.

[13] M. J. Bellman, T.-H. Cheng, R. J. Downey, and W. E. Dixon, “Stationary cycling induced by switched functional electrical stimulation control,” in *Proc. Am. Control Conf.*, 2014, pp. 4802–4809.

[14] M. J. Bellman, T.-H. Cheng, R. Downey, and W. E. Dixon, “Cadence control of stationary cycling induced by switched functional electrical stimulation control,” in *Proc. IEEE Conf. Decis. Control*, 2014.

[15] K. Ragnarsson, “Functional electrical stimulation after spinal cord injury: current use, therapeutic effects and future directions,” *Spinal Cord*, vol. 46, pp. 255–274, 2008.

[16] P. Bauer, C. Krewer, S. Golaszewski, E. Koenig, and F. Müller, “Functional electrical stimulation-assisted active cycling-therapeutic effects in patients with hemiparesis from 7 days to 6 months after stroke: A randomized controlled pilot study,” *Arch. Phys. Med. Rehabil.*, vol. 96, no. 2, pp. 188 – 196, 2015.

[17] S. Ferrante, A. Pedrocchi, G. Ferrigno, and F. Molteni, “Cycling induced by functional electrical stimulation improves the muscular strength and the motor control of individuals with post-acute stroke,” *Eur. J. Phys. Rehabil. Med.*, vol. 44, no. 2, pp. 159–167, 2008.

[18] C. L. Sadowsky, E. R. Hammond, A. B. Strohl, P. K. Commean, S. A. Eby, D. L. Damiano, J. R. Wingert, K. T. Bae, and I. John W. McDonald, “Lower extremity functional electrical stimulation cycling promotes physical and functional recovery in chronic spinal cord injury,” *J. Spinal Cord Med.*, vol. 36, no. 6, pp. 623–631, 2013.

[19] H. R. Berry, C. Perret, B. A. Saunders, T. H. Kakebeeke, N. de N. Donaldson, D. B. Allan, and K. J. Hunt, “Cardiorespiratory and power adaptation to stimulated cycle training in paraplegia,” *Med. Sci. Sports Exerc.*, vol. 40, no. 9, pp. 1573–1580, Sep. 2008.

[20] C.-W. Peng, S.-C. Chen, C.-H. Lai, C.-J. Chen, C.-C. Chen, J. Mizrahi, and Y. Handa, “Review: Clinical benefits of functional electrical stimulation cycling exercise for subjects with central neurological impairments,” *J. Med. Biol. Eng.*, vol. 31, pp. 1–11, 2011.

[21] D. J. Reinkensmeyer, J. L. Emken, and S. C. Cramer, “Robotics, motor learning, and neurologic recovery,” *Annual Review of Biomedical Engineering*, vol. 6, no. 1, pp. 497–525, 2004.

[22] L. Marchal-Crespo and D. J. Reinkensmeyer, “Review of control strategies for robotic movement training after neurologic injury,” *J. Neuroeng. Rehabil.*, vol. 6, no. 1, 2009.

[23] V. R. Edgerton, R. D. de Leon, S. J. Harkema, J. A. Hodgson, N. London, D. J. Reinkensmeyer, R. R. Roy, R. J. Talmadge, N. J. Tillakaratne, W. Timoszyk, and A. Tobin, “Retraining the injured spinal cord,” *J. Physiol.*, vol. 533, no. 1, pp. 15–22, 2001.

[24] V. Edgerton and R. R. Roy, “Paralysis recovery in humans and model systems,” *Curr. Opin. Neurobiol.*, vol. 12, no. 6, pp. 658–667, 2002.

[25] O. Raineteau and M. E. Schwab, “Plasticity of motor systems after incomplete spinal cord injury,” *Nat. Rev. Neurosci.*, vol. 2, pp. 263–273, 2001.

[26] L. L. Cai, A. J. Fong, C. K. Otoshi, Y. Liang, J. W. Burdick, R. R. Roy, and V. R. Edgerton, “Implications of assist-as-needed robotic step training after a complete spinal cord injury on intrinsic strategies of motor learning,” *Journal of Neuroscience*, vol. 26, no. 41, pp. 10 564–10 568, 2006.

[27] W. E. Dixon and M. Bellman, “Cycling induced by functional electrical stimulation: A control systems perspective,” *ASME Dyn. Syst. & Control Mag.*, vol. 4, no. 3, pp. 3–7, Sept 2016.

[28] V. H. Duenas, C. A. Cousin, A. Parikh, P. Freeborn, E. J. Fox, and W. E. Dixon, “Motorized and functional electrical stimulation induced cycling via switched repetitive learning control,” *IEEE Trans. Control Syst. Tech.*, to appear.

[29] A. Farhoud and A. Erfanian, “Fully automatic control of paraplegic FES pedaling using higher-order sliding mode and fuzzy logic control,” *IEEE Trans. Neural Syst. Rehabil. Eng.*, vol. 22, no. 3, pp. 533–542, 2014.

[30] R. J. Downey, T.-H. Cheng, M. J. Bellman, and W. E. Dixon, “Closed-loop asynchronous electrical stimulation prolongs functional movements in the lower body,” *IEEE Trans. Neural Syst. Rehabil. Eng.*, vol. 23, no. 6, pp. 1117–1127, 2015.

[31] N. Sharma, K. Stegath, C. M. Gregory, and W. E. Dixon, “Nonlinear neuromuscular electrical stimulation tracking control of a human limb,” *IEEE Trans. Neural Syst. Rehabil. Eng.*, vol. 17, no. 6, pp. 576–584, Jun. 2009.

[32] C. M. Gregory, W. E. Dixon, and C. S. Bickel, “Impact of varying pulse frequency and duration on muscle torque production and fatigue,” *Muscle Nerve*, vol. 35, no. 4, pp. 504–509, Apr. 2007.

[33] S. A. Binder-Macleod, E. E. Halden, and K. A. Jungles, “Effects of stimulation intensity on the physiological responses of human motor units,” *Med. Sci. Sports. Exerc.*, vol. 27, no. 4, pp. 556–565, Apr. 1995.

[34] K. J. Hunt, B. Stone, N.-O. Negård, T. Schauer, M. H. Fraser, A. J. Cathcart, C. Ferrario, S. A. Ward, and S. Grant, “Control strategies for integration of electric motor assist and functional electrical stimulation in paraplegic cycling: Utility for exercise testing and mobile cycling,” *IEEE Trans. Neural Syst. Rehabil. Eng.*, vol. 12, no. 1, pp. 89–101, Mar. 2004.

[35] J. Szecsi, A. Straube, and C. Fornusek, “Comparison of the pedalling performance induced by magnetic and electrical stimulation cycle ergometry in able-bodied subjects,” *Med. Eng. Phys.*, vol. 36, no. 4, pp. 484–489, 2014.

[36] D. Liberzon, *Switching in Systems and Control*. Birkhauser, 2003.

[37] S. Arimoto, S. Kawamura, and F. Miyazaki, “Bettering operation of dynamic systems by learning: A new control theory for servomechanism or mechatronics systems,” in *Proc. IEEE Conf. Decis. Control*, Dec. 1984, pp. 1064–1069.

[38] D. A. Bristow, M. Tharayil, and A. G. Alleyne, “A survey of iterative learning control: a learning-based method for high performance tracking control,” *IEEE Control Syst. Mag.*, vol. 26, no. 3, pp. 96–114, Jun. 2006.

[39] H.-S. Ahn, Y. Chen, and K. L. Moore, “Iterative learning control: brief survey and categorization,” *IEEE Trans. Syst. Man Cybern. Part C Appl. Rev.,*, vol. 37, no. 6, pp. 1099–1121, Nov. 2007.

[40] Y. Wang, F. Gao, and F. J. Doyle, “Survey on iterative learning control, repetitive control, and run-to-run control,” *J. Process Control*, vol. 19, no. 10, pp. 1589–1600, Dec. 2009.

[41] C. T. Freeman, E. Rogers, J. H. Burridge, A.-M. Hughes, and K. L. Meadmore, *Iterative Learning Control for Electrical Stimulation and Stroke Rehabilitation*, 1st ed., ser. Control, Automation and Robotics. Springer-Verlag London Ltd, 2015.

[42] H.-S. Ahn, K. L. Moore, and Y. Chen, *Iterative learning control: robustness and monotonic convergence for interval systems*, E. Sontag, M. Thoma, A. Isidori, and J. van Schuppen, Eds. Springer, 2007.

[43] W. Messner, R. Horowitz, W.-W. Kao, and M. Boals, “A new adaptive learning rule,” *IEEE Trans. Autom. Control*, vol. 36, no. 2, pp. 188–197, Feb. 1991.

[44] W. E. Dixon, E. Zergeroglu, D. M. Dawson, and B. T. Costic, “Repetitive learning control: A lyapunov-based approach,” *IEEE Trans. Syst. Man Cybern. Part B Cybern.*, vol. 32, pp. 538–545, 2002.

[45] J.-X. Xu and J. Xu, “On iterative learning from different tracking tasks in the presence of time-varying uncertainties,” *IEEE Trans. Syst. Man Cybern. Part B Cybern.*, vol. 34, no. 1, pp. 589–597, February 2004.

[46] M. Sun, S. S. Ge, and I. M. Mareels, “Adaptive repetitive learning control of robotic manipulators without the requirement for initial repositioning,” *IEEE Trans. Robot.*, vol. 22, no. 3, pp. 563–568, Jun. 2006.

[47] C. T. Freeman, E. Rogers, A.-M. Hughes, J. H. Burridge, and K. L. Meadmore, “Iterative learning control in health care: Electrical stimulation and robotic-assisted upper-limb stroke rehabilitation,” *IEEE Control Syst. Mag.*, vol. 32, no. 1, pp. 18–43, Feb. 2012.

[48] P. Sampson, C. Freeman, , S. Coote, S. Demain, P. Feys, K. Meadmore, and A.-M. Hughes, “Using functional electrical stimulation mediated by iterative learning control and robotics to improve arm movement for people with multiple sclerosis,” *IEEE Trans. Neural Syst. Rehabil. Eng.*, vol. 24, no. 2, pp. 235–248, Feb. 2016.

[49] T. Seel, C. Werner, J. Raisch, and T. Schauer, “Iterative learning control of a drop foot neuroprosthesis - generating physiological foot motion in paretic gait by automatic feedback control,” *Control Eng. Pract.*, vol. 48, pp. 87–97, Mar. 2016.

[50] X. Zhao, Y. Chu, J. Han, and Z. Zhang, “SSVEP-based brain-computer interface controlled functional electrical stimulation system for upper extremity rehabilitation,” *IEEE Trans. Syst., Man, Cybern., Syst*, vol. 46, no. 7, pp. 947–956, July 2016.

[51] E. H. Copur, C. T. Freeman, B. Chu, and D. S. Laila, “Repetitive control of electrical stimulation for tremor suppression,” *IEEE Trans. Control Syst. Technol.*, pp. 1–13, 2017.

[52] K.-M. Wang, T. Schauer, H. Nahrstaedt, and J. Raisch, “Iterative learning control of cadence for functional electrical stimulation induced cycling in paraplegia,” in *Proc. Conf. of the Int. Funct. Electrical Stimulation Soc.*, Sep. 2009, pp. 71–73.

[53] A. Hock and A. Schoellig, “Distributed iterative learning control for a team of quadrotors,” in *Proc. IEEE Conf. Decis. Control*, December 2016, pp. 4640–4646.

[54] J. Li, D. W. C. Ho, and J. Li, “Distributed adaptive repetitive consensus control framework for uncertain nonlinear leader-follow multi-agent systems,” *Journal of the Franklin Institute*, vol. 352, no. 11, pp. 5342–5360, November 2015.

[55] X. Bu, Q. Yu, Z. Hou, and W. Qian, “Model free adaptive iterative learning consensus tracking control for a class of nonlinear multiagent systems,” *IEEE Trans. Syst., Man, Cybern., Syst*, vol. PP, no. 99, 2017.

[56] D. Meng and K. L. Moore, “Learning to cooperate: Networks of formation agents with switching topologies,” *Automatica*, vol. 64, pp. 278–293, February 2016.

[57] C. Peng, L. Sun, and M. Tomizuka, “Distributed and cooperative optimization-based iterative learning control for large-scale building temperature regulation,” in *IEEE International Conference on Advanced Intelligent Mechatronics*, July 2017, pp. 1606–1611.

[58] J. Zhang and C. C. Cheah, “Passivity and stability of human-robot interaction control for upper-limb rehabilitation robots,” *IEEE Trans. on Robot.*, vol. 31, no. 2, pp. 233–245, 2015.

[59] P. Y. Li and R. Horowitz, “Control of smart exercise machines-part i: Problem formulation and nonadaptive control,” *IEEE/ASME Trans. Mechatron.*, vol. 2, no. 4, pp. 237–247, 1997.

[60] V. Duenas, C. Cousin, A. Parikh, and W. E. Dixon, “Functional electrical stimulation induced cycling using repetitive learning control,” in *Proc. IEEE Conf. Decis. Control*, 2016.

[61] C. Cousin, V. H. Duenas, C. Rouse, and W. E. Dixon, “Motorized functional electrical stimulation for torque and cadence tracking: A switched lyapunov approach,” in *Proc. IEEE Conf. Decis. Control*, 2017, pp. 5900–5905.

[62] M. Bellman, “Control of cycling induced by functional electrical stimulation: A switched systems theory approach,” Ph.D. dissertation, University of Florida, 2015.

[63] J. Zhang, C. C. Cheah, and S. H. Collins, “Experimental comparison of torque control methods on an ankle exoskeleton during human walking,” in *Proc. IEEE Int. Conf. Robot. Autom.*, May 2015, pp. 5584–5589.

[64] M. A. Holgate, A. W. Bohler, and T. G. Sugar, “Control algorithms for ankle robots: A reflection on the state-of-the-art and presentation of two novel algorithms,” in *Proc. IEEE RAS EMBS Int. Conf. Biomed. Robot. Biomechatron.*, October 2008, pp. 97–102.

[65] D. Quintero, D. J. Villareal, and R. D. Gregg, “Preliminary experiments with a unified controller for a powered knee-ankle prosthetic leg across walking speeds,” in *Proc. IEEE RJS Int. Conf. Intell. Robot. Syst.*, October 2016, pp. 5427–5433.

[66] D. J. Villareal, H. A. Poonawala, and R. D. Gregg, “A robust parameterization of human gait patterns across phase-shifting perturbations,” *IEEE Trans. Neural Syst. Rehabil. Eng.*, vol. 25, no. 3, pp. 265–278, March 2017.

[67] B. J. Fregly and F. E. Zajac, “A state-space analysis of mechanical energy generation, absorption, and transfer during pedaling,” *J. Biomech.*, vol. 29, no. 1, pp. 81–90, 1996.

[68] B. E. Lawson, E. D. Ledoux, and M. Goldfard, “A robotic lower limb prosthesis for efficient bicycling,” *IEEE Trans. on Robot.*, vol. 33, no. 2, pp. 432–445, April 2017.

[69] I. Landau and R. Horowitz, "Synthesis of adaptive controllers for robot manipulators using a passive feedback systems approach," in *Proc. IEEE Int. Conf. Robot. Autom.*, Apr. 1988, pp. 1028–1033.

[70] B. Brogliato, R. Lozano, B. Maschke, and O. Egeland, *Dissipative Systems Analysis and Control: Theory and Applications*, 2nd ed. Springer-Verlag London Ltd, 2007.

[71] T. Hatanaka, N. Chopra, and M. W. Spong, "Passivity-based control of robots: Historical perspective and contemporary issues," in *Proc. IEEE Conf. Decis. Control*, Dec. 2015, pp. 2450–2452.

[72] V. Ghanbari, M. Xia, and P. J. Antsaklis, "A passivation method for the design of switched controllers," in *Proc. Am. Control Conf.*, Jul. 2016, pp. 1572–1577.

[73] K. L. Moore, M. Ghosh, and Y. Q. Chen, "Spatial-based iterative learning control for motion control applications," *Meccanica*, vol. 42, no. 2, pp. 167–175, April 2007.

[74] H.-S. Ahn and Y. Chen, "State-dependent periodic adaptive disturbance compensation," *IET Control Theory Appl.*, vol. 1, no. 4, pp. 1008–1014, July 2007.

[75] J.-X. Xu and D. Huang, "Spatial periodic adaptive control for rotary machine systems," *IEEE Trans. Autom. Control*, vol. 53, no. 10, pp. 2402–2408, November 2008.

[76] M. Lješnjanin, Y. Tan, D. Oetomo, and C. T. Freeman, "Spatial iterative learning control: Output tracking," *IFAC-PapersOnLine*, vol. 50, no. 1, pp. 1977–1982, July 2017.

[77] J. Liu, X. Dong, D. Huang, and M. Yu, "Composite energy function-based spatial iterative learning control in motion systems," *IEEE Trans. Control Syst. Technol.*, vol. PP, no. 99, pp. 1–8, 2017.

[78] N. Fischer, R. Kamalapurkar, and W. E. Dixon, "LaSalle-Yoshizawa corollaries for nonsmooth systems," *IEEE Trans. Autom. Control*, vol. 58, no. 9, pp. 2333–2338, Sep. 2013.

[79] J. L. Krevolin, M. G. Pandy, and J. C. Pearce, "Moment arm of the patellar tendon in the human knee," *J. Biomech.*, vol. 37, no. 5, pp. 785–788, 2004.

[80] T. Watanabe, R. Futami, N. Hoshimiya, and Y. Handa, "An approach to a muscle model with a stimulus frequency-force relationship for FES applications," *IEEE Trans. Rehabil. Eng.*, vol. 7, no. 1, pp. 12–18, Mar. 1999.

[81] E. P. Widmaier, H. Raff, and K. T. Strang, *A.J. Vander, J.H. Sherman, and D.S. Luciano's Human Physiology: The Mechanisms of Body Function*, 9th ed. McGraw-Hill, New York, 2004.

[82] T. S. Buchanan, D. G. Lloyd, K. Manal, and T. F. Besier, "Neuromusculoskeletal modeling: Estimation of muscle forces and joint moments and movements from measurements of neural command," *J. Appl. Biomech*, vol. 20, no. 4, pp. 367–395, 2004.

[83] R. L. Lieber and J. Friden, "Functional and clinical significance of skeletal muscle architecture," *Muscle Nerve*, vol. 23, no. 11, pp. 1647–1666, Nov. 2000.

[84] O. M. Rutherford and D. A. Jones, "Measurement of fibre pennation using ultrasound in the human quadriceps in vivo," *Eur. J. Appl. Physiol. Occup. Physiol.*, vol. 65, pp. 433–437, 1992.

[85] A. F. Filippov, "Differential equations with discontinuous right-hand side," in *Fifteen papers on differential equations*, ser. American Mathematical Society Translations - Series 2. American Mathematical Society, 1964, vol. 42, pp. 199–231.

[86] F. Clarke, *Optimization and Nonsmooth Analysis*. Reading, MA: Addison-Wesley, 1983.

[87] R. Downey, M. Merad, E. Gonzalez, and W. E. Dixon, "The time-varying nature of electromechanical delay and muscle control effectiveness in response to stimulation-induced fatigue," *IEEE Trans. Neural Syst. Rehabil. Eng.*, vol. 25, no. 9, pp. 1397–1408, September 2017.

[88] J. Szecsi, C. Krewer, F. Müller, and A. Straube, "Functional electrical stimulation assisted cycling of patients with subacute stroke: Kinetic and kinematic analysis," *Clin. Biomech.*, vol. 23, no. 8, pp. 1086–1094, October 2008.

[89] E. Ambrosini, S. Ferrante, G. Ferrigno, F. Molteni, and A. Pedrocchi, "Cycling induced by electrical stimulation improves muscle activation and symmetry during pedaling in hemiparetic patients," *IEEE Trans. Neural Syst. Rehabil. Eng.*, vol. 20, no. 3, pp. 320–330, May 2012.

[90] T. W. J. Janssen and D. D. Pringle, "Effects of modified electrical stimulation-induced leg cycle ergometer training for individuals with spinal cord injury," *J. Rehabil. Res. Dev.*, vol. 45, no. 6, pp. 819–830, 2008.

[91] H. Kawai, M. Bellman, R. Downey, and W. E. Dixon, "Closed-loop position and cadence tracking control for FES-cycling exploiting pedal force direction with antagonistic bi-articular muscles," *IEEE Trans. Control Syst. Tech.*, to appear.

[92] V. H. Duenas, C. Cousin, V. Ghanbari, and W. E. Dixon, "Passivity-based learning control for torque and cadence tracking in functional electrical stimulation (FES) induced cycling," in *Proc. Am. Control Conf.*, 2018.

[93] W. E. Dixon, A. Behal, D. M. Dawson, and S. Nagarkatti, *Nonlinear Control of Engineering Systems: A Lyapunov-Based Approach*. Birkhauser: Boston, 2003.

[94] H. K. Khalil, *Nonlinear Systems*, 3rd ed. Upper Saddle River, NJ: Prentice Hall, 2002.

[95] R. Sepulchre, M. Janković, and P. V. Kokotović, *Constructive Nonlinear Control*. New York: Springer-Verlag, 1997.

[96] T. Sadikhov and W. M. Haddad, "On the equivalence between dissipativity and optimality of discontinuous nonlinear regulator for filippov dynamical systems," *IEEE Trans. Autom. Contol*, vol. 59, no. 5, pp. 423–436, February 2014.

[97] J. M. Caputo and S. H. Collins, "A universal ankle-foot prosthesis emulator for human locomotion experiments," *J. Biomech. Eng.*, vol. 136, no. 035002, pp. 1–10, March 2014.

[98] S. Obuz, R. J. Downey, J. R. Klotz, and W. E. Dixon, "Unknown time-varying input delay compensation for neuromuscular electrical stimulation," in *IEEE Multi-Conf. Syst. and Control*, Sydney, Australia, Sep. 2015, pp. 365–370.

[99] S. Obuz, R. J. Downey, A. Parikh, and W. E. Dixon, "Compensating for uncertain time-varying delayed muscle response in isometric neuromuscular electrical stimulation control," in *Proc. Am. Control Conf.*, 2016, pp. 4368–4372.

[100] R. J. Downey, M. J. Bellman, H. Kawai, C. M. Gregory, and W. E. Dixon, "Comparing the induced muscle fatigue between asynchronous and synchronous electrical stimulation in able-bodied and spinal cord injured populations," *IEEE Trans. Neural Syst. Rehabil. Eng.*, vol. 23, no. 6, pp. 964–972, 2015.

[101] R. Kamalapurkar, J. A. Rosenfeld, A. Parikh, A. R. Teel, and W. E. Dixon, "Invariance-like results for nonautonomous switched systems," *IEEE Trans. Autom. Control*, to appear.

[102] R. Kamalapurkar, B. Reish, G. Chowdhary, and W. E. Dixon, "Concurrent learning for parameter estimation using dynamic state-derivative estimators," *IEEE Trans. Autom. Control*, vol. 62, no. 7, pp. 3594–3601, July 2017.

## BIOGRAPHICAL SKETCH

Victor H. Dueñas was born in March 1992 in Ciudad Juárez, México. He received his B.S. in Mechanical Engineering from the University of Texas at El Paso in 2014. Victor joined the Nonlinear Controls and Robotics (NCR) research group to pursue his doctoral research under the advisement of Dr. Warren E. Dixon in 2015. He received his M.S. in Mechanical Engineering from the University of Florida in 2016, where he was awarded the Graduate School Fellowship by the same department in 2014. His research interests include nonlinear and adaptive control for rehabilitation robotics, neuromuscular control, and switched systems.